BNL-25940

UNIVERSIDADE ESTADUAL DE CAMPINAS

CAMPINAS - BRASIL

The Effects of Stoichiometry and Neutron Irradiation in Superconducting A-15 Compounds

A dissertation submitted in partial satisfaction of the requirements for the degree Doctor of Philosophy in Physics

by

Sergio Moehlecke

Committee in Charge:

Professor Daltro Garcia Pinatti, Co-chairman
Professor Alan Robert Sweedler, Co-chairman
Professor Erich Meyer
Professor Michael Collver
Professor Georgi Lucki

1978

To

Marion, Sabrina, Eduardo and André

TABLE OF CONTENTS

LIST OF TABLES

LIST OF TABLES (CONT'D)

LIST OF FIGURES

LIST OF FIGURES (CONT'D)

LIST OF FIGURES (CONT'D)

LIST OF FIGURES (CONT'D)

LIST OF FIGURES (CONT'D)

LIST OF FIGURES (CONT'D)

LIST OF FIGURES (CONT'D)

LIST OF FIGURES (CONT'D)

LIST OF FIGURES (CONT'D)

LIST OF FIGURES (CONT'D)

ACKNOWLEDGEMENT

I would like to express my gratitude to Dr. A. R. Sweedler under whose supervision this work was prepared and especially for his constant friendship. In the same spirit I want to extend my thanks to all my colleagues in Brookhaven National Laboratory that have contributed to this work and particularly to Dr. D. E. Cox, Dr. M. Strongin, Dr. R. Viswanathan, Dr. C.L.Snead, Dr. D. Dew-Hughes, Dr. R. Caton and Dr. T. Luhaman.

I would like to thank R. H. Jones for expert technical assistance. I am greatly indebted to Dr. M. Suenaga and Dr. D. Curinsky of the Brookhaven National Laboratory and to Dr. D. G. Pinatti, Dr. R. C. C. Leite and Dr. J. E. Ripper Fº of the Instituto de Física-Unicamp for creating the opportunity of this work.

I would like to thank Conselho Nacional de Desenvolvimento Científico e Tecnológico and U. S. Energy Research and Development Administration for financial support.

ABSTRACT OF THE DISSERTATION

The Effects of Stoichiometry and Neutron Irradiation in

Superconducting A-15 Compounds

by

Sergio Moehlecke

Doctor of Philosophy in Physics

Universidade Estadual de Campinas - Campinas 1978

Professor Daltro G.Pinatti - Co-Chairman

Professor Alan R.Sweedler - Co-Chairman

The A-15 (A_3B) compounds comprise an important class of superconducting compounds. In order to gain a clearer understanding of the parameters influencing the superconductivity in these materials, several A-15 compounds have been prepared and the effects, of varying stoichiometry, heat treatment, and irradiation with high energy neutrons (E > 1 MeV) on the superconducting transition temperature T_c, Bragg-William order parameter S, and the lattice parameter a_o, have been studied. The systems investigated include Nb_3Ge, Nb_3Al, Nb_3Pt, Nb_3Ir, V_3Ga, V_3Si and Mo_3Os.

Some of the results may be summarized as follows:

1 - For Nb_3Al, Nb_3Pt and V_3Ga, T_c is a strong function of composition, reaching a maximum value at the ideal stoichiometric

composition of 3A: 1B, if that composition exists in the equilibrium phase diagram.

2 - Irradiation with high energy neutrons at temperatures of $\sim$150°C results in drastic lowering of T_c for Nb_3Al, Nb_3Pt and Nb_3Ge, but not for Mo_3Os.

3 - T_c can be recovered by annealing, the recovery temperature being in the range 300-800°C depends on the particular compound.

4 - The order parameter S, decreases with increasing neutron fluence (decreasing T_c), and is also recoverable upon annealing at the appropriate temperature.

5 - The lattice parameter a_o, increases with increasing neutron fluence, and is also restored to its original value by annealing.

A simple hard sphere model is developed to calculate the dependence of a_o on composition within the A-15 phase. Excellent agreement is obtained for the measured values in the Nb-Al, Nb-Pt and V-Ga systems.

The results for both compositionally and irradiation induced disorder can be undestood on the basis of site-exchange taking place between the A and B sites in the A-15 structure.

I. INTRODUCTION

Since 1954, when Hardy and Hulm[1] reported the A-15 compound V_3Si superconducting with a transition temperature, T_c, of 17 K and Matthias et al.[2] reported a T_c of 18.05 K for Nb_3Sn, the phenomenon of superconductivity has received a great deal of attention with hopes for achieving even higher temperatures. At the present time Nb_3Ge has the highest T_c of (~23 K) of any known compound.[3] In addition to high transition temperatures, the A-15 compounds have large critical currents and high upper critical fields making them suitable for technological applications. There are 66 compounds that have already been synthesized with the A-15 structure of which 46 are known to be superconductors.

In the A-15 compounds, of chemical composition A_3B, the A atoms are the transition metals Ti, Zr, V, Nb, Ta, Cr, and Mo, and the B atoms come mainly from the groups IIIB and IVB of the periodic table and the precious metals Os, Ir, Pt and Au. This structure has a primitive cubic cell of 8 atoms, and belongs to the space group O_h^3-Pm3n. The cubic unit cell has 2 B atoms at 000, 1/2 1/2 1/2, and 6 A atoms at 1/4 0 1/2, 1/2 1/4 0, 0 1/2 1/4, 3/4 0 1/2, 1/2 3/4 0, 0 1/2 3/4. The B atoms have twelve nearest neighbors (CN12) at a distance $r_A+r_B=\sqrt{5}\, a_o/4$. The A atoms have a larger coordination number of 14, the CN14 polyhedron around each A atom contains two A atoms at a distance $a_o/2$, four B atoms at a distance

$\sqrt{5}\ a_o/4$, and eight A atoms at a distance $2r_A = \sqrt{6}\ a_o/4$ (a_o is the lattice parameter, r_A and r_B are the atomic radii of the A and B atoms respectively, in the A-15 structure).

A noticeable feature of this structure is the ortogonal chains of A atoms along the three (100) directions, each chain bisecting a face of the cube. The interatomic distance between the A atoms in one chain is the shortest distance between the atoms in the A-15 structure and is less than in the pure A crystal.

In the last few years, extensive experimental data has been obtained regarding the different physical properties of the A-15 compounds. Some of this data have been collected and systematized in a few review articles[4-9] where related theoretical models were also analyzed. Despite the large body of knowledge obtained on the properties of these materials, there does not yet exist any reliable way to predict the T_c of new materials or to obtain new materials with desirable superconducting properties.

The subject of this investigation does not attempt to search for new materials with high T_c's in the A-15 compounds but rather to study some of the available high T_c compounds and to understand what favorable set of parameters brings about higher transition temperatures. As a framework of analysis of the superconducting properties we use the changes in T_c produced by high energy neutron irradiation, rapid quenching from high temperatures, composition

variations and annealing. It has been known[10-12] that the transition temperature is very sensitive to these parameters which manifest themselves in the crystallographic structure of the A-15 compounds and that is why this latter has received special attention in this investigation.

Several A-15 compounds (Nb-Ge, Nb-Al, Nb-Pt, V-Ga, Mo-Os and Nb-Ir) are studied here. In the next chapter we describe how the samples were prepared and characterized, the different heat treatments, and how the parameters were measured. In Chapter III, the results are presented for each system separately and finally in the last chapter these results are discussed and compared with previous work, and some conclusions are drawn. The parameters that have to be optimized to obtain a high T_c in any A-15 system will be discussed. Even though an answer to what materials will have a high T_c cannot be definitely given, some insight has been gained in this area. For Nb_3Si for example, a good candidate for high T_c's,[13] the problem is in developing new techniques for synthesizing this compound in the A-15 structure at the correct stoichiometry.

II. EXPERIMENTAL TECHNIQUE

A) Sample Preparation

All the samples used here were arc-cast in an ultra high-purity (UHP) argon arc furnace using a nonconsumable tungsten electrode, with the exception of the Nb_3Ge. The starting materials used are listed in Table I.

The Nb_3Ge samples were prepared by a chemical vapor deposition process described previously[14]. Briefly stated, the process consists of hydrogen reduction of a mixture of the chlorides of Nb and Ge, deposition taking place on the inside of Cu tubes held at 900°C. After deposition the Cu was dissolved in HNO_3, and the Nb_3Ge was left in the form of very brittle flakes about 50μm thick. Nb_3Al was prepared by mechanically mixing Nb and Al powders in the desired proportions (with 25% by weight of Al added due to losses during melting) and pressed to about 5 tons in the form of pellets. The V-Ga alloys were formed by wrapping small pieces of V & Ga together with V wire in a spring form with 20% excess of Ga added. Nb_3Pt, Nb_3Ir and Mo_3O_s presented no problems in the arc furnace as the weight losses were low due to the high melting temperatures of the components.

The samples (1 to 3g) were remelted at least four times and inverted on the water-cooled cooper heart between each melt.

TABLE I

MATERIAL	FORM & SOURCE	PURITY & REMARKS
Nb	POWDER (18Mesh); SPECPURE - JOHNSON MATTHEY CHEMICALS LIMITED	Fe = 3ppm; Al = 1ppm; Ti = 20ppm; Ca = 1ppm; Si<1ppm; Ta<50ppm
V	ROD; MATERIALS RESEARCH CORP.	Marz Grade Etched: HNO_3/H_2O
Mo	ELECTRO-REFINED CRYSTALS; NATIONAL BUREAU OF MINES	99.99%
Al	POWDER (200 Mesh); RESEARCH ORGANIC/INORGANIC CHEMICAL CORP.	99.9%
Ga	ROD; LEICO INDUSTRIES	99.9999%
Pt	ROD; ENGELHARD INDUSTRIES	99.999% Etched: Aqua Regia
Ir	ROD; ENGELHARD INDUSTRIES	99.999% Etched: Aqua Regia
Os	POWDER; VARLACOID	99.9%

The composition was determined by weight losses (to the nearest 0.00001g), assuming that it came only from the low melting temperature element. Melting Nb, V or Mo alone gave negligible weight loss. The composition was determined to better than 1 at.% and in the case of Nb_3Pt, Nb_3Ir and Mo_3Os samples to better than 0.2 at.%. Selected samples had the composition and homogeneity checked after heat treatments by electron microprobe analysis and no change in composition or inhomogeneity was detected within the accuracy of this technique[15]. For the Nb_3Ge samples spectrographic and chemical analysis were performed to determined impurity levels and composition.

B) Heat Treatments

After casting, the samples were submitted to a series of heat treatments with the objective of obtaining single phase, homogeneity, high critical temperature and maximum order. To obtain this, three different kinds of heat treatments were done on each sample. First, a high temperature anneal (1400 - 2000°C) for a short time (5 min. - 12 hrs.). These treatments were designed to remove all traces or coring or segregation present in the as-cast specimens and to accelerate the attainment of equilibrium in the subsequent anneals. After this, the heat treatment was done at high and medium temperatures (1000 - 1900°C) for a longer time (2 hrs. - 8 days) until equilibrium was achieved, followed by a fast cooling. This treatment is the most critical to obtain good results and depends strongly on composition, the

phase diagram and the system involved. Finally, a low temperature heat treatment (600 - 1000°C) for a long period (2 - 70 days) was used to obtain maximum order.

The low temperature heat treatments were carried out in a Ni-Cr resistance furnace with the temperature controlled by two Cr-Al thermocouples (±5°C). The samples were wrapped in Ta foils and sealed in quartz tubes under ½ atm of ultra high purity argon. After the anneals, the samples were removed from the furnace and cooled by radiation.

For the high temperature heat treatment, two kinds of furnaces were used. In the first,(Centorr, model 15-2x5W-30, Centorr Associates, Inc.) heating was accomplished by a W resistance coil and temperatures of up to 2000°C could be maintained for long periods of time. The samples were wrapped in Ta foils to avoid contamination where located in the center of the furnace in contact with a W-5Re/W-26Re thermocouple Mo sheathed and under a UHP argon atmosphere (2 - 3 atm). The thermocouple was calibrated against the melting point of Pt to within ±20°C. No appreciable change in weight or any change in color of the surface of the samples were observed. To cool the sample from 1900°C to 800°C in this furnace takes about 2 minutes. In order to obtain homogeneous samples the as-cast button was broken into small pieces (~0.1g) to increase the cooling rate and provide more uniform cooling.

Another furnace was constructed to obtain faster quenches

(~1/10 sec. from 1900°C to 300°C) similar in design to that previously reported[16]. It consists of a Ta tube heated resistively and thermally insulated with "Zircar" (ZrO_2 - Union Carbide). The specimen (≤0.3g) is suspended in the center of the tube, next to a W-5Re/W-26Re thermocouple Mo sheathed (±30°C), by W or Nb wire hung in fine fuse wire. The specimen is quenched by applying 50V to the fuse wire to explode it and the sample falls into liquid Ga. The heat treatment is done in one atmosphere of UHP argon and the weight losses are negligible. When the losses become appreciable (long-term anneal and/or high temperature) the composition of the sample can be maintained by etching the sample surfaces as losses are only due to volitalization of the low melting elements from the surfaces (~100μm - thick)[17]. The specimen surface (some times contaminated with tantalum oxides evaporated from the Ta tube) and the Ga adsorbed were removed by cleaning the sample in a ultra-sonic cleaver with hot water and then etching with aqua regia ($HF+HNO_3+H_2O$; 1:1:2). The accuracy of the temperature indicated by the calibrated thermocouple was periodically checked against the melting point of pure platinum.

C) Metallography

The samples were mounted in epoxy resin and their surfaces polished with SiC paper (grit numbers 400A and 600A) and a final polish was done with alumina in a cloth-covered wheel.

The grain boundaries in the A-15 phase of Nb_3Ge and Nb_3Al were observed by etching the specimens in a solution of 2g Cr O_3 in 100 ml HF for 1 to 5 minutes. The Nb_3Pt and Nb_3Ir samples were etched in a solution of $1HNO_3+1H_2SO_4+1HF+1H_2O$ for 1 to 3 seconds to show the grain boundaries and even sub-boundaries in the grain were developed. This same solution also revealed the grains in the Mo_3Os and V_3Ga systems after etching for 1 - 3 minutes, but in this latter system, surface stains form rather rapidly on the etched specimen. This staining can be prevented by dipping the specimens in a $1NH_4OH + 10H_2O$ solution for 30 - 60 seconds.

Individual phases of the Nb_3Ge and Nb_3Al samples were distinguished by means of their different thickness oxide layer formation during anodization. Each sample was made the anode of an electrolytic cell. The sample surface was immersed in a solution of dilute citric acid (1:10), was touched with a Nb needle where 22½ volts were applied for 1 second to 3 minutes. This treatment resulted in different colors across the samples due to interference effects by which the phases were identified. The following general observations were made: body-centered cubic niobium appears blue, the A-15 cubic phase appear pink, while tetragonal or hexagonal phases appear orange. When an over-anodization occurs the oxide layers can be decreased by etching in a dilute solution of hydrofluoric acid (1:5). A proper balance between these two treatments can improve the color

contrast, especially when there is finely divided structures in the phase boundaries.

D) Lattice Parameter

The lattice parameter measurements were made with a Debye-Scherrer 114.5 mm camera (Straumanis method) using Ni-filtered Cu Kα radiation (Norelco, Philips Electronics, Inc., 40kV and 15 mA). The samples were powdered to -325 mesh (45μm), assembled in a glass capillary (0.3 mm) and, normally, exposured for 6 hours. The lattice parameter, a_o, of the A-15 phase was determined by extrapolating to $\theta=90^o$ the measured values of the reflections in the back-reflection region using the Nelson-Riley function. This procedure gives an accuracy of ±0.001Å or better.

For neutron-irradiated samples short exposure times (1 to 4 hours), small quantities of material (~1mg) and higher energy in the x-ray beam (50 kV and 20 mA) were used to decrease the γ-radiation background of the sample.

It was also possible to observe second phase present in amounts greater than 5% (volume fraction) and identify them by indentifying the lines with standard ASTM charts. Photographs were also taken on an IRD Guinier focusing camera with Cu Kα radiation, high-purity Si powder being used as an internal standard. This technique gives improved resolution and sensitivity and is very useful for impurity phase identification.

E) Long Range Order Parameter

To determine the degree of long range order (LRO), the samples were prepared by grounding the material (30 - 300mg) in an agate mortar under cyclohexane (to reduce oxidation due to heating and reduce strains) to a - 400 mesh (38μm) particle size. The particle size were further decreased by grounding (~½ hour) in the same conditions. The powder was transferred to an aluminum sample holder into which a shallow rectangular trough 2.5 x 1.5 x 0.025 cm had been machined, compacted and leveled with a glass slide. The specimen was mounted on a General Electric XRD5 diffractometer with a fine-focus Cu target equipped with a Canberra semiautomatic 6511 step-scanning system for digital data collection. A graphite monochromator mounted on the detector arm was used to eliminate CuKβ radiation and improve the signal-to-noise ratio. Scans were taken over the first twenty peaks (20 - 120 deg.) with a scanning speed of 0.05 degree per minute and extra time was devoted to weak peaks if necessary. With this procedure, peaks having about 0.1% the intensity of the strongest peak are easily detected.

Shifting the position of the sample holder normally resulted in a change (~10%) in the integrated intensities due to differences in particle size. This effect was observed to persist even when the sample holder was rotated during the scan. More consistent results were obtained mixing the sample with silicon powder and moving it to four or five different positions, taking an average

integrated intensity for each peak. The standard deviation obtained for these peaks was usually considerably larger than the errors due to counting statistics, uncertainties in background or target stability, and was, therefore, taken as the error in the intensity. Using a smaller mesh (10μm) the number of scans were reduced to two or three different positions.

The calculated integrated intensities include the usual analytical expression for the Lorentz polarization factors, multiplicity factors, and of the monchromator was taken into account. The expression of the structure factor for the A-15 structure used was:

$$F = \left\{ \bar{f}_B \left[1 + \cos 2\pi\left(\frac{h+k+1}{4}\right)\right] + 2\,\bar{f}_A \left[\cos 2\pi\left(\frac{h}{4} + \frac{1}{2}\right) + \right.\right.$$

$$\left.\left. + \cos 2\pi\left(\frac{h}{2} + \frac{k}{4}\right) + \cos 2\pi\left(\frac{k}{2} + \frac{1}{4}\right)\right]\right\} \exp\left(-\frac{B\sin^2\theta}{\lambda}\right)$$

where $\bar{f}_A$ and $\bar{f}_B$ represent the average scattering factors for A and B sites in the A-15 structure given by:

$$\bar{f}_A = \left(\frac{3-x}{3}\right) f_A + \left(\frac{x}{3}\right) f_B$$

$$\bar{f}_B = \left(1-x-y\right) f_B + \left(x + y\right) f_A \ .$$

Defined in this way we can write a generalized expression for the A-15 phase, which includes compositional and positional

parameters, $(A_{3-x}B_x)[B_{1-x-y}A_{x+y}]$. The parameter y determines the departure from the ideal stoichiometric ratio and may be positive or negative depending on whether the alloy is B poor (<25 at.%) or B rich (>25 at.%). The parameter x determines the fractional occupation of the A and B sites of a given composition. The parameters x and y can be related to the conventional Bragg-Williams LRO parameter, S, by noting that for nonstoichiometric compositions one must assign different values of S to each crystallographic site (<25 at.% or >25 at.%). An order parameter for the A sites, S_A, and for the B sites, S_B, is defined in the following manner:

$$S_A = \frac{P_A - \Gamma_A}{1 - \Gamma_A} = 1 - \frac{4x}{3(1-y)}$$

and

$$S_B = \frac{P_B - \Gamma_B}{1 - \Gamma_B} = 1 - \frac{4(x+y)}{3+y}$$

where $P_A = (3-x)/3$ is the fraction of A sites occupied by A atoms, $P_B = 1-x-y$ is the fraction of B sites occupied by B atoms, $\Gamma_A = (3+y)/4$ is the fraction of A atoms in alloy, and $\Gamma_B = (1-y)/4$ is the fraction of B atoms in alloy. Note that for stoichiometric alloys (i.e., $y = 0$) $S_A = S_B$.

Least-squares refinement of the integrated intensity data was carried out with a computer program which permits each peak or composite peak to be specified in terms of the reflections

from any phase which can possibly contribute. Beyond the A-15 phase, appropriate structure factor expressions were used for Si and other phases which were present. For the scattering factors neutral atoms were assumed and appropriately corrected for dispersion effects[18]. Instrumental factors were also considered, and an overall Debye-Waller factor, B, was assumed, since attempts to refine individual values for A and B sites did not usually produce any significant improvement. The agreement between observed and calculated intensities was indicated by the usual reliability R factors, defined as:

$$R \text{ factor} = \Sigma / I_{obs} - I_{calc} / \Sigma I_{obs}$$

$$\text{weighted R factor} = \{\Sigma w (I_{obs} - I_{calc})^2 / \Sigma w (I_{obs})^2\}^{\frac{1}{2}}$$

where $w = 1/\sigma^2$, σ is the standard deviation. With this procedure, the error in the determination of the LRO parameter was $\Delta S = \pm 0.02$. To certify that no preferred orientation was included in the observed values greater than the assumed errors, the intensity ratios of the peaks 200, 211, 321, 420, 332 and 521 was compared in each scan since these reflections contribute in the same way to the structure factors[19].

The peaks which have the structure factors given by only the difference in the scattering factors ($f_B - f_A$), such as (110), (220), (310), (411), (330), (422), (510), (431), (530), (433),

(620), and (541) are the superstructure peaks and are called difference peaks or difference lines.

From these intensities measurements, the amount of second phase was also determined, using standard methods[20].

F) Critical Temperature

The superconducting transition temperature, T_c, was detected by an AC mutual-inductance bridge operating at a frequency of 27 Hz. The sample was mounted on a sapphire block where a calibrated Ge thermometer was incrusted. The sample holder was inserted into the secondary coil of the mutual-inductance coil which was located in the outer vacuum jacket of a double-vacuum-space Dewar. The double vacuum space enabled the measuring coils to be kept at 4.2K while the sample could be warmed to temperatures above 4.2K by a heater attached to the sapphire. This avoided coil drift at high temperatures. Bellow 4.2K, the temperature was determined by monitoring the vapor pressure of liquid He. The accuracy of the T_c's are ±0.1K. The transition temperature was defined as illustrated in Fig. 1 and unless indicated, the T_c adopted was where 50% of normal to superconducting transition occurs, T_{c3} of Fig. 1 . ΔT_c was defined as $T_{c2} - T_{c4}$.

G) Neutron-Irradiations

The samples for irradiation were crushed (to - 50 mesh for T_c and post-irradiation anneals, ~70 mg each; to - 325 mesh for a_o, ~8 mg each; and to - 400 mesh for LRO, ~60 mg each) and

Figure 1

Schematic representation of transition from normal to superconducting state defining different T_c values noted in text.

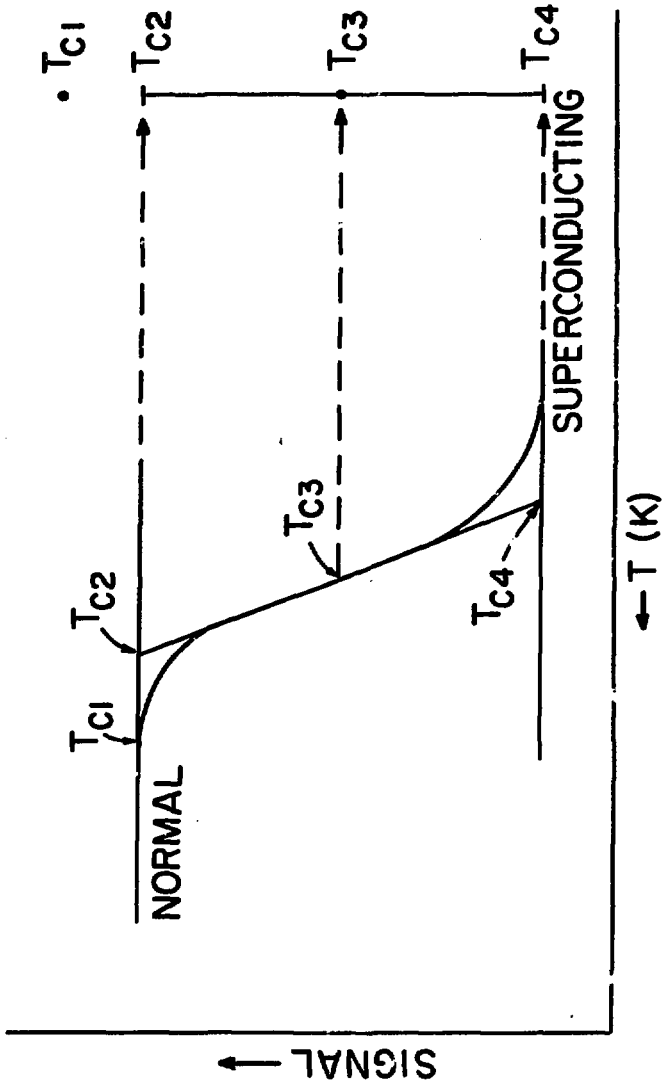

Fig. 1

sealed in 4 mm quartz tubes under ½ atmosphere of UHP He exchange gas. In this manner, it was possible to measure T_c and to carry out annealing studies after irradiation without the need to remove the radioactive samples from the quartz capsules, minimizing any possible radioactive contamination. All irradiations were performed in the Brookhaven High Flux Beam Reactor (HFBR). The ampoles were placed in Al capsules, designed to accommodate up to fifteen samples at a time, and were immersed in the reactor's cooling water. The temperature during irradiation measured with a thermocouple inserted in a Sn powder located at the same position where the samples were irradiated, averaged at 140 ± 30°C. All irradiations were carried out under as nearly identical conditions as possible, and the fluence was determined from the product of the irradiation time and the fast flux (E>1MeV). In each Al capsule a Ni monitor was included and the neutron activation of the reaction $Ni^{58}(n,p)Co^{58}$ was measured. As a result of these measurements and from other kinds of monitors, the flux (E>1MeV) was determined to be $1.0 \pm 0.1 \times 10^{14} n/cm^2$ sec.

In a few irradiated samples, hysteresis or a decrease in height of the S-N transition signal or no transition at all was observed, probably due to a loss of the He exchange gas during irradiation[21]. These ampoles were recapsulated after irradiation with new He exchange gas. After this procedure, no hysteresis was observed, and the transition height was generally equal to that of the unirradiated value. In order to

obtain consistent results reincapsulating was adopted as a standard procedure. It should be pointed out here that a sample irradiated and showing a normal transition in the sense of no hysteresis and full signal, after recapsulation maintained the same characteristics: i.e., no hysteresis, full signal, same T_c and width of transition, ΔT_c.

Annealing of the neutron irradiated samples was accomplished by placing the quartz capsules in a conventional tube furnace with flowing He. This arrangement was to avoid losses of the He exchange gas that diffuses out of the quartz tubes even at low temperatures.

III. EXPERIMENTAL RESULTS

Nb - Ge: At present, the Nb-Ge system has the highest superconducting transition temperature when prepared by non-equilibrium techniques, such as sputtering[23,24], electron beam deposition[25,26], and chemical vapor deposition[14,27]. The reason why these preparation techniques result in transition temperatures as high as 23K, whereas conventional techniques, such as arc melting or sintering[28-30], result in such lower T_c's of ~6K, is thought to be associated with formation of a metastable stoichiometric Nb_3Ge[23,28,31]. However, an increase in stability of the A-15 structure by addition of impurities[32,33], presence of highly disordered or amorphous material[34], or the elimination of some unknown defect[24] is also attributed to explain this effect. An extensive analysis of this system has not been possible because of the very small quantities of material obtained by sputtering and electron beam vapor deposition techniques. However, recently it has proved possible to prepare relatively large quantities of high T_c material by chemical vapor deposition techniques[14].

We present here a study of Nb_3Ge prepared in this manner. The metastability of the A-15 phase of Nb_3Ge was investigated by studying the effects of high temperature annealing and neutron irradiation on the superconducting and lattice properties of CVD prepared Nb_3Ge.

Several samples were examined, one involving a relatively large quantity of material (~25g - from several CVD runs),

designated Nb_3Ge (II), was used for the annealing studies. Spectrographic analysis of this sample indicated metallic impurities at the following levels: Fe (0.2 wt%), Cu (0.2 wt%), Si(0.2 wt%) and others at less than 100 ppm. Chemical analysis for Nb and oxygen gave values of 75.05 and 1.57 wt.% respectively.

Debye-Scherrer and Guinier photographs of the as-deposited sample showed the principal phase was of A-15 type with a lattice constant of 5.142 $\pm$ 0.002Å. Four other phases were also detected, the principle phase being tetragonal Nb_5Ge_3 with cell parameters a = 10.173 $\pm$ 0.005Å and c = 5.143 $\pm$ 0.003Å. There were also significant amounts of Nb O_2 and Nb O (a = 4.210Å) and a trace of hexagonal Nb_5Ge_3 (a = 7.72Å, c = 5.345Å). To help in the phase identification an arc-melted sample of tetragonal Nb_5Ge_3 was prepared. Chemical analysis for Nb showed this to be very close to stoichiometry (67.9 wt.% against a calculated value of 68.08 wt.%). This material gave a very well resolved x-ray pattern (lattice parameters a = 10.169 $\pm$ 0.003Å, c = 5.139 $\pm$ 0.002Å) and showed quite clearly that there was overlap of many of the principle lines with the A-15 phase.

The diffraction lines of the as-deposited sample were observed to be appreciably broadened compared to those of the Si standard. This could arise from effects such as grain size, microstress, or compositional inhomogeneities, all of which could plausibly result from the vapor deposition process. However, metallographic analyses of the as-deposited material

indicated the average grain size to be of the order of 7μ (Fig. 2) which is too large to be the cause of the observed line broadening[20]. From the general trend of the line widths as a function of increasing 2θ, either microstresses or inhomogeneities, or a combination of both, appear to be mainly responsible for the line broadening. Similar, although more pronounced, effects have been observed in sputtered A-15 niobium-base alloys[35]. Comparing the as-deposited film with those obtained from off-stoichiometry (Nb - rich) arc-melted samples we observed that in the latter all the lines were sharp. As these arc-melted samples are less affected by grain size, microstress, or compositional inhomogeneities effects the line broadening observed in the as-deposited material must originate in the deposition process.

The annealing studies on Nb_3Ge (II) revealed a number of interesting features. At 700°C, some of the NbO_2 had already been converted to NbO. At 850°C, both the NbO_2 and hexagonal Nb_5Ge_3 could no longer be detected but there was no observable change in the lattice parameter of the A-15 phase. At 1000°C there was still no change, but at 1100°C there was quite a definite increase from 5.142 to 5.152Å and at 1350°C a further increase to 5.179Å. The x-ray pattern for both phases (A-15 and tetragonal Nb_5Ge_3) at this point was quite sharp and the (110) line of the A-15 phase was no longer visible in the x-ray film[36]. A substantial increase in the amount of tetragonal phase relative to the A-15 phase was also evident. Within experimental limits

Figure 2

Nb_3Ge as-deposited, etched (2gm CrO_3 + 10mℓHF, 5 min.), average grain size 7μm, 1200X.

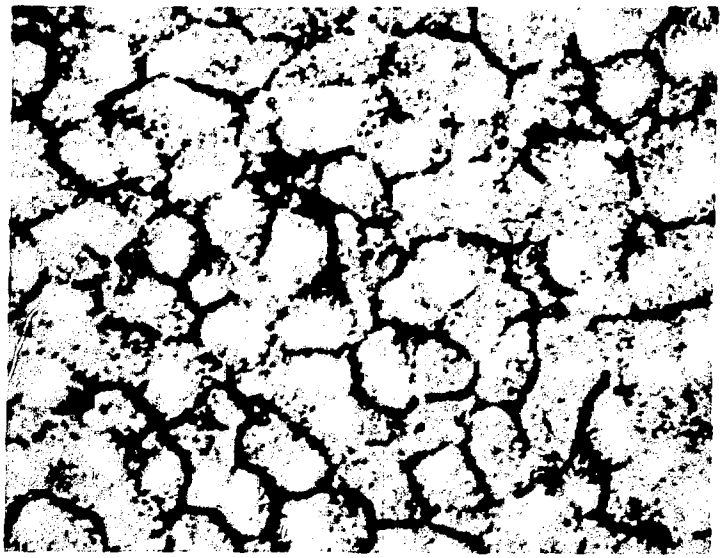

Fig. 2

of error, no change of lattice parameters of the former was observed in the annealing process. Samples which had been annealed at 1150°C and 1250°C were also subjected to further anneals at 1000°C and 1100°C in order to check for reversibility, but the x-ray patterns showed no changes.

The effect of annealing on T_c is summarized in Table II and shown graphically in Fig. 3 together with the lattice parameters. Between 700°C and 900°C Tc remained relatively constant compared to the as-deposited value of 19.4K, exhibiting a small degradation of about 0.4K and an increase in the transition width ΔT_c, from 0.4 to 1.0K. Above 900°C T_c began to slowly decrease and above 1000°C the decrease was fairly rapid until T_c finally leveled off at a value of about 6K for an annealing temperature of 1250°C. Further annealing at 1350°C and 1450°C produced no further change in T_c.

It can also be seen from Fig. 3 that in the temperature range 950°C - 1150°C ΔT_c increases considerably compared to the as-deposited value, and that the difference between the onset transition temperature and T_{c2} also increases over this range. The origin of this broadening is not understood. However, it may be associated with the initial stage of the decomposition process described previously.

The decrease in T_c due to annealing accompanies the increase of the lattice parameter. Furthermore, the decrease was not reversible. Samples annealed at 1000°C and 1100°C for 48 hours after annealing at 1150°C and 1250°C retained their lower T_c values.

Table II

Summary of Data for Chemically Vapor Deposited Nb_3Ge(II) Annealed Samples

Transition Temperature (K)				Lattice Parameter of A-15 Phase	Other Phases Present	Heat Treatment
T_{c1}	T_{c2}	T_{c3}	T_{c4}	a_o Å		
19.9	19.7	19.4	19.3	5.142	T-Nb_5Ge_3(a=10.17$_3$, c=5.14$_3$) NbO_2; NbO; H-Nb_5Ge_3	as deposited
19.7	19.4	18.8	18.1	5.141	T-Nb_5Ge_3; NbO_2; NbO	700°C/48 hrs
19.7	19.3	18.6	17.9	5.142		750°C/48 hrs
19.7	19.3	18.4	17.3	5.144	T-Nb_5Ge_3; NbO; NbO_2	800°C/48 hrs
19.5	19.1	18.1	17.3	5.143	T-Nb_5Ge_3; NbO	850°C/48 hrs
19.6	19.3	18.7	18.3	5.141	T-Nb_5Ge_3; NbO	900°C/48 hrs
19.2	17.5	15.6	14.8	5.143	T-Nb_5Ge_3; NbO	950°C/48 hrs
18.7	17.5	16.0	15.0	N.M.	Not measured	985°C/48 hrs
19.5	17.1	14.8	13.3	5.144	T-Nb_5Ge_3 (a=10.16$_5$, c=5.13$_5$) NbO	1000°C/48 hrs
18.1	14.9	12.6	11.3	5.143	T-Nb_5Ge_3; NbO	1050°C/48 hrs
15.0	9.6	8.4	7.5	5.152	T-Nb_5Ge_3 (a=10.16$_0$, c=5.14$_2$) NbO (a=4.210)	1100°C/48 hrs
8.2	7.5	6.6	6.1	5.158	T-Nb_5Ge_3; NbO	1150°C/48 hrs
5.9	5.8	5.7	5.6	5.170	T-Nb_5Ge_3; NbO	1250°C/48 hrs
5.9	5.8	5.6	5.5	5.179	T-Nb_5Ge_3 (a=10.16$_5$, c=5.13$_5$) NbO (a=4.210)	1350°C/48 hrs
6.2	6.1	5.8	5.7	5.177	T-Nb_5Ge_3 (a=10.17$_1$, c=5.14$_2$) NbO (a=4.216)	1450°C/48 hrs
5.9	5.8	5.6	5.5	5.170	T-Nb_5Ge_3 (a=10.16$_3$, c=5.13$_7$) NbO (a=4.210)	1250°C/48 hrs + 1100°C/48 hrs
7.3	7.2	6.3	5.7	5.158	T-Nb_5Ge_3; NbO	1150°C/48 hrs + 1000°C/48 hrs
5.8	5.8	5.6	5.5	5.169	T-Nb_5Ge_3 (a=10.16$_3$, c=5.133) NbO (a=4.210)	1250°C/48 hrs + 1000°C/48 hrs

Figure 3

Effect of annealing on the superconducting transition temperature T_c and lattice parameter a_o of the A-15 phase of Nb_3Ge (II).

(a) T_c vs. annealing temperature. Error bars represent transition widths $\Delta T_c \equiv T_{c_2} - T_{c_4}$.

(b) a_o vs. annealing temperature.

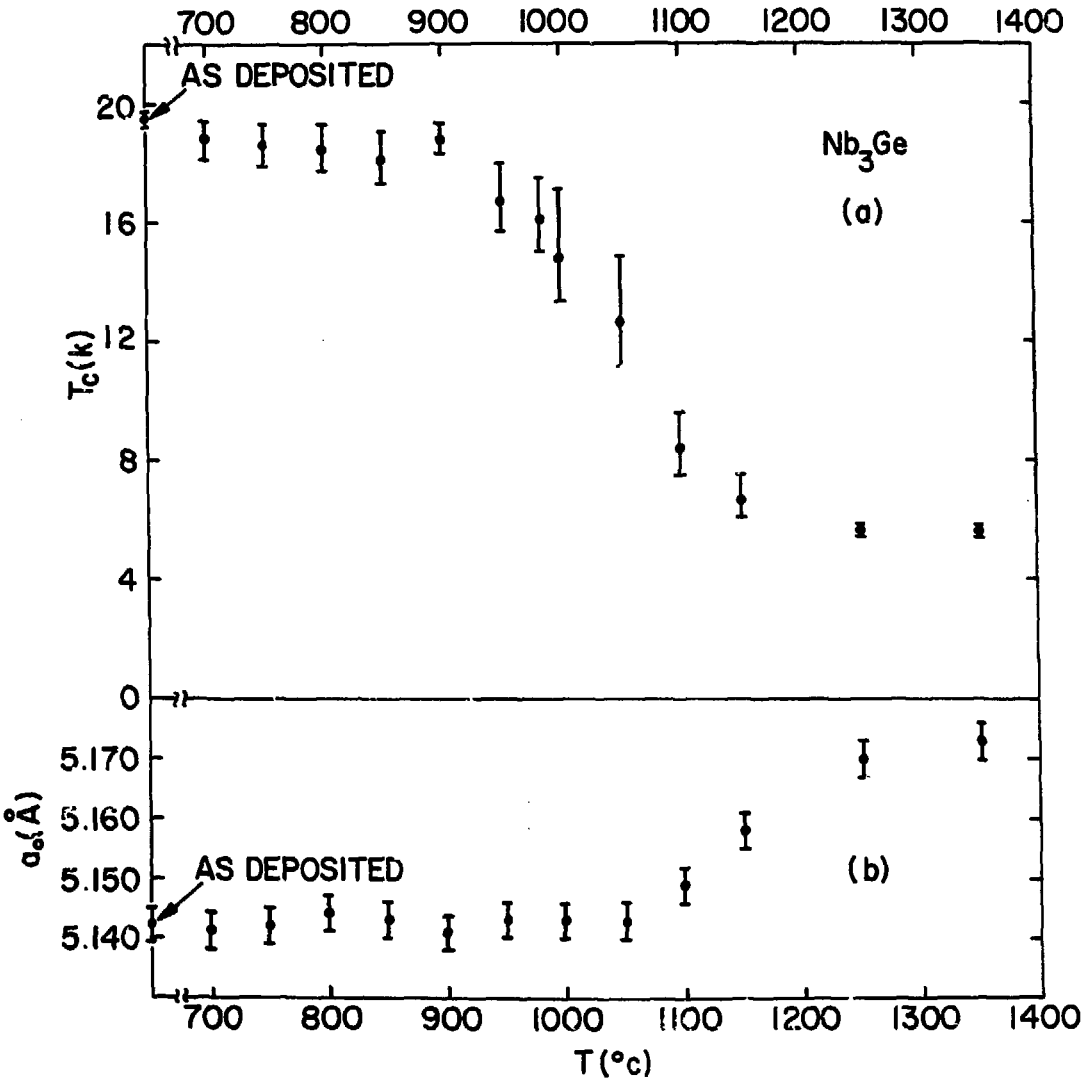
700
800
900
1000
1100
1200
1300
1400
AS DEPOSITED
20
16
12
8
4
0
T_c(k)
Nb_3Ge
(a)
5.170
5.160
5.150
5.140
a_o(Å)
AS DEPOSITED
(b)
T(°c)

Fig. 3

Parts of the diffractometer scans for Nb_3Ge (II), both as-deposited and annealed at 1350°C, are shown in Fig. 4. In addition to the A-15 phase, there are substantial quantities of impurity phases in the as-deposited material (Fig. 4a) as previously observed from the x-ray films. One obvious feature of both patterns is the number of overlapping peaks. However, it is emphasized that every single peak can be accounted for, and that the (110) peak of the A-15 phase is completely free from any overlap of this type. Although quite weak, it can be measured quite accurately, as shown in the inset to each figure.

In spite of the number of impurity phases present, least-squares refinement of the intensity data was possible. The data from the sample annealed at 1350°C were first processed with variable scale and temperature factors for the four phases (including Si), an occupation factor k for the A-15 phase, and the three variable positional parameters for tetragonal Nb_5Ge_3. The positional parameters of NbO have been given previously by Bowmann, et. al.[37]. The impurity phases were assumed to have their ideal stoichiometry.

The compositional parameter (y in $Nb_{3+y}Ge_y$) was assigned several values. Virtually identical fits were obtained in each case, since the scale factor and occupation factor adjust themselves accordingly, while the other parameters attain the same set of final values. From the respective values of the scale factors, the volume fractions of each phase were calculated

Figure 4

X-ray data for Nb_3Ge (II). (a) As-deposited. (b) Annealed at 1350°C for 48 hours. The insert to each pattern shows the (110) peak of the A-15 phase in greater detail.

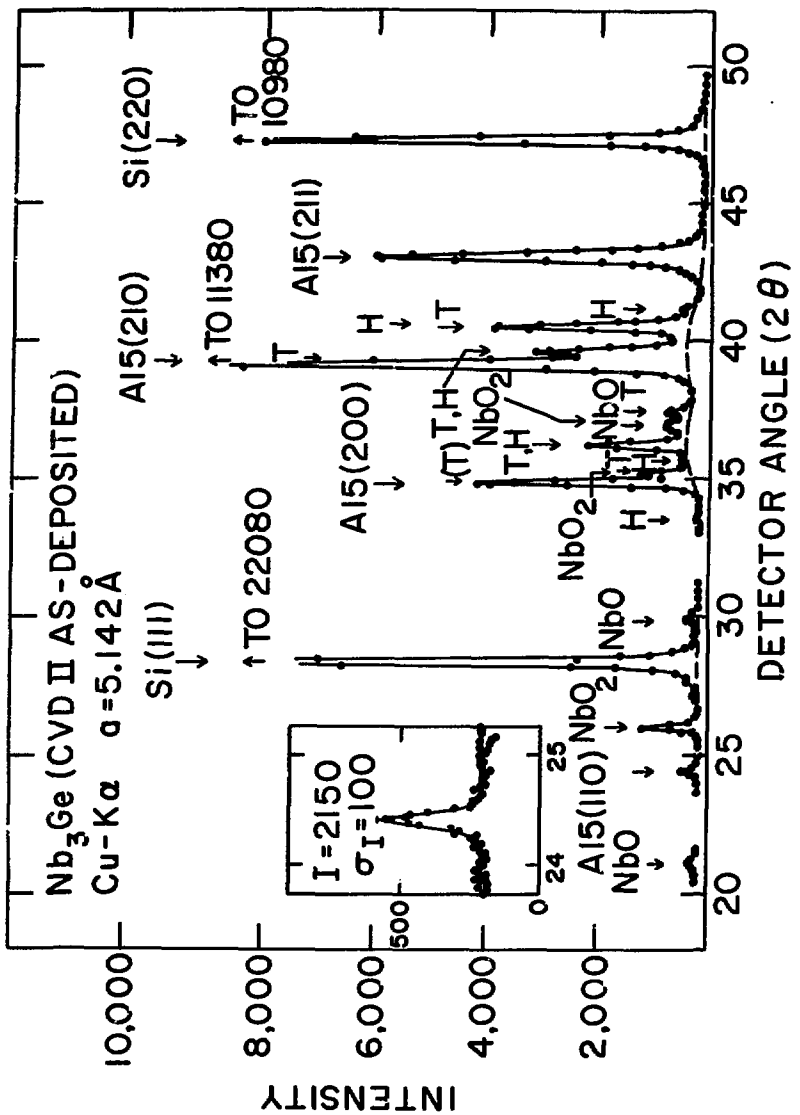
Nb3Ge (CVD II AS-DEPOSITED)
Cu-Kα a=5.142Å
Si(111)
TO 22080
A15(210)
TO 11380
Si(220)
TO 10980
A15(211)
A15(200)
A15(110)
NbO2
NbO
T
H
(T)T,H
T,H
I=2150
σI=100
INTENSITY
DETECTOR ANGLE (2θ)

Fig. 4a

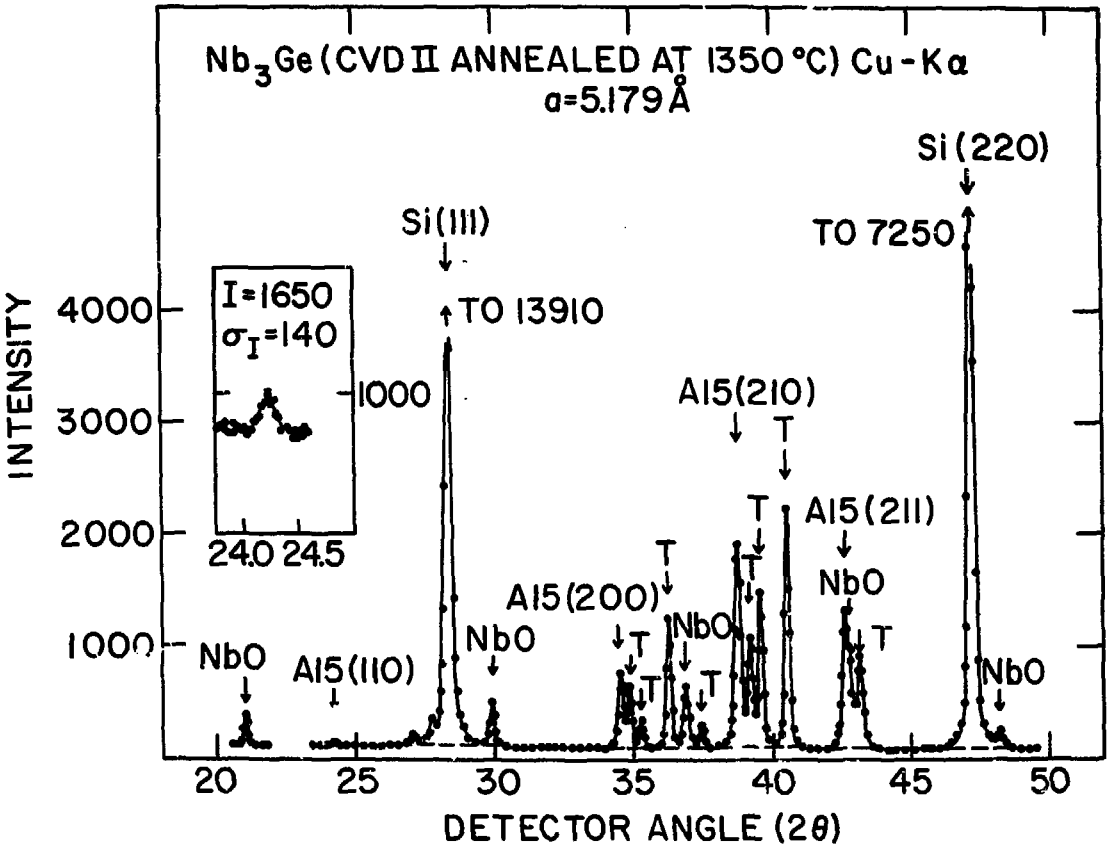
Nb3Ge (CVD II ANNEALED AT 1350 °C) Cu-Kα
a=5.179 Å
Si(220)
Si(111)
TO 7250
TO 13910
I=1650
σI=140
24.0 24.5
A15(210)
A15(211)
A15(200)
NbO
A15(110)
INTENSITY
4000
3000
2000
1000
1000
20
25
30
35
40
45
50
DETECTOR ANGLE (2θ)

Fig. 4b

from standard formulae, and hence the weight percentages of niobium and oxygen for each assumed value of y. By comparison with the chemical analysis figure, the Nb content of the A-15 phase was established as 83 $\pm$ 1 at.%. The oxygen content (1.75 wt.%) agrees quite well with the chemical analysis result of 1.57 wt.%.

Final values of the parameters for this material are given in Table III together with observed and calculated intensities. As indicated by the low R factor of 0.04, the overall fit is very good and each of the three phases is well characterized in spite of the large number of overlapping peaks. The positional parameters found for Nb_5Ge_3 are in excellent agreement with those reported in a recent single crystal study by Jagner and Rasmussen[38] (Nb(2): k-0.0760; Nb(2): y-0.2222; Ge(2): x-0.1654), and the occupation of the A-15 phase is zero within error limits of $\pm$0.8%.

A similar procedure was followed for the as-deposited material. In this case, it is necessary to make allowance for NbO_2 and hexagonal Nb_5Ge_3 as well. The two positional parameters of the latter were permitted to vary, while those of NbO_2 were fixed at the values determined in a recent neutron diffraction study[39]. Both phases were assumed to be stoichiometric. The positional parameters of tetragonal Nb_5Ge_3, and the Debye-Waller factors of hexagonal and tetrogonal Nb_5Ge_3, were fixed at the value given for the latter in Table III. A similar constraint

TABLE III

Least-squares parameters and intensities for Nb_3Ge(II), annealed at 1350°C. k is the percentage of Nb sites occupied by Ge, B the Debye-Waller factor. T denotes tetragonal Nb_5Ge_3.

Standard errors are given in parentheses and refer to the least significant digit.

$Nb_{0.83}Ge_{0.17}$ (a_0 = 5.179Å, T_c = 5.6°K)

k (%)	0.2 (8)
B (Å^2)	0.8 (3)

Tetragonal Nb_5Ge_3 (a = 10.165Å, c = 5.135Å)

Nb(2): k	0.0780 (5)
Nb(2): y	0.2217 (5)
Ge(2): x	0.1671 (6)
B(Å^2)	0.9 (2)

NbO (a = 4.210Å)

B (Å^2)	0.7 (3)

Phase	hkℓ	I_{calc}	I_{obs}	(σ)
NbO	100	15.6	15.2	(0.7)
A15	110	2.6	2.7	(0.2_5)
T	220	0.1	0.3	(0.3)
T	211	1.5	1.5	(0.4)
T	310	2.7	2.2	(1.0)
Si	111	1073.7	1062.7	(50.0)
NbO	110	29.7	28.8	(1.5)
A15	200	63.0	105.1	(1.5)
T	002	41.6		
T	400	17.8	17.9	(0.7)
T	321	92.6	94.2	(2.0)

TABLE III(Cont'd)

Phase	hkℓ	I_{calc}	I_{obs}	(σ)
NbO	111	47.1	50.8	(1.2)
T	112	2.4		
T	330	18.5	16.5	(0.8)
A15	210	213.6	195.4	(10.0)
T	202	90.3	90.3	(7.0)
T	420	110.6	115.5	(7.0)
T	411	193.8	192.7	(5.0)
A15	211	135.7	262.7	(10.0)
NbO	200	46.4		
T	222	74.2		
T	312	0.2	0.4	(0.7)
T	510	1.1	0.5	(0.7)
Si	220	666.9	703.0	(30.0)
T	431	0.8		
NbO	210	7.4		
A15	220	0.3	0.5	(0.7)
T	402	11.9	13.1	(1.0)
T	440	1.8		
T	521	21.3	19.9	(1.5)
T	332	7.6	15.3	(1.5)
T	530	7.3		
NbO	211	10.3	9.4	(0.7)
T	422	0.2	0.0	(0.5)
T	600	0.2	0.0	(0.5)
A15	310	0.5	369.7	(18.5)
Si	311	373.9		
T	620	13.3	11.8	(2.0)
T	213	0.1		

TABLE II[I](Cont'd)

Phase	hkℓ	I_{calc}	I_{obs}	(σ)
T	611	1.0	0.7	(0.5)
T	512	4.2	4.3	(0.5)
T	541	3.0	3.0	(0.5)
A15	222	19.1	42.7	(3.0)
NbO	220	27.3		
T	442	11.9	28.3	(3.0)
T	323	15.9		
T	631	15.1	19.0	(2.0)
A15	320	42.2	71.6	(4.0)
T	532	13.1		
T	710	11.5		
T	550	7.7		
NbO	300	0.7	60.0	(4.5)
NbO	221	2.8		
T	602	15.8		
T	640	0.0		
T	413	39.5		
A15	321	62.1	61.2	(4.6)
Si	400	93.1	86.4	(6.5)
T	622	4.2		
T	721	5.7	9.2	(2.0)
NbO	310	4.0	7.2	(1.0)
T	730	2.0		
T	433	0.2	0.6	(0.6)
A15	400	26.6	29.0	(2.9)
T	004	14.5	15.2	(2.0)
NbO	311	17.8	27.0	(2.7)
T	800	0.0		
T	523	6.2		
T	114	0.0		
T	651	1.5	1.4	(0.7)

TABLE III(Cont'd)

Phase	hkℓ	I_{calc}	I_{obs}	(σ)
Si	331	133.7		
T	712	9.0	154.6	(11.6)
T	552	6.5		
T	204	0.1		
T	642	25.0	45.0	(5.0)
T	820	12.6		
A15	330	0.1		
A15	411	0.2	4.8	(1.5)
T	811	4.5		
T	741	0.1		
NbO	222	8.6	8.3	(1.5)
T	224	0.0		
T	660	11.3		
T	613	0.4	11.0	(0.7)
T	314	0.3		
T	732	5.2	5.2	(0.6)
T	705	0.4		
NbO	320	1.5	1.2	(0.5)
A15	420	16.4		
T	543	1.2	34.3	(3.4)
T	831	15.6		
T	404	2.3	3.1	(1.0)
A15	421	36.5		
NbO	321	4.4		
T	840	0.6	63.9	(6.4)
T	633	6.2		
T	334	2.7		
T	802	9.7		
T	910	3.1		
T	424	18.4	30.4	(7.6)
T	822	0.0		
A15	332	14.1	206.1	(20.6)
Si	422	172.9		

R factor 0.039 Weighted R factor 0.049

was placed on the Debye-Waller factors of NbO_2 and NbO.

This fitting procedure together with the chemical analysis figure for Nb yielded a self-consistent result of 76 $\pm$ 1 at.% for Nb content of the A-15 phase. The oxygen content works out to be 1.97 wt.%, rather higher than the analysis figure. This is probably because there is no way to allow for the diffuse part (broken line in Fig. 4a, between 34 - 42 deg.) of the scattering in the x-ray phase analysis, which would lead to an underestimate of the absolute amounts of the three Nb - Ge phases, and a corresponding overestimate of the amounts of the oxide phases. Allowance was made for this by scaling the fractions of NbO_2 and NbO so as to agree with the oxygen analysis. However, the relative proportions found for the Nb - Ge phases should not be very much affected by the diffuse scattering. The final parameters are given in Table IV. Intensities have not been listed since there are over 150 reflections, but the overall agreement is quite satisfactory.

There is clearly a significant amount of disorder in the as-deposited material amounting to occupation of about 3% of the Nb sites by Ge (S_A = 0.87) and 14% of the Ge sites by Nb (S_B = 0.82). This may be contrasted to the annealed material in which there are essentially no Ge atoms on Nb sites and vice versa. The data of both as-deposited and annealed material are summarized in Table V.

Since there has been considerable interest in and speculation about other kinds of defects and their role in stabilizing

TABLE IV

Least-squares parameters for Nb_3Ge (II) as-deposited. Composition of A15 phase $Nb_{0.76}$ $Ge_{0.24}$ (a_0 = 5.142Å, T_c = 19.4°K). k is the percentage of Nb sites occupied by Ge, B the Debye-Waller factor.

k (%)	3.2 (8)
B ($Å^2$)	0.8 (3)

R factor = 0.066 Weighted R factor = 0.089

TABLE V

Phase Distribution (in wt%) for Nb_3Ge(II)
Prepared by Chemical Vapor Deposition

	As-depostied at 900°C	Annealed at 1350°C for 48 hours
A-15	54	32
T-Nb_5Ge	35	56
H-Nb_5Ge_3	2	not detected
NbO	3.5	12
NbO_2	5.5	not detected
Atomic % Nb in A-15 phase	76±1	83±1
Lattice parameter of A-15 phase	5.142Å	5.179Å
T_c	19.4k	5.6k

high T_c A-15 phases,[24,32-34] the intensity data for the as-deposited material were also refined on the basis of a vacancy model of the type $Nb_{3-x}\,\square_x\,Ge_{1-x-y}\,Nb_{x+y}$ in which the Nb site defects were assumed to be vacancies rather than Ge atoms. Since it is essentially the ratio of the average scattering factors on the two sites which is determined, a virtually identical fit should be possible. This indeed is the case, and the corresponding occupation factor for vacancies at the composition $Nb_{0.76}\,Ge_{0.24}$ is $3.7 \pm 0.4\%$. The large number of vacancies, necessary to amount for these changes in intensities, should be easily detected by density measurements. However, no indication of vacancies were observed where measurements have been done[17,40,44] certainly not at the level of a few percent.

For the irradiation experiments the yield from one CVD run (about 1.5g) was sufficient and this sample was designated Nb_3Ge(I). The effect of the high energy neutron irradiation on T_c of Nb_3Ge(I) is shown in Fig. 5. We see that T_c is severely degraded with increasing fluence. The as-deposited T_{c3} value of 20.2K is depressed to 4.2K for a fluence of 2.6×10^{19} n/cm^2, and further increase in fluence only depress T_c to 3.4K at $5 \times 10^{19} n/cm^2$ where T_c appears to reach a saturation region. There is an increase in the superconducting transition width when T_c begins to decrease but at high fluences, where T_c saturates, the widths are narrow, even narrower then the unirradiated material.

Figure 5

Effect of high-energy neutron irradiation (E>1 MeV) on the superconducting transition temperature T_c of Nb_3Ge (I) and Nb_3Ge (III), this latter used for the long range order measurements. Also included is the T_c of Nb_3Ge (IV) as-deposited.

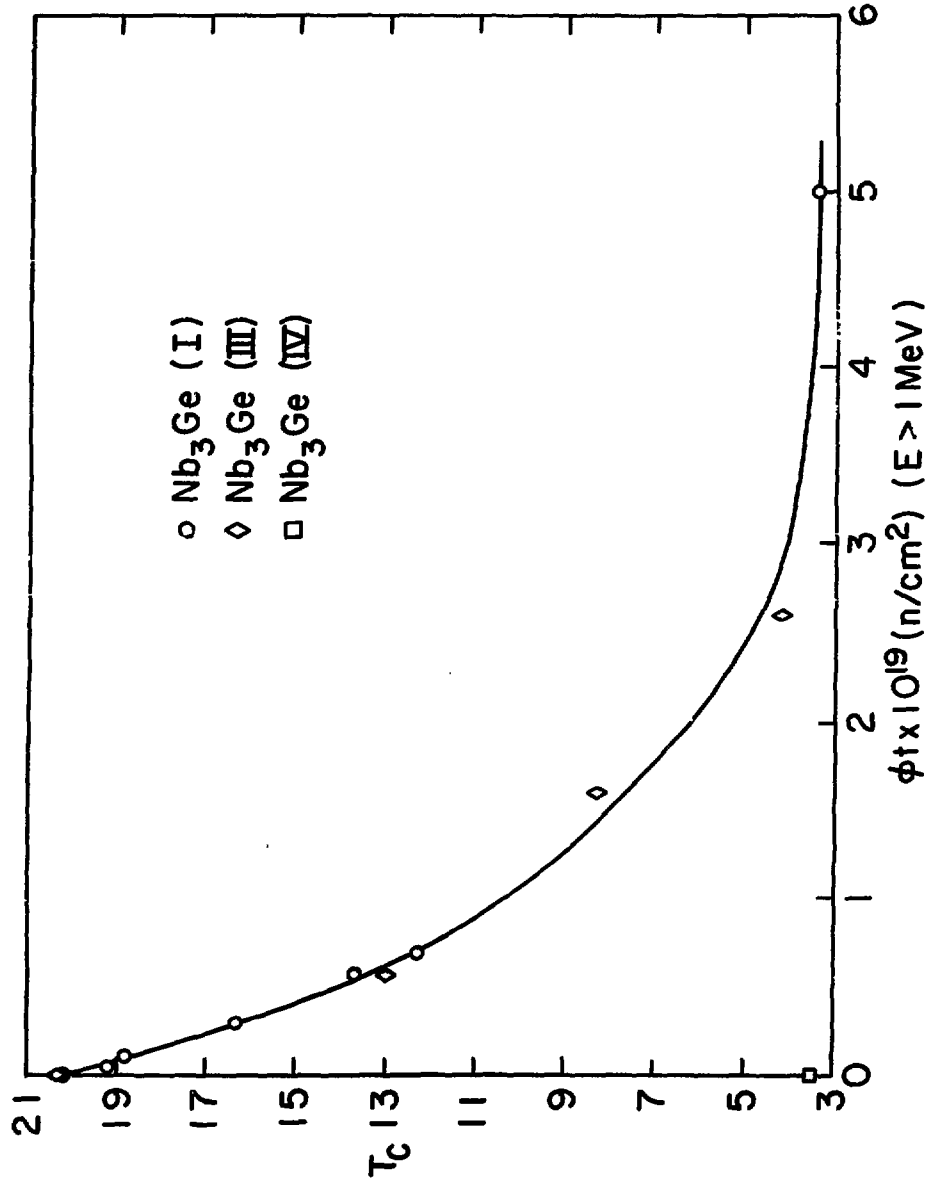
o Nb_3Ge (I)
◇ Nb_3Ge (III)
□ Nb_3Ge (IV)
T_c
21
19
17
15
13
11
9
7
5
3
0
1
2
3
4
5
6
$\phi t \times 10^{19}$ (n/cm^2) (E > 1 MeV)

Fig. 5

The lattice parameter of the A-15 phase as a function of Tc for the same irradiation doses of Fig. 5 is shown in Fig. 6 and the data is summarized in Table VI. We see a rather large increase in a_o as a function of neutron fluence similar to that observed as a function of annealing temperature (Fig. 3). The value of a_o was initially 5.143Å and increased to 5.161Å after exposure to a fluence of 2.6×10^{19} $n/_{cm}2$, at this point T_c begins to saturate but the lattice continues to expand.

Apart from this lattice expansion the Debye-Scherrer patterns remained unchanged[45] up to a fluence of 2.6×10^{19} $n/_{cm}2$. There was, however, in the most heavily irradiated sample ($5 \times 10^{19} n/_{cm}2$), some line broadening in the high angle region and a clear decrease in intensity of these lines compared to the low angle region. This sample also presents a rather large lattice expansion, 5.19 ± 0.01Å. The large error in the lattice parameter is because only the three first strongest lines (200, 210 and 211) could be used in the lattice determination.

The long range order measurements in neutron irradiated samples was performed with about 2g., designed as Nb_3Ge(III). This as-deposited sample had an a_o of 5.1415Å and a T_c of 20.3K before irradiation. Part of the diffractometer scan of the unirradiated material is shown in Fig. 7, and refinement showed that the material contained about 10 wt.% of tetragonal and 8 wt.% of hexagonal Nb_5Ge_3 respectively, and a trace of NbO

Figure 6

Superconducting transition temperature T_c vs. lattice parameter a_o of the A-15 phase for neutron irradiated Nb_3Ge (I) and Nb_3Ge (III), this latter used for the long range order measurements. Also included is Nb_3Ge (IV) as-deposited.

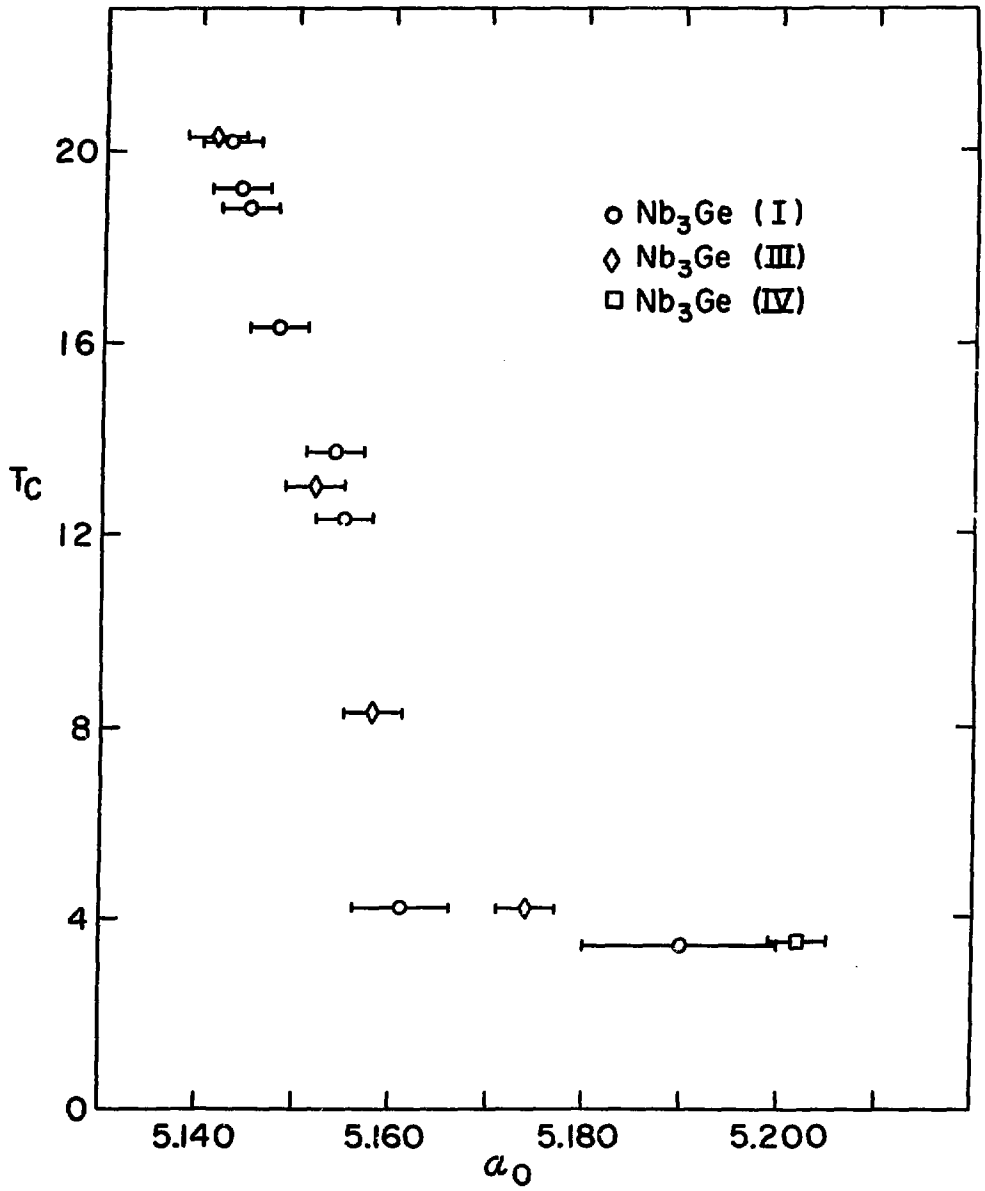
20
16
12
8
4
0
T_C
5.140
5.160
5.180
5.200
a_0
o Nb_3Ge (I)
◊ Nb_3Ge (III)
□ Nb_3Ge (IV)

Fig. 6

TABLE V I

Nb_3Ge(I) Neutron Irradiated

Transition Temperature T_{c3}(K)	Transition Widths ΔTc	Fluence $\phi t(n/cm^2)$	Lattice Parameter a_o(Å)
20.2	0.9	0	5.143 ± 0.003
19.2	1.8	5.0×10^{17}	5.144 ± 0.003
18.8	1.0	1.1×10^{18}	5.145 ± 0.003
16.3	1.5	3.0×10^{18}	5.148 ± 0.003
13.7	1.0	5.8×10^{18}	5.154 ± 0.003
12.3	1.3	7.0×10^{18}	5.155 ± 0.003
4.2	0.2	2.6×10^{19}	5.161 ± 0.005
3.4	0.6	5.0×10^{19}	5.19 ± 0.01

Figure 7

X-ray data for Nb_3Ge (III). The insert shows the (110) peak of the A-15 phase in greater detail.

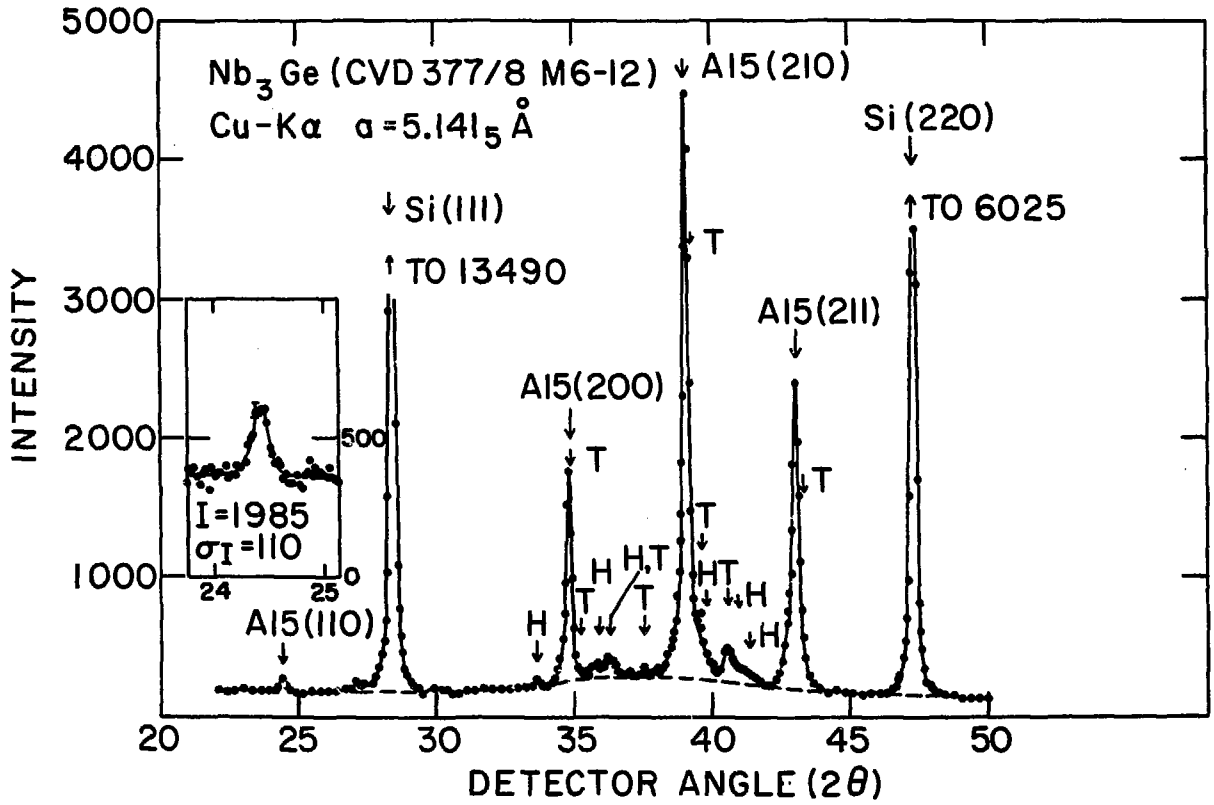
Nb3Ge (CVD 377/8 M6-12)
Cu-Kα a=5.141₅ Å
A15(210)
Si(220)
Si(111)
TO 13490
TO 6025
A15(211)
A15(200)
A15(110)
I=1985
σI=110
INTENSITY
DETECTOR ANGLE (2θ)
5000
4000
3000
2000
1000
500
0
20
25
30
35
40
45
50
24
25
T
H
H,T
HT

Fig. 7

(from chemical analysis, ~0.4 wt.%). In view of the close similarity of the values of a_o and T_c with those of Nb_3Ge(II), a Nb content of 76 ± 1 at % was assumed. Except for the two positional parameters of hexagonal Nb_5Ge_3, the other parameters and Debye-Waller factors of the impurity phases were fixed at the values listed in Table III. Final parameter values are listed in Table VII, together with observed and calculated intensities. A Nb site occupation factor of about 4% (S_A = 0.84) was obtained, (this would be about 5% if the stoichiometric composition were assumed), quite consistent with the value obtained for Nb_3Ge(II).

The long range order parameter of the irradiated material, Nb_3Ge(III), was measured at fluences of 5.8 x 10^{18}n/cm^2, 1.6 x 10^{19}n/cm^2 and 2.5 x 10^{19}n/cm^2, where T_c's of 13.0 K, 8.3 K and 4.2 K (Fig. 5) and a_o's of 5.152Å, 5.158Å and 5.174Å (Fig. 6), respectively, were obtained. Each measurement was done using approximately 50 mg. of powdered (≥-400 mesh) Nb_3Ge(III) mixed with Si and packed in the Al sample-holder covered with a thin (0.025 mm) Be foil. This latter was used to avoid eventual contamination from the radioactive powder and because Be has a low absorption coefficient and no peak overlap with the A-15 phase of Nb_3Ge. The background γ-radiation of these irradiated materials was reduced by shielding the diffractometer counter and using a monochromator. The refinement procedures were the same applied to the unirradiated material described previously (see also Table VII). Part of the diffractometer scan for the most

TABLE VII

Least-squares parameters and intensities for Nb_3Ge(III) k is the percentage of Nb sites occupied by Ge, B the Debye-Waller factor. T and H denote tetragonal and hexagonal Nb_5Ge_3 respectively.

$Nb_{0.76}Ge_{0.24}$ ($a = 5.141_5$Å, $T_c = 20.3^{\circ}K$)

k (%)	4.0 (6)
B (Å^2)	0.7 (2)

Hexagonal Nb_5Ge_3 ($a = 7.65$Å, $c = 5.33$Å)

Nb (2): x	0.256 (8)
Ge: x	0.619 (7)

Phase	hkℓ	I_{calc}	I_{obs}	(σ)
A15	110	4.9	4.9_3	(0.3_5)
H	200	1.5	1.4	(0.5)
Si	111	481.8	498.6	(25.0)
NbO	110	1.7	1.9	(0.6)
H	002	2.4	2.8	(1.0)
A15	200	79.1		
T	002	3.6	85.0	(5.0)
T	400	1.6		
H	210	4.3	6.6	(2.0)
H	102	2.7		
T	321	8.1	13.3	(3.0)
NbO	111	2.7		
T	112	0.2	2.8	(1.0)
T	330	1.6	2.9	(1.0)

TABLE VII(Cont'd)

Phase	hkℓ	I_{calc}	I_{obs}	(σ)
A15	320	55.5		
H	410	0.8		
H	213	2.7		
H	402	1.7		
T	631	1.3	70.6	(7.1)
T	532	1.1		
T	710	1.0		
T	550	0.7		
T	602	1.4		
T	640	0.0		
T	413	3.4		
A15	321	78.8	75.4	(7.5)
Si	400	43.6		
T	622	0.4	43.5	(6.5)
T	721	0.5		
A15	400	34.5		
T	004	1.3	36.6	(3.7)
H	313	0.4		
Si	331	63.1		
T	712	0.8		
T	552	0.6		
T	204	0.0	68.7	(5.0)
T	642	2.2		
T	820	1.1		
H	331	0.5		
H	420	0.9		
A15	411	0.4		
A15	330	0.2	0.4	(0.6)
T	224	0.0		
A15	420	21.0		
H	511	1.3		
H	323	0.8		
H	332	0.3	26.6	(4.0)
H	304	1.8		
T	831	1.4		
T	404	0.2		
T	802	0.8		

TABLE VII(Cont'd)

Phase	hkℓ	I_{calc}	I_{obs}	(σ)
A15	421	48.9		
T	840	0.1		
T	633	0.3	58.6	(7.5)
T	334	0.2		
T	910	0.3		
T	424	1.6		
Si	422	83.0	90.8	(9.1)
T	822	0.0		
A15	332	18.1	18.5	(3.0)
A15	422	0.3		
Si	511	34.4		
Si	333	11.5	46.1	(4.6)
H	521	0.7		
T	842	0.7		

R factor 0.043 Weighted R factor 0.068

heavily irradiated (2.5×10^{19} n/cm^2) and the unirradiated Nb_3Ge(III) are shown in Fig. 8. From this figure we can see that the neutron irradiated pattern has the A-15 peaks shifted to lower angle with no line broadening (see right insets of Fig. 8) while no lattice expansion were observed for the other phases present. Although quite weak, the difference (110) peak (left insets of Fig. 8) that was not visible in the x-ray films can be clearly observed even in this significantly disordered material. The final parameters for all the irradiations are summarized in Table VIII and Fig. 9 gives how T_c varies with the amount of disorder, where we can see that T_c approach a saturation before the order parameter goes to zero.

A diffractometer scan was also taken for the most heavily irradiated material of Nb_3Ge(I) (5×10^{19} n/cm^2) and part of this scan is shown in Fig. 10 together with the Nb_3Ge(I) unirradiated. A large lattice expansion can be observed from the A-15 peaks and now an expansion of the tetragonal Nb_5Ge_3 lattice parameters is also observed (a = 10.20±0.01Å, c = 5.16±0.005Å).[46] From the inset of Fig. 10 we can see that the difference (110) peak is already covered by the background statistics. The high angle peaks are broad and weak as observed from the x-ray films and a value for the order parameter could not be obtained since no difference peak was resolved, T_c at this fluence was (3.4 K) essentially saturated.

Another chemical vapor deposited material, designed Nb_3Ge(IV), was with an unusually high a_o of 5.202Å (Fig. 6)

Figure 8

X-ray data for Nb_3Ge (III) irradiated ($2.5 \times 10^{19} n/cm^2$) and unirradiated. The right insets show (400) reflection with no line broadening. The decrease in the (110) peaks is clearly visible (left insets).

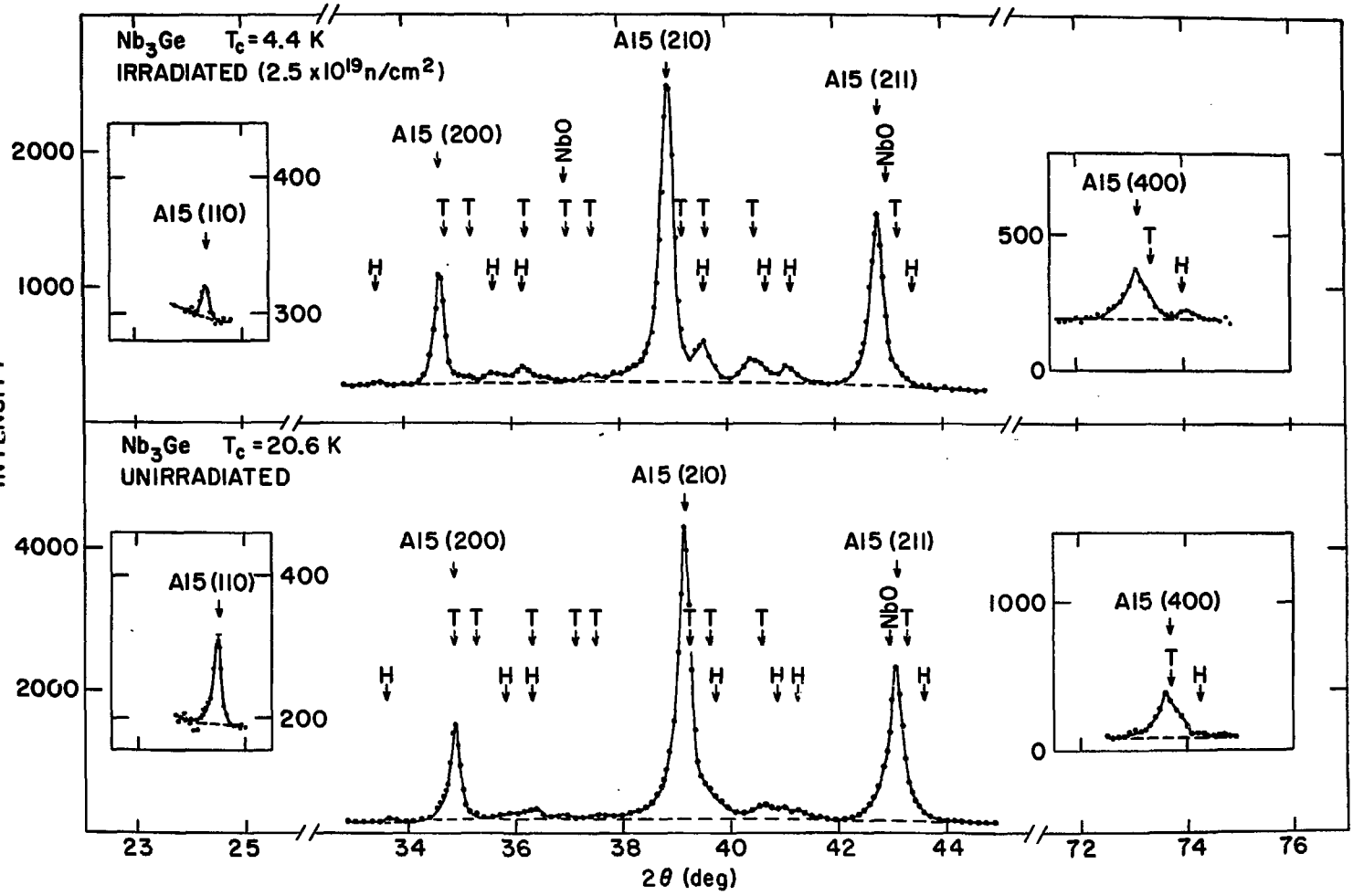
Nb3Ge Tc = 4.4 K
IRRADIATED (2.5 x10^19 n/cm^2)
A15 (210)
A15 (211)
A15 (200)
NbO
NbO
A15 (110)
A15 (400)
2000
1000
400
300
500
0
Nb3Ge Tc = 20.6 K
UNIRRADIATED
A15 (210)
A15 (200)
A15 (211)
NbO
A15 (110)
A15 (400)
4000
2000
400
200
1000
0
T
H
INTENSITY
23
25
34
36
38
40
42
44
72
74
76
2θ (deg)

Fig. 8

TABLE VIII

Nb_3Ge(III) Neutron Irradiated

LRO Measurements

ϕt(n/cm^2)	T_{c3}(K)	ΔT_c(K)	a_o(Å)	k(%)[a]	S_A	S_B	B(Å^2)	X[b]
0	20.3	1.63	5.1415 ±0.002	4.0	0.84	0.79	0.7	0.12
5.8×10^{18}	13.0	2.05	5.152 ±0.003	6.0	0.75	0.71	0.7	0.18
1.6×10^{19}	8.3	1.29	5.158 ±0.003	8.2	0.66	0.62	0.2	0.25
2.5×10^{19}	4.2	0.34	5.174 ±0.003	12.9	0.46	0.44	1.1	0.39

(a) - k(%) = percentage of Nb sites occuppied by Ge($\frac{100x}{3}$ = k(%)).

(b) - X from $(Nb_{3-x}Ge_x)$ $[Ge_{1-x-y}Nb_{x+y}]$, is a measure of the order parameter.

Figure 9

Superconducting transition temperature T_c, as a function of the amount of disorder for Nb_3Ge (III) neutron irradiated.

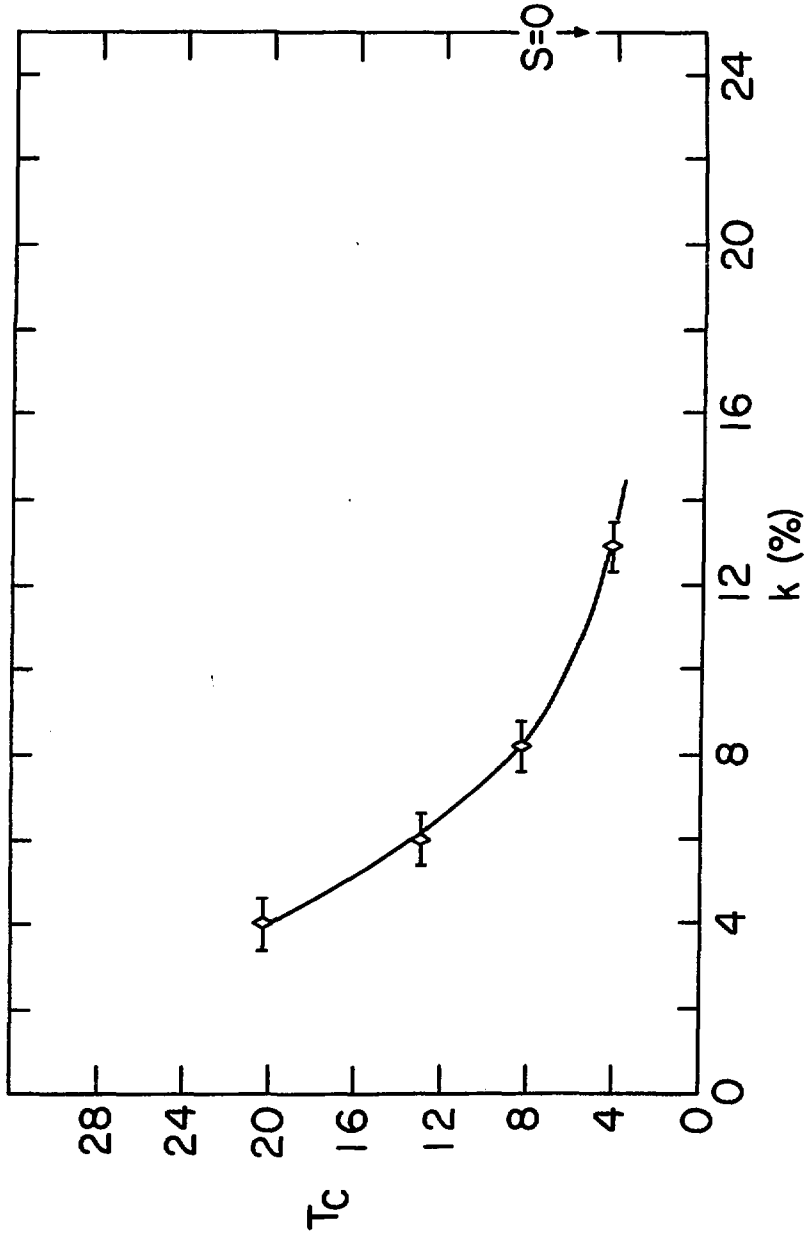

Fig. 9

Figure 10

X-ray data for Nb_3Ge (I) unirradiated and irradiated ($5x10^{19}n/cm^2$). The inserts show the (110) peak - (unirradiated) and arrow indicate where this peak - should be for the most heavily irradiated material.

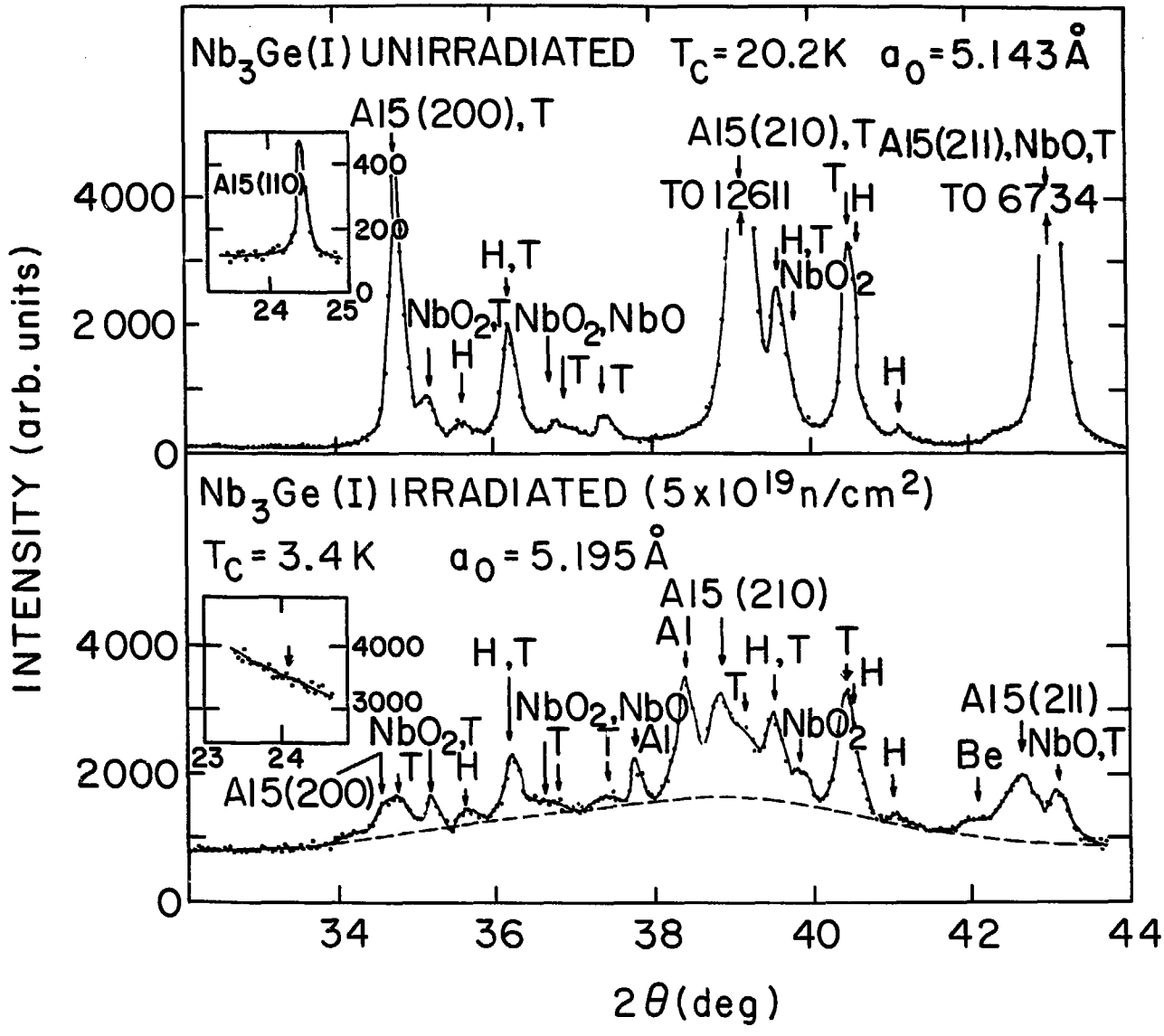
Nb3Ge(I) UNIRRADIATED Tc=20.2K a0=5.143Å
A15(200),T
A15(110)
A15(210),T
A15(211),NbO,T
TO 12611
TO 6734
H,T
NbO2,T
NbO2,NbO
NbO2
H
T
Nb3Ge(I) IRRADIATED (5x10^19 n/cm^2)
Tc=3.4 K
a0=5.195Å
A15(210)
Al
A15(200)
A15(211)
Be
NbO,T
INTENSITY (arb. units)
2θ(deg)

Fig. 10

and low T_c of 3.5 K (ΔT_c = 0.4 K)(Fig. 5). It is interesting to note that these parameters are very similar to those of Nb_3Ge irradiated until the saturation region, only obtained by a different process. The diffraction pattern showed that this material was contaminated with about 3 wt.% of tetragonal Nb_5Ge_3. One small additional peak was observed with a d-spacing of 2.40Å and an intensity 2 - 3% of that of the strongest A-15 peak. This could conceivably arise from a sub-oxide of Nb with approximate composition Nb_6O[47] although no other peak characteristic of this phase could be seen. Refinement of the A-15 intensities corrected for tetragonal Nb_5Ge_3 yielded a set of occupation factors as a function of composition which are listed in Table IX. Although there was not enough sample for chemical analysis, the high a_o and low T_c strongly suggest that the Nb content is significantly higher than 83 at.%, and the results summarized in Table IX are therefore indicative of little or no occupancy of Nb sites by Ge.

In contrast to the depressions in T_c due to annealing described previously (Fig. 3), the T_c's for the neutron irradiated samples were recoverable to close to the unirradiated value by annealing. Fig. 11 shows the results for isochronal annealing of Nb_3Ge(I) which has been irradiated to three different fluences 7×10^{18}, 2.6×10^{19} and 5×10^{19} n/cm^2 and for which T_c of the unirradiated material (T_c = 20.2 K) had been depressed to 12.3 K, 4.2 K and 3.4 K respectively. The data presented are for successive anneals on the same sample for periods

TABLE IX

Least-squares parameters for Nb_3Ge(IV)(a_o = 5.202Å, T_c = 3.5°K). k is the percentage of Nb sites occupied by Ge, B the Debye-Waller factor.

	Assumed composition (at % Nb)		
	84	86	88
k (%)	4.3 (4)	2.2 (4)	0.2 (4)
B ($Å^2$)	0.6 (1)	0.6 (1)	0.6 (1)

R factor = 0.019 Weighted R factor = 0.036

Figure 11

Isochronal annealing curve of Nb_3Ge (I) irradiated to three different fluences.

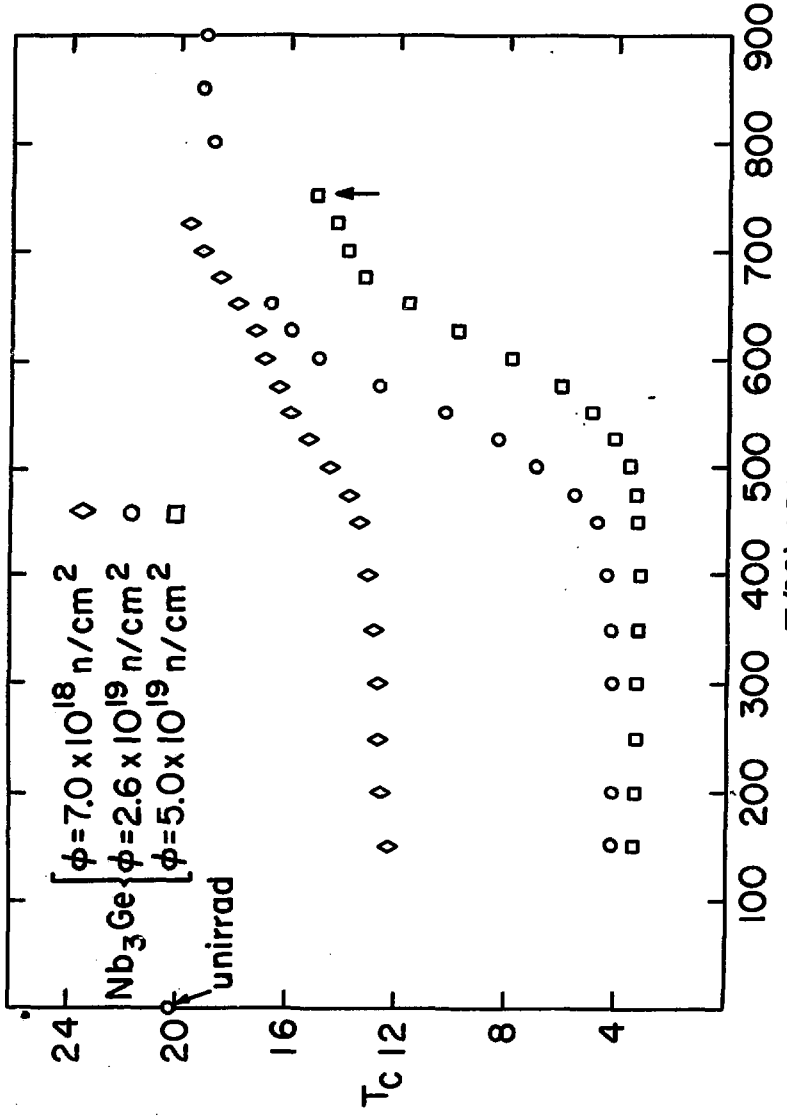
Nb_3Ge
$\phi=7.0\times10^{18}$ n/cm^2
$\phi=2.6\times10^{19}$ n/cm^2
$\phi=5.0\times10^{19}$ n/cm^2
unirrad
T_c
T(°C)/2hrs
24
20
16
12
8
4
100
200
300
400
500
600
700
800
900

Fig. 11

of two hours at the temperature indicated. Very little recovery of T_c is seen in the temperature range 200°C to 400°C. Above 400°C recovery progress and the rate of recovery is less for the lower fluences. The final values of T_c at 750°C also depends on the amount of damage, being lower for the highest fluence.[48]

The results of isothermal annealing of Nb_3Ge(I) are shown in Fig. 12. These data were obtained from a single sample irradiated at a fluence of $2.6 \times 10^{19} n/cm^2$. The annealing temperature was chosen as 550°C, which is approximately the temperature at which the maximum rate of increase in T_c occurred in the isochronal anneals for this fluence. At this temperature the recovery of T_c as a function of time is gradual, reaching about 60% of its unirradiated value after 6 hours and 80% after 4 days.

A diffractometer scan was also taken for the Nb_3Ge(I) sample irradiated to $5 \times 10^{19} n/cm^2$ (see Fig.10) and isochronally annealed until 750°C (point indicated by an arrow in Fig. 11) and part of this scan is shown in Fig. 13. This sample has T_c of 15.0K (ΔT_c = 1.7K) and a_o of 5.148 ± 0.002Å. An increase in the amount of tetragonal Nb_5Ge_3 and NbO and a decrease of NbO_2 were also observed. This latter behavior is very similar to that observed in the annealing study of Nb_3Ge(II), and with these changes in the amount of second phases the stoichiometry of the A-15 phase is changed by 1.5 at.% (76 → 77.5 at.% Nb). The final parameters for these two compositions are given in Table X. From these results we can see that not only the lattice parameter but also

Figure 12

Isothermal annealing of Nb_3Ge (I) irradiated to a fluence of $2.6 \times 10^{19} n/cm^2$. Annealing temperature was $550^{\circ}C$ and each point represents successive anneals on the same sample for time indicated. Error bars represents transition widths ΔT_c.

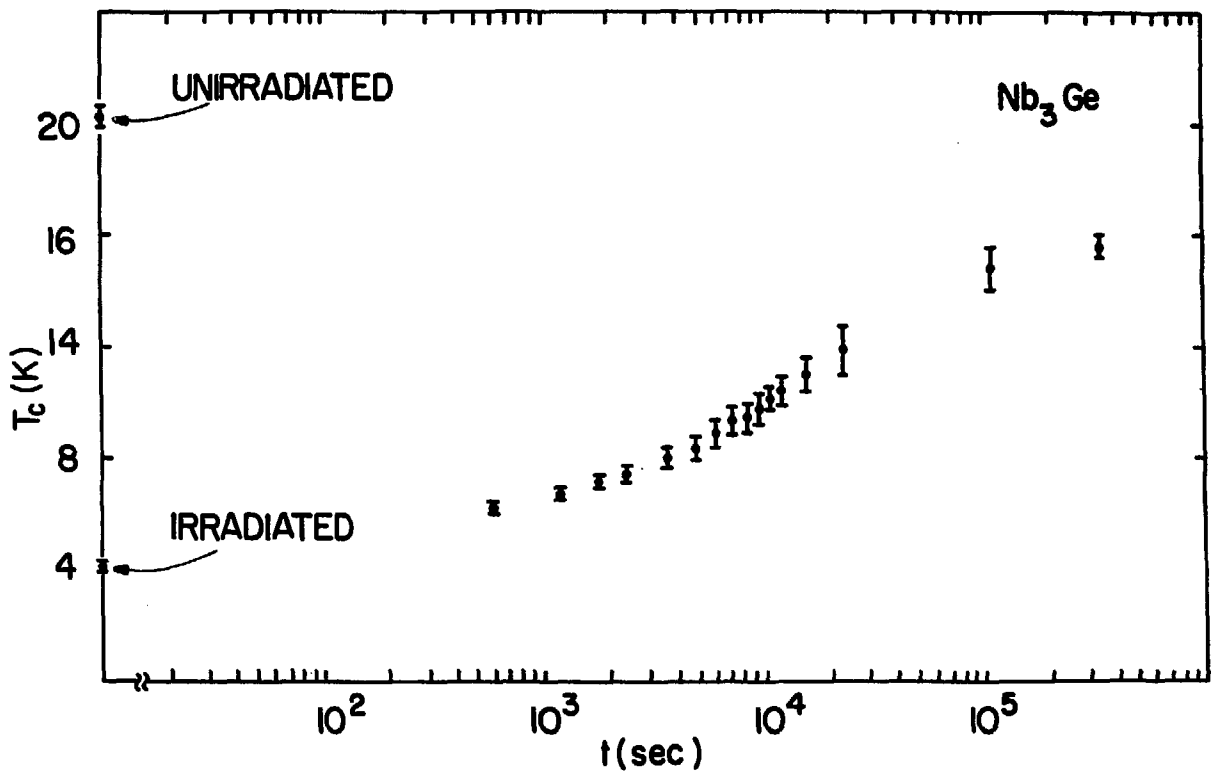
UNIRRADIATED
IRRADIATED
Nb_3Ge
20
16
14
8
4
T_c (K)
10^2
10^3
10^4
10^5
t(sec)

Fig. 12

Figure 13

X-ray data for Nb_3Ge (I) irradiated to $5x10^{19}n/cm^2$ and isochronally anneled until 750^oC (point indicated by an arrow in Fig. 11).

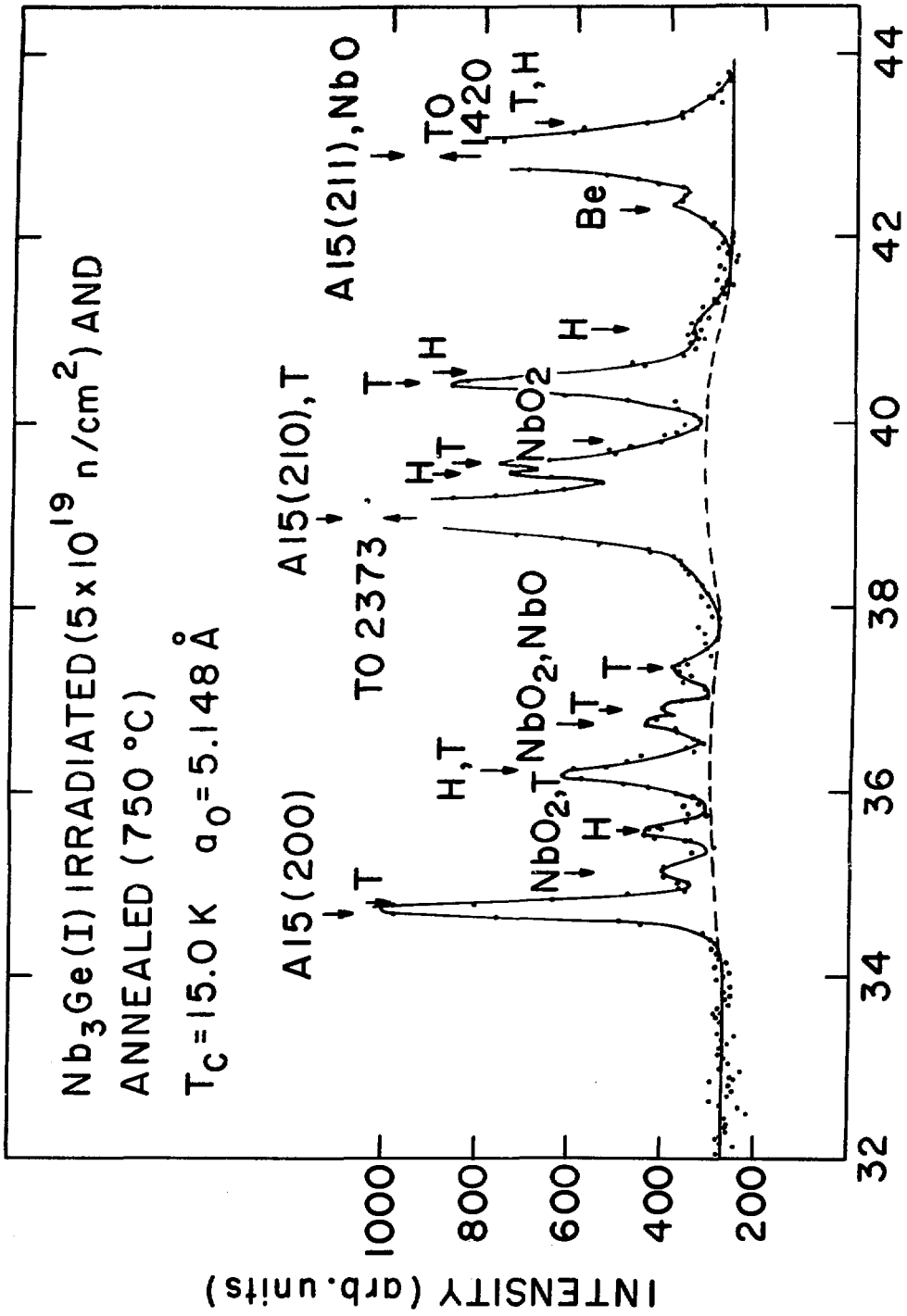
Nb_3Ge(I) IRRADIATED (5×10^{19} n/cm^2) AND
ANNEALED (750 °C)
T_c=15.0 K a_o=5.148 Å
A15(200)
T
NbO_2,T
H
H,T
NbO_2,T
NbO_2,NbO
T
T
A15(210),T
TO 2373
H,T
T
H
NbO_2
H
A15(211),NbO
TO 1420
T,H
Be
INTENSITY (arb. units)
2θ (deg)
1000
800
600
400
200
32
34
36
38
40
42
44

Fig. 13

TABLE X

Nb_3Ge(I) irradiated ($\phi t = 5 \times 10^{19} n/cm^2$) and isochronally annealed until 750°C ($T_c = 15.0K$, $a_o = 5.148 \pm 0.002Å$)

	76 at.% Nb	77.5 at.% Nb
X	0.09 (2)	0.04 (2)
S_A	0.88 (4)	0.94 (4)
S_B	0.83 (4)	0.82 (4)
$B(A^2)$	0.4 (3)	0.4 (3)

Nb_3Ge(I) unirradiated ($T_c = 20.2K$, $a_o = 5.143 \pm 0.003Å$)

	76 at.%Nb
X	0.06 (2)
S_A	0.92 (3)
S_B	0.87 (3)
$B(Å^2)$	0.3 (2)

the long range order parameter is recovered with the recovery of T_c.

Nb - Al: The A-15 phase in the Nb - Al system was first described by Wood et al.[49] and Corenzwit[50] found it to be superconducting at 18 K. Since then, several studies[17,51-60] have concerned themselves with the T_c dependence on stoichiometry. However, some conflicting results remain particularly with respect to the width of the homogeneity range of the A-15 phase at high temperatures. From the different homogeneity ranges proposed in the literature[40,61-63] the two currently accepted are those proposed by Lundin and Yamamoto[40] and Sveshnikov et al.[63] The niobium-rich side of these two phase diagrams are shown in Fig. 14(full lines, Ref. 63 and dashed lines, Ref. 40 . According to Lundin and Yamamoto[40] the A-15 phase forms peritectically at 1960°C with a composition $Nb_{75}Al_{25}$ from niobium solid solution (23.0 at.% Al) and the liquid (32.0 at.% Al). The homogeneity range of the A-15 phase extends to both sides of its stoichiometric composition. The maximum solubility for this phase is 32.0 at.% Al at 1870°C on the aluminum-rich side and 17.5 at.% Al at about 1000°C on the niobium-rich side. Sveshnikov et al.[63] report that the A-15 phase forms by a peritectoid reaction (α + σ) at 1730°C at a composition Nb_{74} Al_{26}. Here the homogeneity range is only half that of Lundin and Yamamoto ranging from 26 at.% Al at 1730°C to 19 at.% Al at 1000°C. As these two homogeneity ranges are so different

Figure 14

Niobium-rich side of the Nb-Al phase diagram (full lines, ref. 63 and dashed lines, ref. 40). Some of our results are also represented.

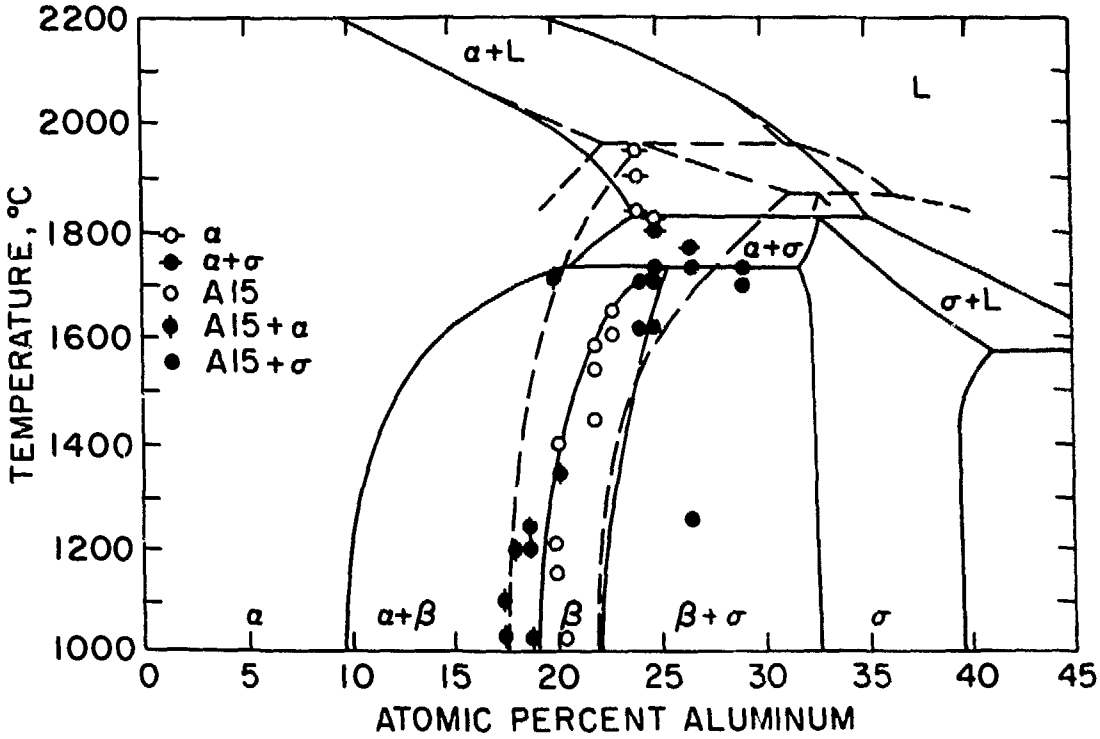
2200
2000
1800
1600
1400
1200
1000
TEMPERATURE, °C
α+L
L
α+σ
σ+L
α
α+β
β
β+σ
σ
α
α+σ
A15
A15+α
A15+σ
0
5
10
15
20
25
30
35
40
45
ATOMIC PERCENT ALUMINUM

Fig. 14

it is difficult to do any further studies in this system before doing a careful analysis of the equilibrium phase diagram in this region with well characterized samples. An attempt to accomplish this is the first part of this study.

Between 17.4 at.% Al and 29.4 at% Al, thirteen samples with different compositions were prepared and submitted to a series of heat treatments (sample preparation, heat treatment and cooling techniques are described in Chapter II). The homogeneity and the phases present in the samples were identified from x-ray films, diffractometer scans, microprobe and metallographic analyses. Some of the results are represented in Fig. 14. A strong dependence on heat treatment with composition was observed. Annealing a sample with a composition close to stoichiometry above 1800°C for 3 to 5 minutes followed by a rapid quench resulted in a single phase niobium solid solution. Heat treating this sample between 1800°C and 1730°C for 5 minutes followed by a rapid quench resulted in a niobium solid solution plus sigma phase (Nb_2 Al). The same results were observed for a sample with 27 at.% Al. The weight loss analysis indicate that the small losses observed can not account for the large change in composition necessary to explain these results. We also want to point out here that the same samples annealed at these temperatures but cooled by radiation show A-15 plus sigma phase with a trace or no niobium solid solution. These results can be clearly understood in terms of the equilibrium diagram proposed by Sveshnikov et al.[63] but

they are in disagreement with Lundin and Yamamoto where all these samples should have been single phase A-15.

Long-term anneals at medium temperatures (1730°C - 1000°C) in off-stoichiometry Nb-rich samples showed A-15 or A-15 plus niobium solid solution (Figs. 15-18) while close to stoichiometry and Al-rich samples all show A-15 plus sigma (Figs. 19-22). Direct cooling from the melt resulted in single phase A-15 material only for a composition of 21.9 at.% Al. By appropriate heat treatment single phase samples at 20.2, 23, and 23.2 at.% Al were also prepared. It can be seen from the micrographs of Figs. 19-22 that the amount of sigma phase begins to increase with increasing Al contend after 24.5 at.% Al. This latter sample contains about 6% of sigma phase resulting in a corrected composition of 24.1 at.% Al. A great attempt was done to anneal this sample and others close to stoichiometry (25.3 and 25.4 at.% Al) in the region between 1700°C and 1730°C where Sveshnikov et al.[63] found a single A-15 phase. No success was obtained as the sigma phase was observed to precipitate. This might be due to the possibility that the stoichiometric composition is metastable at low temperatures and the rapid quench technique used here is not fast enough to prevent precipitations or the stoichiometric composition does not exist at all in the equilibrium phase diagram of the Nb - Al system. According to these results the homogeneity range of the A-15 phase extends from 20 at.% Al at 1030°C to about 24 at.% Al at 1730°C and is in much

Figure 15

$Nb_{81.3}Al_{18.7}$; annealed 8 days 1030°C + 1 week 750°C, anodized (dilute citric acid, 5 sec.) + etched (HF 10%, 15 sec.), matrix - Nb_{ss} (blue); A-15 (pink), 400X.

Figure 16

$Nb_{79.8}Al_{20.2}$; annealed 42 hs. 1350°C + 1 week 750°C, anodized (dilute citric acid, 5 sec.) + etched (HF 10%, 15 sec.); A-15, 400X.

Fig. 15

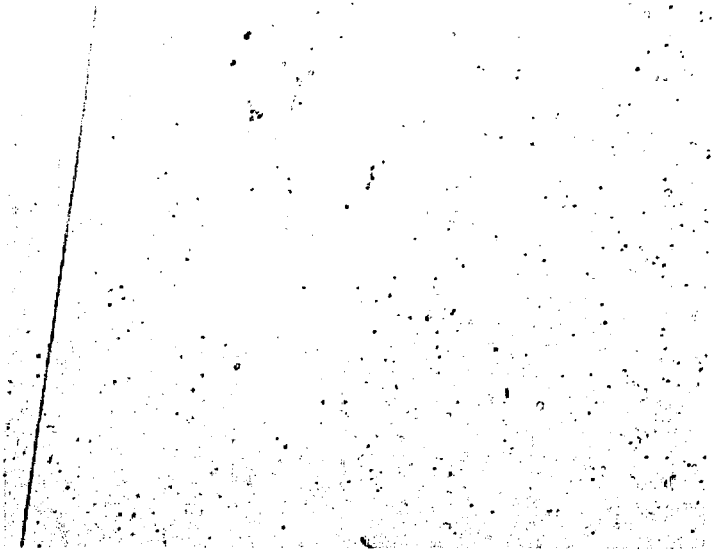

Fig.16

Figure 17

$Nb_{78.1}Al_{21.9}$; annealed 17 hs. 1550°C + 1 week 750°C, etched ($Cr\ O_3$ + HF, 10 min.); A-15, 400X.

Figure 18

$Nb_{77}Al_{23}$; annealed 12 hs. 1650°C + 203 hs. 750°C, etched ($Cr\ O_3$ + HF, 10 min.); A-15, 400X.

Fig. 17

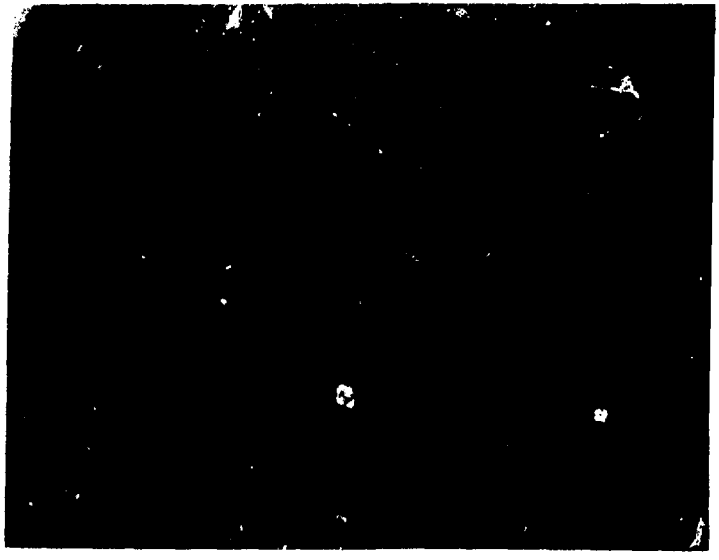

Fig. 18

Figure 19

$Nb_{75.5}Al_{24.5}$; annealed 10 hs. 1700°C + 1 week 750°C, anodized (dilute citric acid, 15 sec.), matrix A-15(light blue), σ (pink), 400X.

Figure 20

$Nb_{74.7}Al_{25.3}$; annealed 10 hs. 1730°C + 1 week 750°C, anodized (dilute citric acid, 4 sec.), matrix A-15 (light blue), σ (pink), 400X.

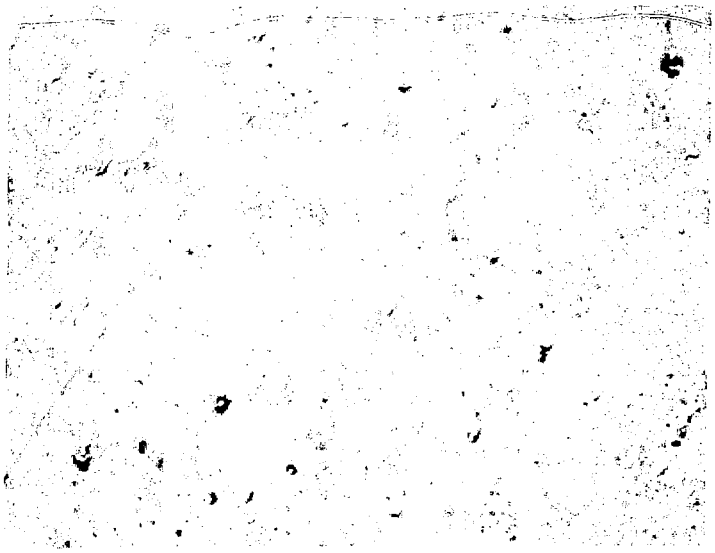

Fig. 19

Fig. 20

Figure 21

$Nb_{73}Al_{27}$; annealed 10 hs. 1730°C + 1 week 750°C, anodized (dilute citric acid, 5 sec.), matrix A-15 (light blue), σ (pink), 400X.

Figure 22

$Nb_{70.6}Al_{29.4}$; annealed 10 hs. 1730°C + 1 week 750°C, anodized (dilute citric acid, 5 sec.), matrix A-15(light blue), σ (pink), 400X.

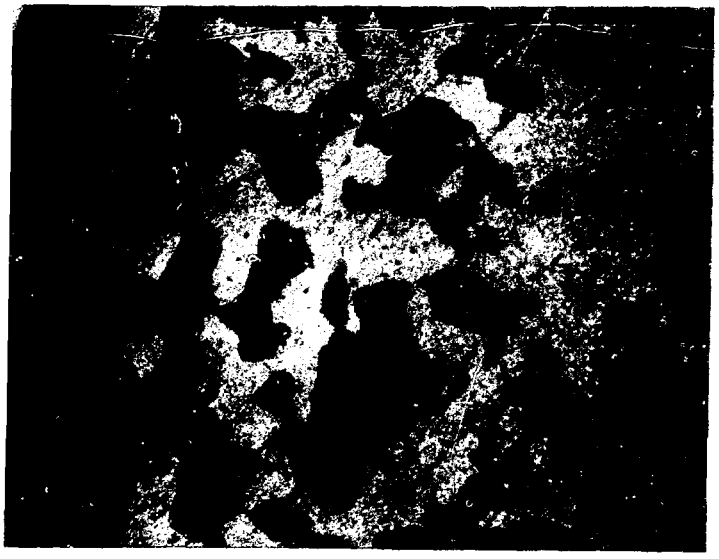

Fig. 21

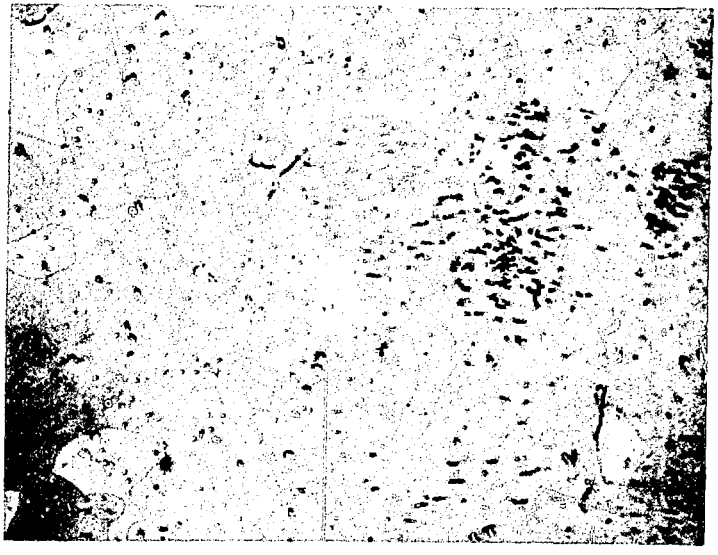

Fig. 22

better agreement with the phase diagram proposed by Sveshnikov et al.[63] than by Lundin and Yamamoto[40].

The superconducting critical temperature, T_c, and the lattice parameter, a_o, were measured, and the results are summarized in Table XI. In the arc-melted samples T_c is nearly independent of composition. This is probably due to inhomogeneities and large amounts of second phases present in these samples, which is very similar to the results obtained by sputtering and quenching from the liquid state[56]. After a proper high temperature heat treatment and a long time low temperature (750°C) anneal, a strong T_c dependence on composition is obtained (2.6 K/at.% Al), as can be seen from Fig. 23. T_c is about 10.2 K at 18.7 at.% Al and at 20.2 at.% Al it starts to increase until 18.6 K at 24.5 at.% Al, and further increase in the Al content does not increase T_c further. Similar behavior has been previously observed.[17,54,55,57] Also shown in Fig. 23 is the lattice parameter of these same samples, where we can see that a_o decreases from 5.196 ± 0.002Å at 20.2 at.% Al to 5.184 ± 0.001Å at 24.5 at.% Al and remains unchanged with increasing Al content. From this T_c and a_o dependence on composition, we conclude that the homogeneity range of the A-15 phase is restricted to 20.2 to 24.5 at.% Al at 1730°C in agreement with the previous metallographic results (Figs.15-22).

The low temperature anneal normally increases T_c about 1 K in the samples cooled by radiation from high temperatures with a negligible or small decrease (≤0.02%) in a_o while no changes

Summary of Data for A-15 Phase of Nb-Al

Composition	Heat Treatment	T_{c1}	T_{c3}	ΔT_c	a_o	Remarks
$Nb_{81.3}Al_{18.7}$	As Cast	16.71	15.35	1.76	N.M.	A-15+Nb_{SS}
$Nb_{81.3}Al_{18.7}$	10 min. 1730°C+24 hrs 1240°C+48 hrs 725°C	11.93	10.23	1.09	5.196 ±0.002	A-15+Nb_{SS}
$Nb_{79.8}Al_{20.2}$	As Cast	16.79	13.94	1.32	N.M.	A-15+Nb_{SS}
$Nb_{79.8}Al_{20.2}$	42 hrs 1350°C+1 week 750°C	15.84	10.46	3.59	5.196 ±0.002	A-15
$Nb_{78.1}Al_{21.9}$	As Cast	17.27	16.42	1.33	N.M.	A-15
$Nb_{78.1}Al_{21.9}$	17 hrs 1550°C+1 week 750°C	17.52	14.94	3.56	5.191 ±0.001	A-15
$Nb_{77}Al_{23}$	As Cast	17.18	17.09	0.11	N.M.	A-15+σ
$Nb_{77}Al_{23}$	12 hrs 1650°C+203 hrs 750°C	18.66	17.71	1.36	5.186 ±0.001	A-15
$Nb_{75.5}Al_{24.5}$	As Cast	17.45	17.34	0.11	N.M.	A-15+σ
$Nb_{75.5}Al_{24.5}$	10 hrs 1700°C+1 week 750°C	18.67	18.60	0.11	5.184 ±0.001	A-15+σ
$Nb_{74.7}Al_{25.3}$	As Cast	17.37	17.17	0.23	N.M.	A-15+σ
$Nb_{74.7}Al_{25.3}$	10 hrs 1730°C+1 week 750°C	18.75	18.61	0.19	5.183 ±0.001	A-15+σ
$Nb_{73}Al_{27}$	As Cast	17.52	17.02	0.61	N.M.	A-15+σ
$Nb_{73}Al_{27}$	10 hrs 1730°C+1 week 750°C	18.67	18.49	0.30	5.184 ±0.001	A-15+σ
$Nb_{70.6}Al_{29.4}$	As Cast	17.18	14.74	2.23	N.M.	A-15+σ
$Nb_{70.6}Al_{29.4}$	10 hrs 1730°C+1 week 750°C	18.67	18.44	0.34	5.184 ±0.001	A-15+σ

N.M. - Not Measured

Figure 23

Superconducting transition temperature, T_c, and lattice parameter, a_o, vs. composition for the Nb-Aℓ system.

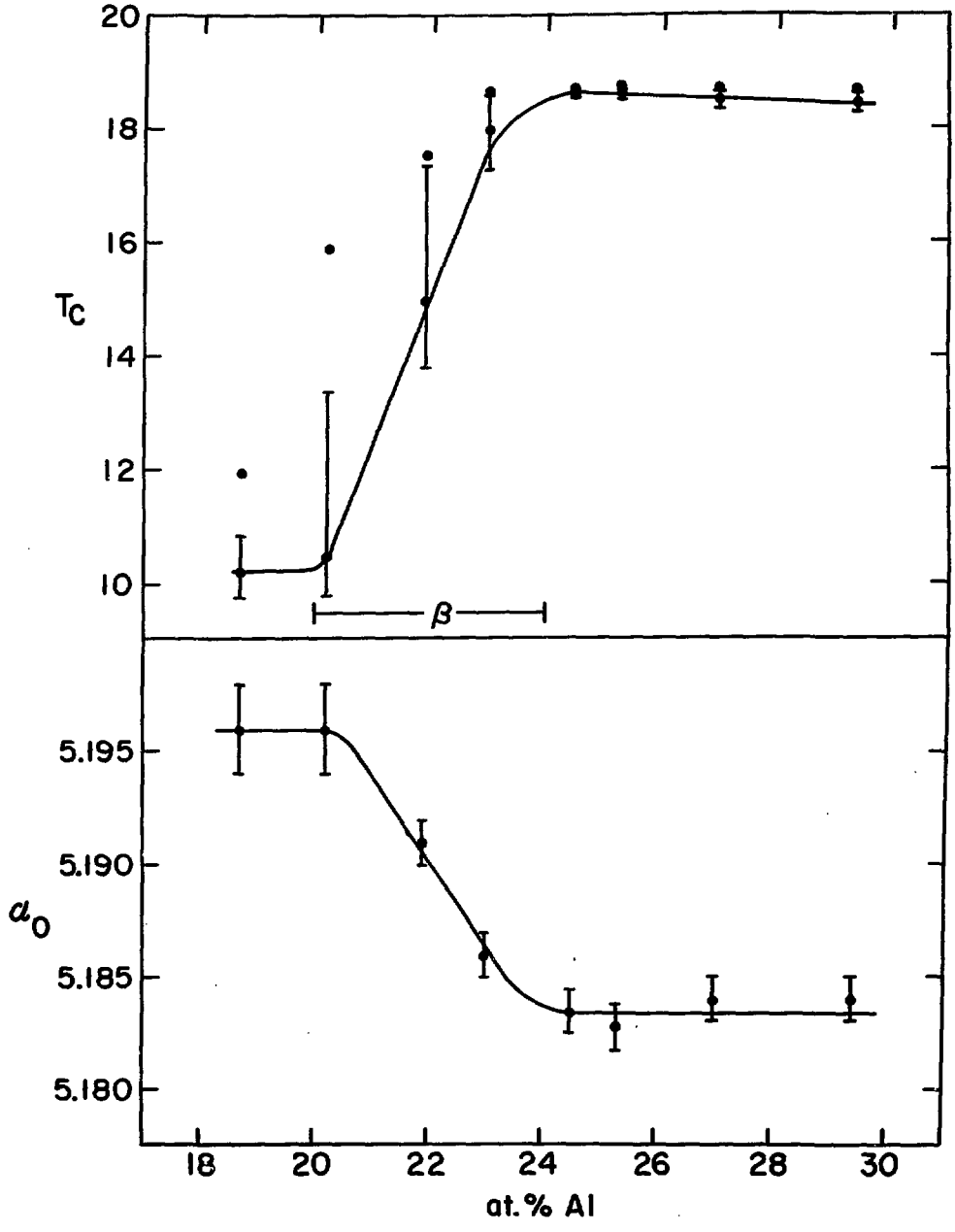
20
18
16
14
12
10
T_C
β
5.195
5.190
5.185
5.180
a_0
18
20
22
24
26
28
30
at.% Al

Fig. 23

in the amount of second phase were observed at these temperatures (750°C). However, fast quenching from high temperatures a sample with 25.4 at.% Al, depressed T_c by 2.4 K (from 18.5 - 16.1 K) and increased a_o by 0.06%. Annealing this latter sample for 6 days at 750°C recovered both T_c and a_o to the original pre-quenched value.

Diffractometer scans were taken in several of these samples, and a typical spectrum is shown in Fig. 24. This sample (23 at.% Al) was annealed 12 hours at 1650°C plus 203 hours at 750°C and had a T_c of 17.7 K and a_o of 5.186 $\pm$ 0.001Å and is single phase as can be seen from the figure. For the least-squares refinement of the integrated intensities of this sample it was necessary to take an average intensity for each peak after five scans due to preferred-orientation effects. These effects were observed in other compositions and probably came from the large grain size of these arc-melted samples ($\sim$ 100μ) (see Figs.17 and 18).

The final parameters are summarized in Table XII, together with observed and calculated intensities. As indicated by the occupation factor k there is no Nb site occupied by Al and the sample is ordered to the maximum value permitted by the composition (S_B = 0.89 $\pm$ 0.02).

The effect of high energy neutron irradiations on T_c of Nb - Al for different compositions is shown in Fig. 25 and the data are summarized in Table XIII. These samples received a

Figure 24

X-ray data for $Nb_{0.77}Al_{0.23}$

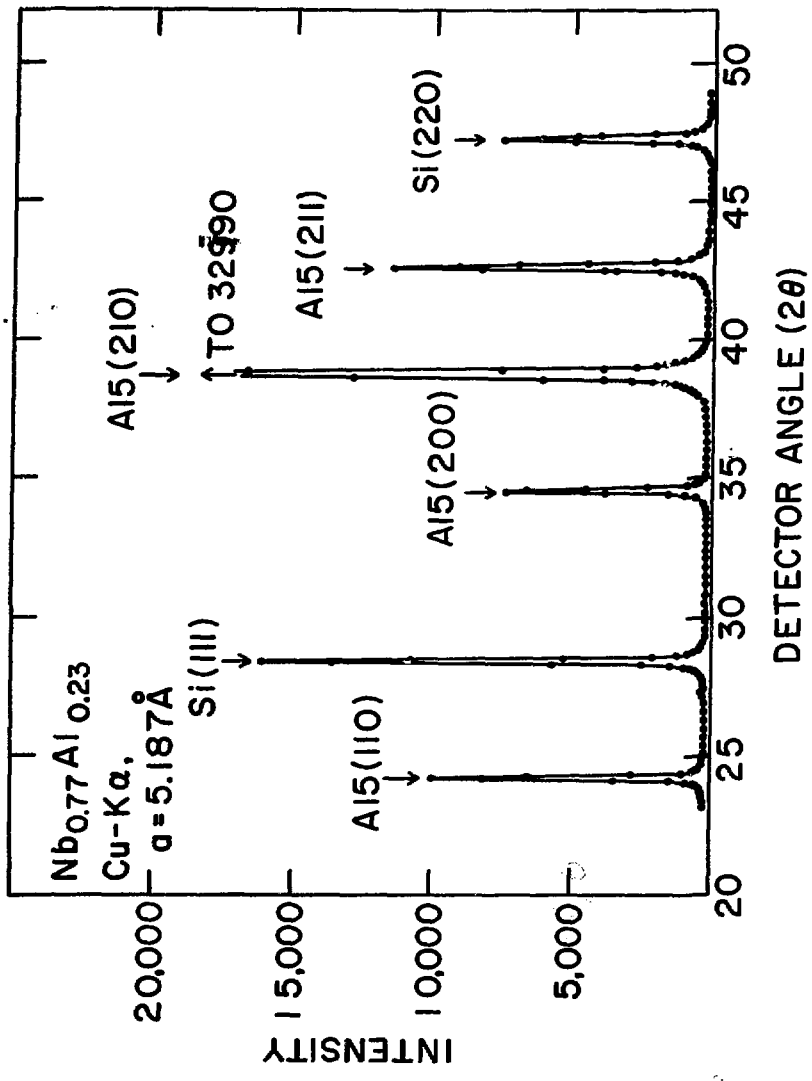
$Nb_{0.77}Al_{0.23}$
Cu-Kα,
a=5.187Å
Si(111)
A15(110)
A15(210)
TO 3290
A15(211)
A15(200)
Si(220)
INTENSITY
20,000
15,000
10,000
5,000
20
25
30
35
40
45
50
DETECTOR ANGLE (2θ)

Fig. 24

TABLE XII

Least-squares parameters and intensities for $Nb_{0.77}Al_{0.23}$ (a = 5.186Å, T_c = 17.7 °K). k is the percentage of Nb sites occupied by Al, B the Debye-Waller factor.

k (%)	-0.2 (7)
B ($Å^2$)	0.4 (2)

Phase	hkℓ	I_{calc}	I_{obs}	(σ)
A15	110	34.5	36.7	(3.5)
Si	111	65.0	66.1	(3.5)
A15	200	28.9	27.7	(3.5)
A15	210	185.0	173.5	(25.0)
A15	211	63.3	66.3	(4.5)
Si	220	42.2	39.5	(4.5)
A15	220	4.8	5.0	(1.0)
A15	310	6.6	30.1	(2.0)
Si	311	24.3		
A15	222	26.3	29.5	(4.5)
A15	320	39.0	35.8	(3.5)
A15	321	31.1	32.7	(4.0)
Si	400	6.3	6.8	(1.0)
A15	400	19.2	14.2	(2.0)
Si	331	9.3	9.5	(1.5)
A15	411	2.5	4.1	(1.0)
A15	330	1.2		
A15	420	8.7	9.4	(1.0)
A15	421	36.0	40.3	(5.0)

TABLE XII (Cont'd)

Phase	hkℓ	I_{calc}	I_{obs}	(σ)
A15	332	7.6	23.8	(5.0)
Si	422	12.6		
A15	422	1.7	1.6	(1.0)
Si	333	1.8	7.1	(1.0)
Si	511	5.3		
A15	510	1.6	4.8	(1.0)
A15	431	3.2		
A15	432	26.6		
A15	520	13.3	42.1	(3.5)
Si	440	4.5		
A15	521	11.6	13.5	(1.5)

R factor 0.069 Weighted R factor 0.084

Figure 25

Superconducting transition temperature, T_c, vs. composition of Nb-Aℓ unirradiated and irradiated to different neutron fluences (E > 1 MeV). The samples with more than 24 at.% Aℓ contain σ phase.

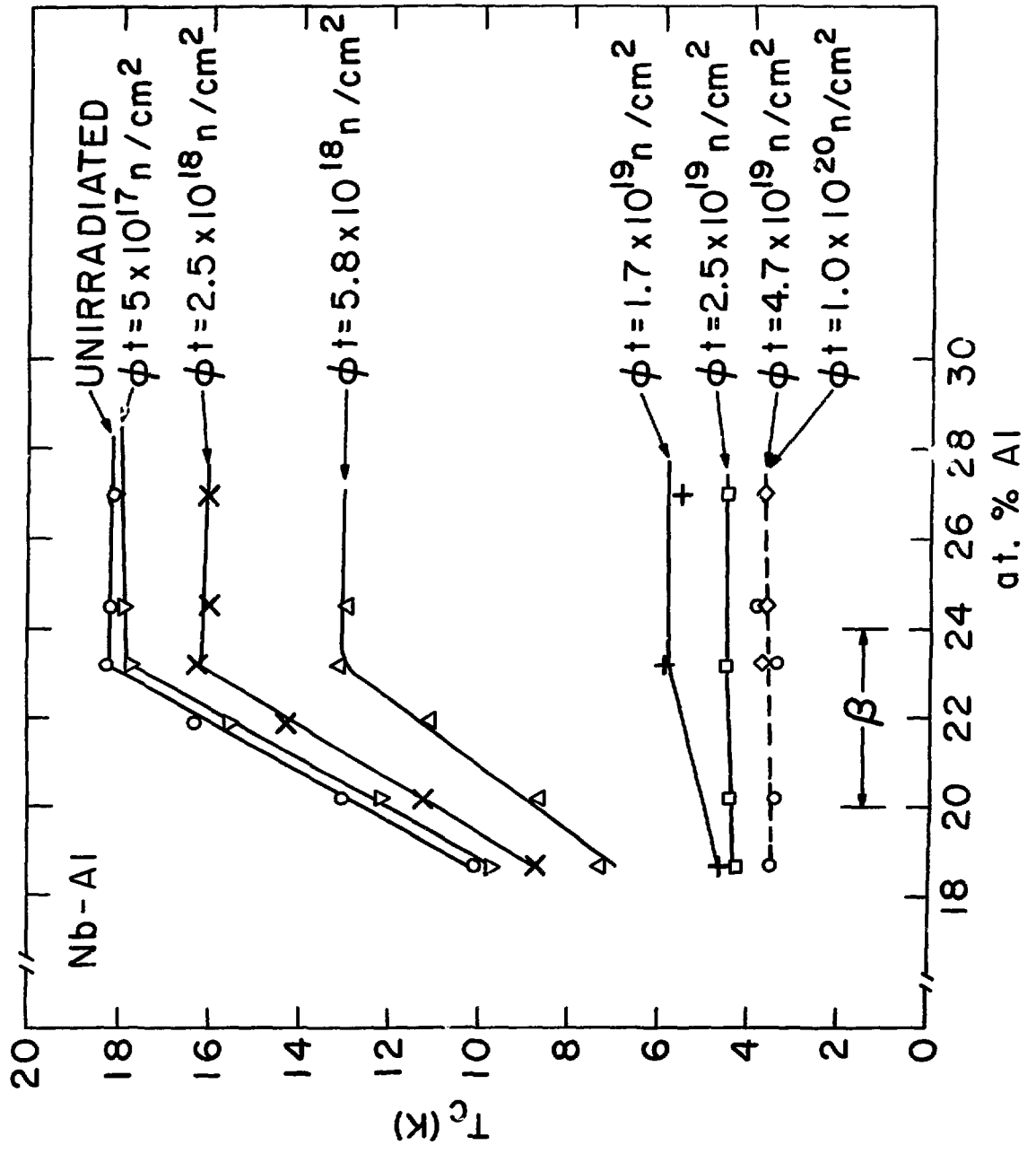
Nb-Al
UNIRRADIATED
$\phi t = 5 \times 10^{17} n/cm^2$
$\phi t = 2.5 \times 10^{18} n/cm^2$
$\phi t = 5.8 \times 10^{18} n/cm^2$
$\phi t = 1.7 \times 10^{19} n/cm^2$
$\phi t = 2.5 \times 10^{19} n/cm^2$
$\phi t = 4.7 \times 10^{19} n/cm^2$
$\phi t = 1.0 \times 10^{20} n/cm^2$
β
T_c (K)
at. % Al
0
2
4
6
8
10
12
14
16
18
20
18
20
22
24
26
28
30

Fig. 25

TABLE XIII

Summary Data of Neutron Irradiated Nb-Al

	$Nb_{81.3}Al_{18.7}$ (a)				$Nb_{79.8}Al_{20.2}$ (b)				$Nb_{78.1}Al_{21.9}$ (c)			
$\phi t (n/cm^2)$	T_{c1}	T_{c3}	ΔT_c	a_o	T_{c1}	T_{c3}	ΔT_c	a_o	T_{c1}	T_{c3}	ΔT_c	a_o
0	11.75	10.15	1.49	5.196±0.002	17.55	13.10	4.35	5.193±0.001	17.60	16.37	3.15	5.188±0.001
$5x10^{17}$	11.60	9.77	1.96	-	17.21	12.23	4.74	-	16.73	15.60	2.62	-
$2.5x10^{18}$	10.26	8.78	1.36	5.201±0.002	15.87	11.33	3.44	-	15.71	14.28	2.24	-
$5.8x10^{18}$	7.72	7.32	0.37	5.204±0.002	12.03	8.68	2.78	-	12.10	11.18	1.28	-
$1.7x10^{19}$	4.96	4.71	0.18	5.2105±0.002	-	-	-	-	-	-	-	-
$2.5x10^{19}$	4.58	4.28	0.25	5.210±0.002	4.72	4.51	0.20	-	-	-	-	-
$4.7x10^{19}$	-	-	-	5.2115±0.002	-	-	-	5.2095±0.001	-	-	-	5.2055±0.001
$1.0x10^{20}$	4.02	3.56	0.40	-	4.56	3.72	0.69	-	-	-	-	-

(a) - anneal: 10 min. 1730°C + 24 hrs 1200°C + 48 hrs 725°C (A-15 + Nb_{SS})

(b) - anneal: 10 min. 1720°C + 10 hrs 1410°C + 48 hrs 750°C (A-15)

(c) - anneal: 10 min. 1740°C + 5 hrs 1500°C + 48 hrs 725°C (A-15)

TABLE XIII (Cont'd)

	$Nb_{76.8}Al_{23.2}$ (d)				$Nb_{75.5}Al_{24.5}$ (e)				$Nb_{73}Al_{27}$ (f)			
ϕt (n/cm^2)	T_{c1}	T_{c3}	ΔT_c	a_o	T_{c1}	T_{c3}	ΔT_c	a_o	T_{c1}	T_{c3}	ΔT_c	a_o
0	18.45	18.29	0.36	5.183±0.001	18.47	18.25	0.30	5.184±0.001	18.26	18.15	0.25	5.182±0.001
$5x10^{17}$	17.90	17.78	0.17	-	18.22	17.98	0.35	-	18.25	18.13	0.19	-
$2.5x10^{18}$	16.45	16.32	0.54	-	16.28	16.02	0.33	-	16.40	16.11	0.38	-
$5.8x10^{18}$	13.37	13.16	0.46	-	13.34	12.99	0.52	-	-	-	-	-
$1.7x10^{19}$	6.12	5.98	0.17	-	-	-	-	-	5.86	5.62	0.36	-
$2.5x10^{19}$	4.74	4.58	0.19	-	-	-	-	-	4.80	4.59	0.21	-
$4.7x10^{19}$	4.41	3.80	0.55	-	4.48	3.75	0.69	5.2025±0.001	4.26	3.77	0.59	5.2005±0.001
$1.0x10^{20}$	4.65	3.45	0.65	-	5.92	3.92	1.67	-	-	-	-	-

(d) - anneal: 15 min. 1920°C + 1 week 750°C (A-15)

(e) - anneal: 15 min. 1920°C + 1 week 750°C (A-15 + σ)

(f) - anneal: 7 hrs 1780°C + 96 hrs 750°C (A-15 + σ)

different heat treatment than those of Table XI(Fig. 23) and a small increase in the amount of second phase and inhomogeneity were observed. Since the T_c and a_o dependence on composition differs only slightly from the previous results, we can assume that the stoichiometry of these samples has not changed significantly. The upper curve of Fig. 25 represent the T_c's of the unirradiated samples and the lower the irradiated, in terms of increasing fluences. In each of these curves, all samples with different compositions were irradiated at the same time, to insure they received the same neutron dose. From this figure we can see that T_c decreases for all compositions with increasing fluence but the rate of depression of T_c is more pronounced as we approach stoichiometry. For example, a sample with 23.2 at.% Al has its T_c of 18.29K decreased to 13.16K after a fluence of $5.8 \times 10^{18} n/cm^2$ while an off-stoichiometry with 18.7 at.% Al has his T_c of 10.15K decreased to only 8.78K after the same neutron dose. At high fluences ($1.0 \times 10^{20} n/cm^2$) all compositions reach essentially the same T_c (~3.5K), which is shown by a horizontal line in Fig. 25. It is also interesting to note that the rates of depression of T_c are the same for samples with more than 23.2 at.% Al which confirms the previous metallographic result that these samples have actually a composition close to 24 at.% Al. Figure 26 shows the same data as a function of fluence for different compositions. Here, we can more clearly see some of the previous observations (Fig. 25), especially the large satu-

Figure 26

Superconducting transition temperature, T_c, against neutron fluence (E > 1 MeV) for various compositions in the Nb-Aℓ system. The samples with more than 24 at% Aℓ contain σ phase. This figure also shows the results for pure niobium neutron irradiated.

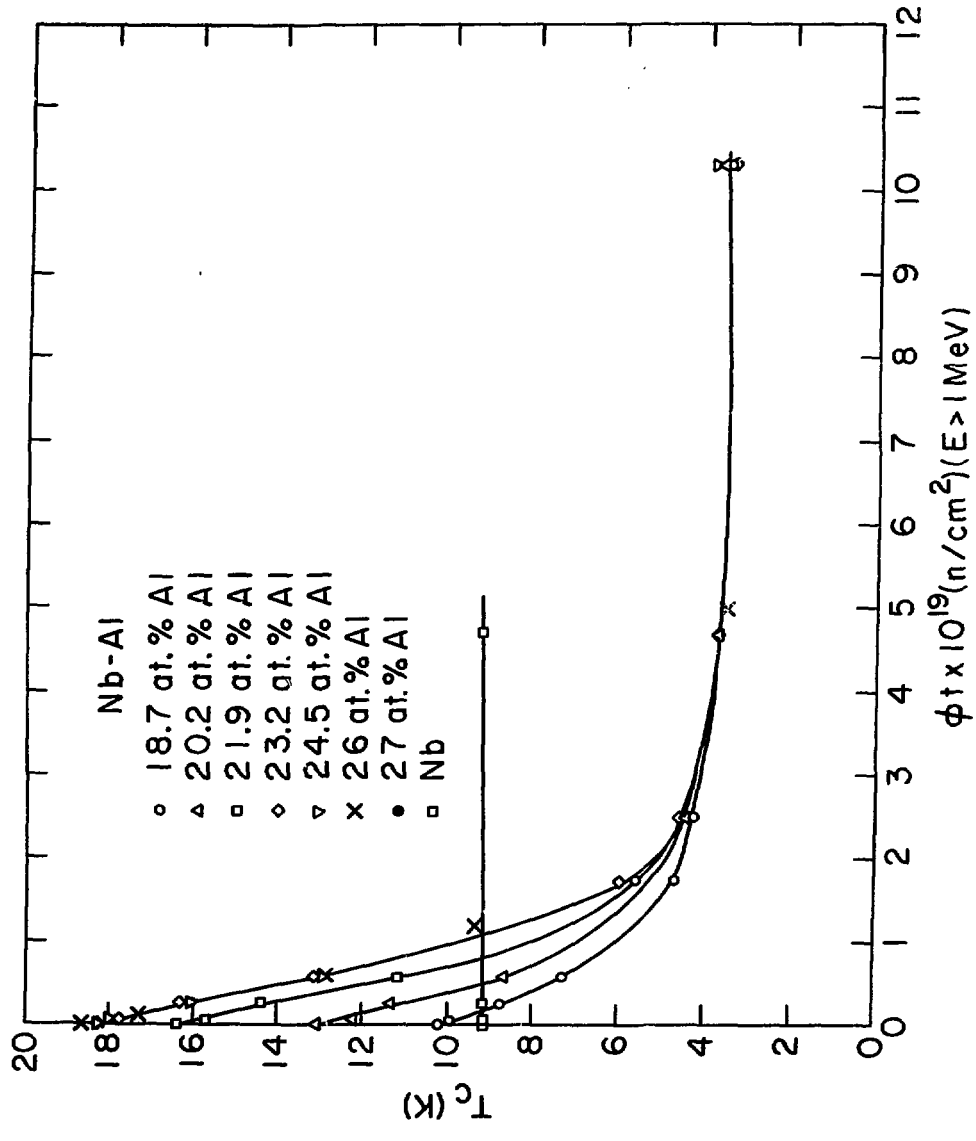
Nb-Al
18.7 at.% Al
20.2 at.% Al
21.9 at.% Al
23.2 at.% Al
24.5 at.% Al
26 at.% Al
27 at.% Al
Nb
T_c (K)
$\phi t \times 10^{19} (n/cm^2)(E>1 MeV)$

Fig. 26

ration region above $4.7 \times 10^{19} n/cm^2$ which is common for all compositions. Also included is the data from Sweedler and Cox [64] for neutron irradiated Nb_{74} Al_{26}. We see that these data fits very well the curve given by the samples with compositions higher than 23.2 at.% Al (upper curve of Fig. 26). This figure also shows the results for pure niobium where no depression in T_c was observed up to $4.7 \times 10^{19} n/cm^2$. It is interesting to note, although no decrease in T_c was observed, a decrease in the transition widths occurred from 0.29K (unirradiated) to 0.09K at $4.7 \times 10^{19} n/cm^2$.

The superconducting transition widths, ΔT_c, for Nb - Al (Table XII) show, as a general trend, a small or negligible increase at low fluences but a significant decrease is observed at high fluences. Further increases in fluences, in the saturation region, seems to increase again the widths. The initial rather random variation of the width in some of these samples may be associated with the inhomogeneities in the starting materials.

The lattice parameter, a_o, of the irradiated samples are given in Figs. 27 and 28. Fig. 27 shows the lattice parameter of the unirradiated and irradiated samples at 4.7×10^{19} n/cm^2 for different compositions and Fig. 28 shows how a_o expands as a function of fluence for 26[64] and 18.7 at.% Al. From these two figures we see that for a given fluence the lattice parameter is expanded by a constant factor in all the

Figure 27

Lattice parameter, a_o, vs. composition for Nb-Al unirradiated and irradiated to $4.7 \times 10^{19} n/cm^2$.

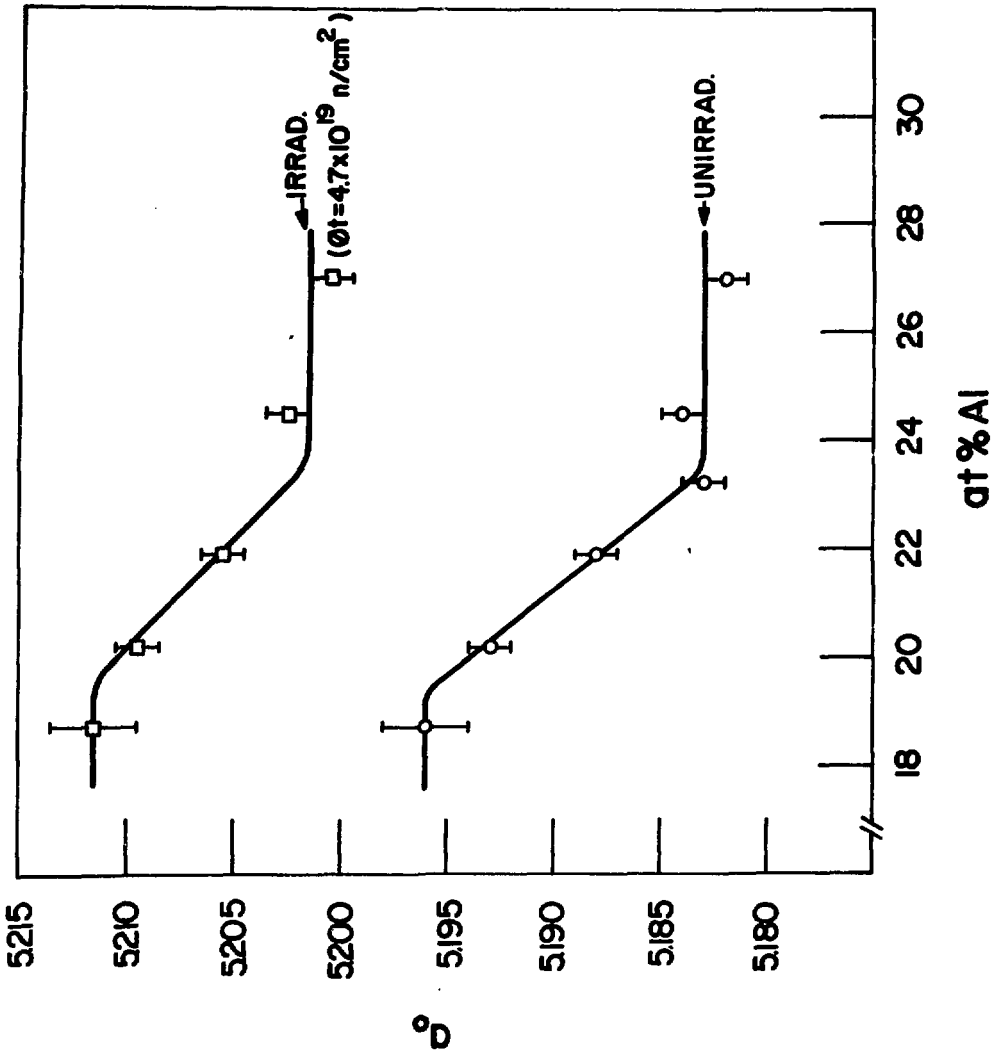
IRRAD.
(Øt=4.7x10^19 n/cm^2)
UNIRRAD.
5215
5210
5205
5200
5195
5190
5185
5180
°D
18
20
22
24
26
28
30
at % Al

Fig. 27

Figure 28

Lattice parameter, a_o, against neutron fluence (E>1 MeV) for samples with 18.7 and 26 at.% Aℓ.

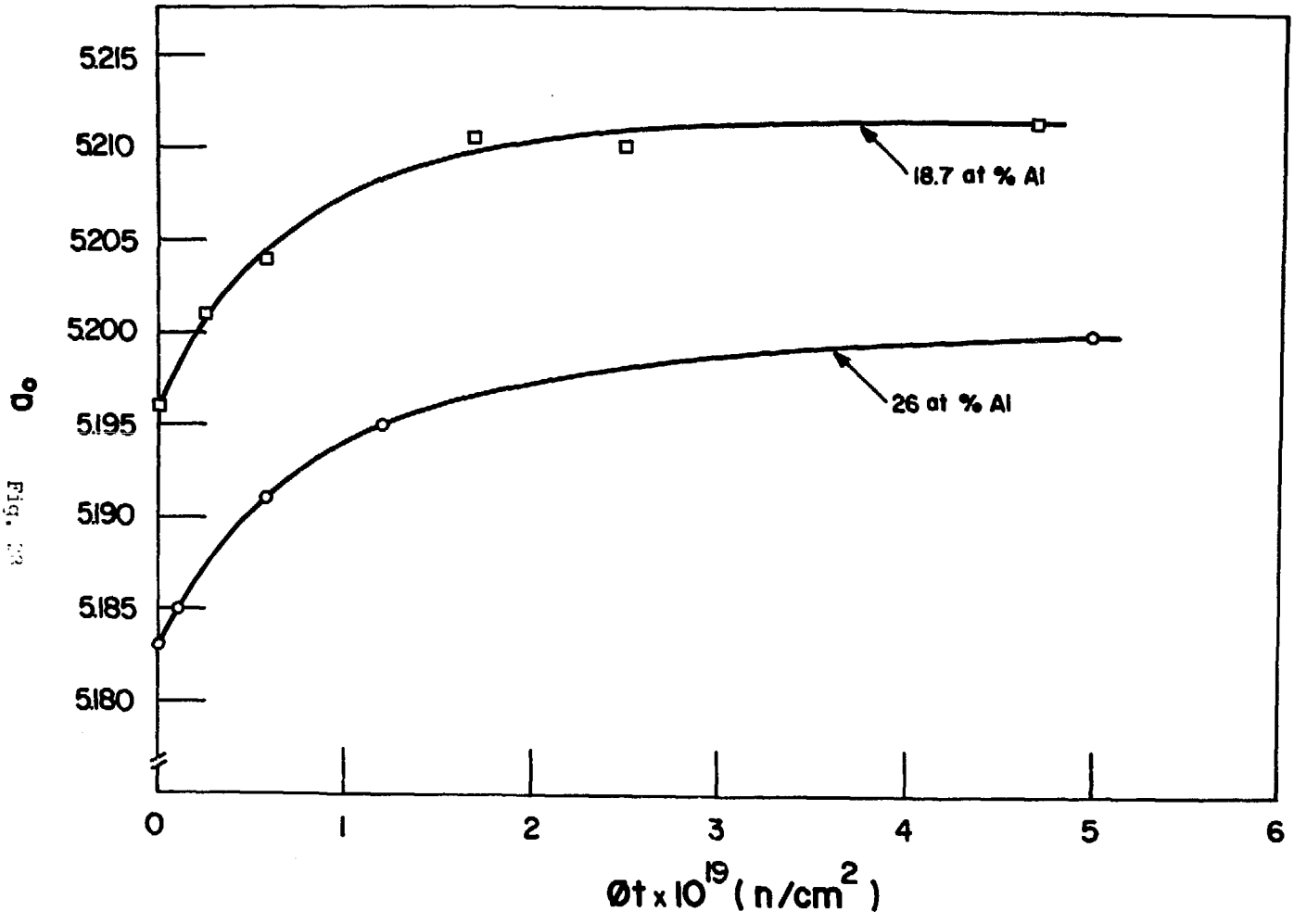
5.215
5.210
5.205
5.200
5.195
5.190
5.185
5.180
a_o
18.7 at % Al
26 at % Al
0
1
2
3
4
5
6
$\phi t \times 10^{19}$ (n/cm^2)

Fig. 23

compositions (Fig. 27) and that the a_o dependence on fluence is the same for different compositions (Fig. 28). These behaviors of a_o are in great contrast with those of T_c shown in Figs. 25 and 26 .

From the Debye-Scherrer x-ray patterns we observe that the intensities of all the difference lines decrease with increasing fluence and after a fluence of $4.7 \times 10^{19} n/cm^2$ all the difference lines could no longer be observed in the x-ray films, except the (110) line which is the most intense of the difference lines. These observations cannot be attributed to the fact that these lines were overshadowed by the increase with fluence of the γ-radiation background as other structure lines with calculated intensities equivalent or smaller than the difference lines, like the (420) line, were clearly visible even at high fluences where these difference lines could not be observed. This decrease in intensity of the difference lines with fluence imply a decrease in the long-range order parameter, which has also been measured in this system.[64] In contrast to the Nb_3Ge observations, no line broadening was noted even in the most heavily irradiated samples. Also, no large lattice expansions were observed at high fluences (see Fig. 28).

An x-ray film was also taken for pure Nb irradiated to $1.5 \times 10^{20} n/cm^2$. This film showed that the b.c.c. lattice parameter of Nb did not change at this fluence but a clear broadening of the high angle lines was observed.

Fig. 29 shows how T_c of three samples with different compositions (18.7, 20.2 and 23.2 at.% Al) irradiated to a fluence of 4.7 x 10^{19}n/cm^2, recovers with an isochronal anneal. All three samples had a similar T_c at 4.7 x 10^{19}n/cm^2 and were annealed at the same time during the two hours isochronal anneal. From Fig. 29 we can see that there is nearly no recovery of T_c below 400°C and at this temperature and above the rate of recovery of T_c is similar for all compositions. At higher temperatures (>575°C) the curves split and the T_c's of the samples tend to the original unirradiated values. At 800°C, T_c is not only completely recovered, but also show some enhancements with respect to the unirradiated material, of more than 1K in some cases. An unirradiated sample with 20.2 at.% Al received the same isochronal anneal as the three irradiated sample and no change in T_c or ΔT_c were observed until 800°C, which may indicate that some radiation enhancement of diffusion[65] had taken place. The transition width, ΔT_c, of the three irradiated samples, quite narrow (~0.5K) after a fluence of 4.7 x 10^{19}n/cm^2, begin to broaden above 500°C and then narrowed as T_c approached the final value. The width at 800°C was close to the unirradiated value.

In Fig. 30 we present the isochronal anneal of a sample with 26 at.% Al irradiated at a fluence of 5 x 10^{19}n/cm^2 where T_c and a_o were measured for the same sample during the anneal. The results are presented in percentage of recovery for a direct comparison. From these results we can see that the lattice

Figure 29

Isochronal annealing curve for neutron irradiated samples of Nb-Aℓ with different compositions. Note enhancement of T_c - with respect to unirradiated value.

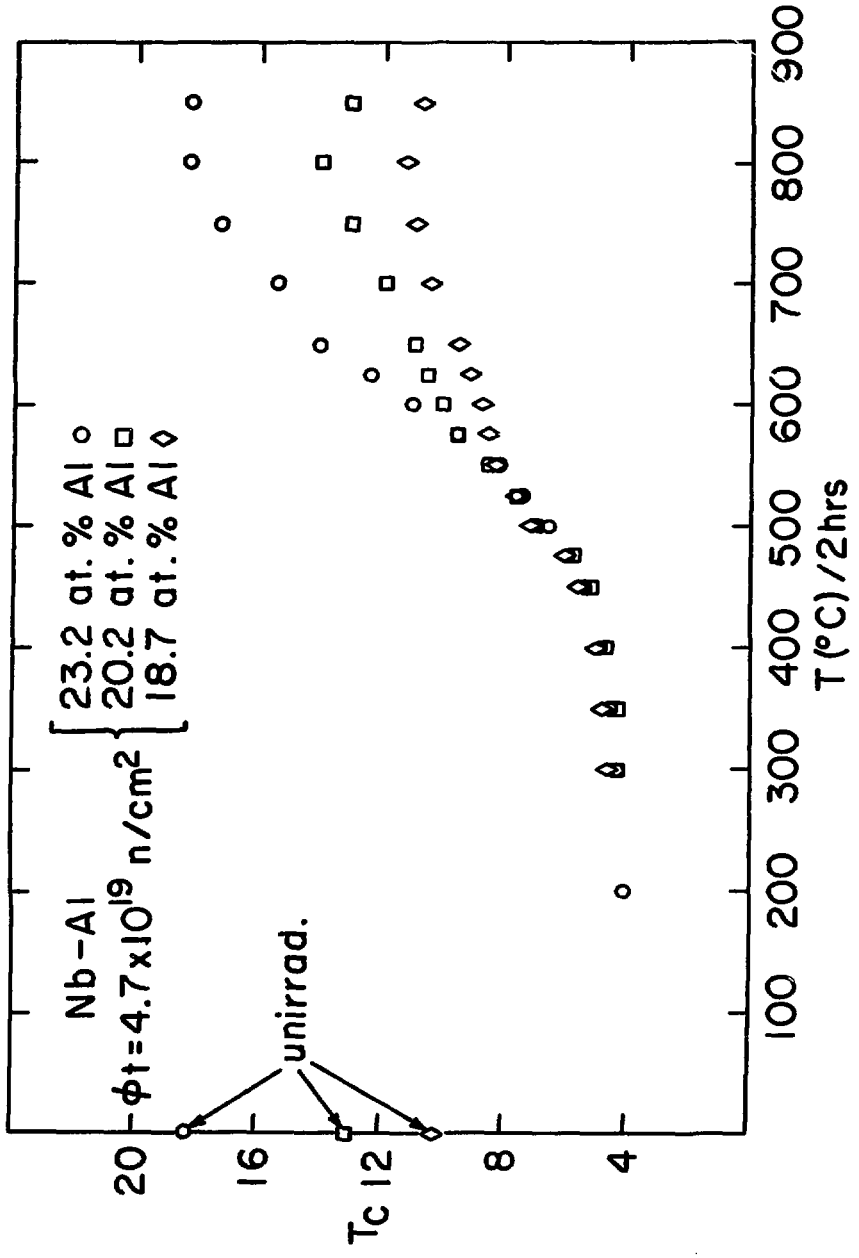
Nb-Al
$\phi t = 4.7 \times 10^{19}$ n/cm^2
23.2 at.% Al ○
20.2 at.% Al □
18.7 at.% Al ◇
unirrad.
Tc
20
16
12
8
4
100
200
300
400
500
600
700
800
900
T(°C)/2hrs

Fig. 29

Figure 30

Percentage recovery of the lattice parameter, a_o, and transition temperature, T_c, as a function of isochronal anneals for neutron irradiated $Nb_{74}Al_{26}$.

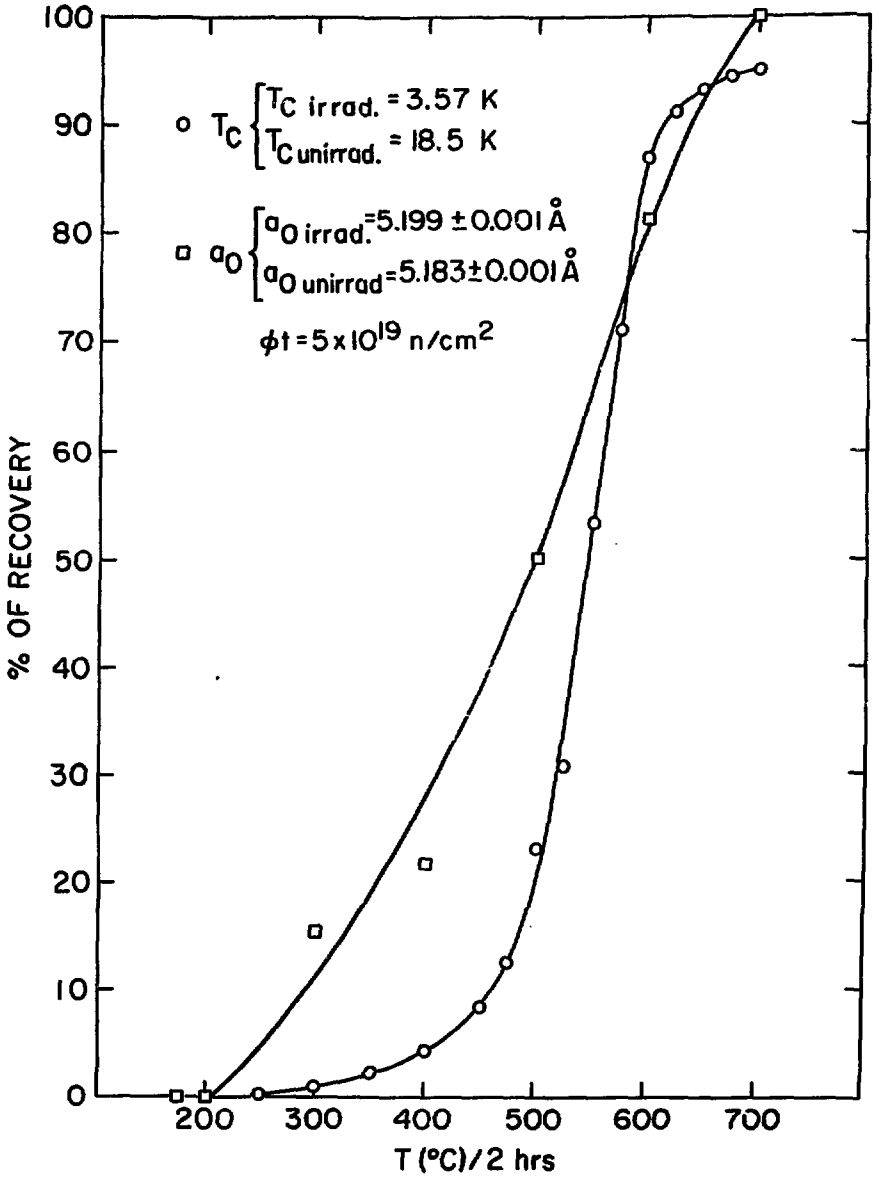
100
90
80
70
60
50
40
30
20
10
0
% OF RECOVERY
o T_C T_C irrad. = 3.57 K
T_C unirrad. = 18.5 K
□ a_0 a_0 irrad. = 5.199 ± 0.001 Å
a_0 unirrad = 5.183 ± 0.001 Å
$\phi t = 5 \times 10^{19}$ n/cm^2
200
300
400
500
600
700
T (°C)/2 hrs

Fig. 30

parameter is also recoverable as T_c is but the rate of recovery is different than T_c. For example, the lattice parameter recovers 15% and 50% at 300°C and 500°C respectively, while T_c recovers only 1% and 23% at these same temperatures. These results may reflect the lack of correlation of a_o with T_c for irradiated materials.

Nb- Pt: In most of the high-T_c Nb-base A-15 compounds such as Nb-Ge and Nb-Al, single phase, homogeneous samples are difficult or impossible to prepare over a wide composition range, and are generally restricted to the Nb-rich side of stoichiometry. However, Waterstrat and Manuszewski[66], recently have investigated the phase diagram for the Nb-Pt system and have reported a broad homogeneity range for the A-15 phase extending from 19 to 28 at.% Pt at high temperatures. As T_c for Nb_3Pt has been reported to be between 10-11K[11,67,68] and the homogeneity range encompasses both sides of stoichiometry, Nb-Pt is an excellent choice for a systematic study of the effects of composition and order on the superconducting properties of these compounds.

Here, an attempt has been made to determine the effects of both composition and ordering on the T_c and lattice parameter in the Nb-Pt system. The effects of ordering at different compositions have been investigated by measuring the long range order parameter of samples with different heat treatments and using the disorder produced as a result of irradiation with high energy neutrons coupled with isochronal anneals.

The composition of the samples investigated ranged from 19 to 29.1 at.%Pt in 1 at.% steps. After casting, the samples were subjected to a high temperature heat treatment at 1800°C for 12 hours followed by a low temperature anneal at 900°C for 10 days. Selected samples were also annealed at 900°C for periods up to 40 days, and others were rapidly quenched from 1800°C into liquid Ga or splat cooled from the melt. The heat treatments for each composition are summarized in Table XIV with the corresponding T_{c1}, T_{c3}, ΔT_c and a_o values. The homogeneity range of the A-15 phase was found to extend from 19.5 at.%.Pt at 1900°C to 29.1 at.%Pt at 1800°C, in good agreement with Waterstrat and Manuszewski. The two end members of nominal compositions 19 and 29.1 at.%Pt were found to contain about 5 wt% of Nb-rich bcc phase (corrected composition 19.5 at.%Pt) and 1 wt% of σ phase respectively. No impurity phases were detected in any of the other samples.

T_c is shown as a function of composition for various heat treatments in Fig. 31. There is a roughly linear decrease in T_c on both sides of the stoichiometric composition with an average slope of about 1.5K per at.% for those samples receiving a high temperature plus low temperature anneal, with a pronounced peak at the stoichiometric composition. For samples annealed at 1800°C for 12 hours without a subsequent 900°C anneal, roughly the same trend is seen, with the exception of the stoichiometric material where T_c is significantly lower. It is also interesting to note that for compositions on the Pt-rich side of

TABLE XIV

SUMMARY OF DATA FOR THE A-15 PHASE OF Nb-Pt

Sample	T_{c2}(K) (a)	T_{c3}(K) (b)	ΔT_c(K) (c)	a_o(Å) (d)	Remarks
$Nb_{80.5}Pt_{19.5}$	2.40	2.35	0.11	5.1790	A15+5%A2 (k)
$Nb_{79}Pt_{21}$	3.89	3.57	0.63	5.1725	A15 (j)
$Nb_{79}Pt_{21}$	4.26	4.14	0.22		A15 (e)
$Nb_{79}Pt_{21}$	5.77	4.75	1.62	5.1725	A15 (f)
$Nb_{79}Pt_{21}$	7.99	6.15	3.5	5.1715	A15 (h)
$Nb_{77.9}Pt_{22.1}$	5.96	5.75	0.40		A15 (e)
$Nb_{77.9}Pt_{22.1}$	7.29	6.36	1.46	5.167	A15 (f)
$Nb_{76.9}Pt_{23.1}$	7.43	7.34	0.18		A15 (e)
$Nb_{76.9}Pt_{23.1}$	7.59	7.45	0.22	5.1635	A15 (f)
$Nb_{75.9}Pt_{24.1}$	7.24	6.80	1.64		A15 (j)
$Nb_{75.9}Pt_{24.1}$	8.24	8.19	0.10		A15 (e)
$Nb_{75.9}Pt_{24.1}$	8.34	8.29	0.10	5.1590	A15 (f)
$Nb_{75.9}Pt_{24.1}$	8.78	8.48	0.60		A15 (g)
$Nb_{75.9}Pt_{24.1}$	9.13	8.62	0.89		A15 (i)
$Nb_{74.9}Pt_{25.1}$	7.38	7.13	1.38	5.1555	A15 (j)
$Nb_{74.9}Pt_{25.1}$	9.10	9.03	0.13		A15 (e)
$Nb_{74.9}Pt_{25.1}$	10.87	10.67	0.31	5.1545	A15 (f)
$Nb_{74.9}Pt_{25.1}$	11.03	10.87	0.30		A15 (g)
$Nb_{74.9}Pt_{25.1}$	11.02	10.81	0.33		A15 (i)
$Nb_{74.9}Pt_{25.1}$	7.12	6.13	2.69		A15 (splat cooled)
$Nb_{74}Pt_{26}$	8.42	8.28	0.28		A15 (e)
$Nb_{74}Pt_{26}$	8.68	8.57	0.21	5.1515	A15 (f)

TABLE XIV(Cont'd)

Sample	T_{c2}(K) (a)	T_{c3}(K) (b)	ΔT_c(K) (c)	a_o(Å) (d)	Remarks
$Nb_{74}Pt_{26}$	8.73	8.56	0.35		A15 (g)
$Nb_{74}Pt_{26}$	8.65	8.51	0.26		A15 (i)
$Nb_{73}Pt_{27}$	7.34	7.27	0.13		A15 (e)
$Nb_{73}Pt_{27}$	7.30	7.30	0.15	5.1475	A15 (f)
$Nb_{72}Pt_{28}$	6.11	5.97	0.28		A15 (e)
$Nb_{72}Pt_{28}$	6.11	6.00	0.23	5.144	A15 (f)
$Nb_{70.9}Pt_{29.1}$	5.17	4.70	0.47		A15 (j,l)
$Nb_{70.9}Pt_{29.1}$	5.19	5.07	0.23		A15 (e,l)
$Nb_{70.9}Pt_{29.1}$	5.26	5.12	0.25	5.1405	A15+1%σ (f,l)
$Nb_{70.9}Pt_{29.1}$	5.28	5.13	0.28		A15 (h,l)

Key

a) Onset of transition, T_{c2}.

b) Midpoint of transition, T_{c3}.

c) Transition width, $\Delta T_c (=T_{c2}-T_{c4})$.

d) Accurate to ±0.0005Å except where 3 places are given, then accurate to ±0.001Å.

e) 1800°C/12 hours.

f) 1800°C/12 hours + 900°C/10 days.

g) 1800°C/12 hours + 900°C/20 days.

h) 1800°C/12 hours + 900°C/30 days.

i) 1800°C/12 hours + 900°C/40 days.

j) Rapid quench from 1800°C.

k) 1900°C/3 hours + 900°C/10 days.

l) No σ phase detected on Debye-Scherrer films.

Figure 31

Superconducting transition temperature midpoints, T_c, vs. composition for the A-15 phase of Nb-Pt. Solid lines are a guide the eye.

O - 1800°C for 12 hous plus 900°C for 10 days

◊ - 1800°C for 12 hours.

□ - rapidly quenched from 1800°C.

▽ - 1800°C for 12 hours plus 900°C for 30 days.

▼ - 1800°C dor 12 hours plus 900°C for 40 days

Δ - splat cooced from melt.

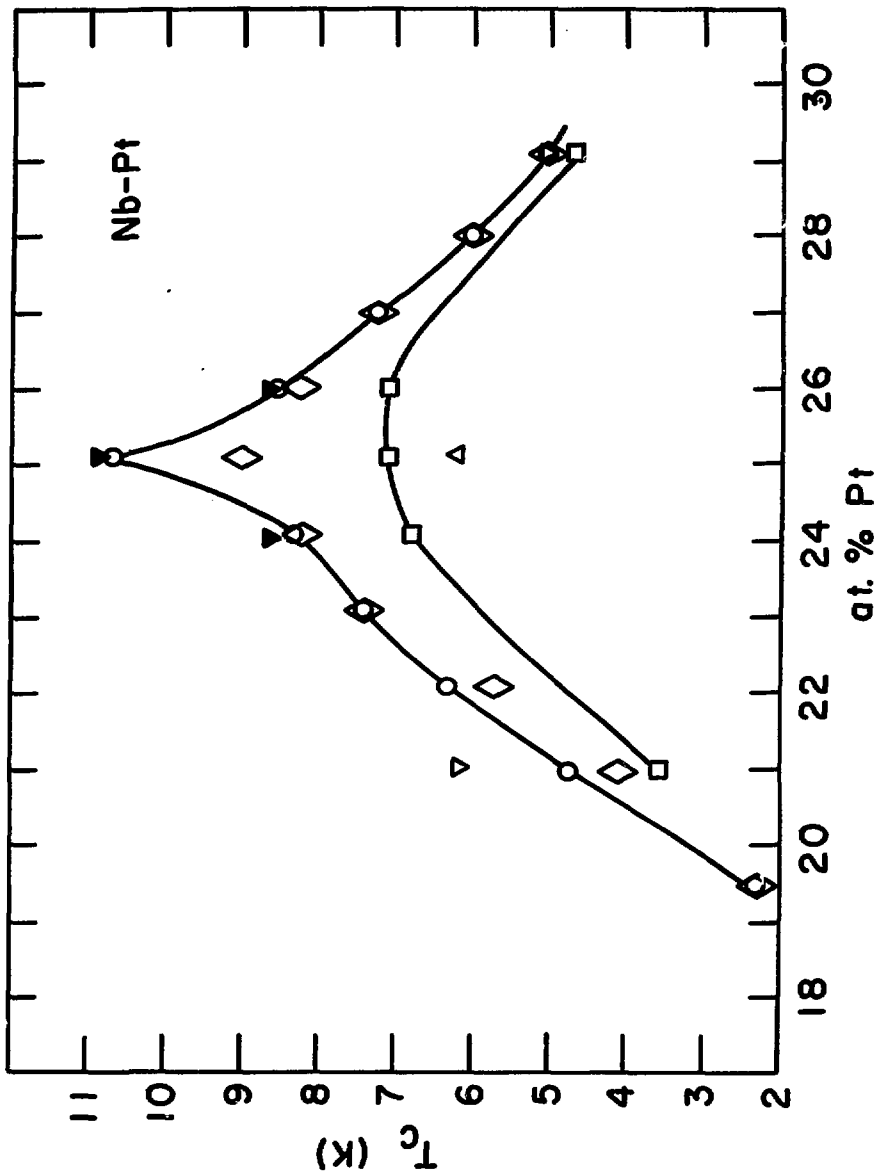

Fig. 31

stoichiometry the 10 day low temperature anneal has little or no effect on T_c while on the Nb-rich side a slight increase in T_c is observed. However, at the stoichiometric composition a substantial increase of about 1.6K is observed. Further annealing at 900°C for up to 40 days resulted in a significant increase on the Nb-rich side but not close to stoichiometry or on the Pt-rich side. For samples rapidly quenched from 1800°C the T_c's are consistently lower than in the case of those receiving high temperature anneals, but nevertheless the same general trend is followed. Finally, the effect of splat cooling from the melt results in a T_c of 6.2K, about 4K lower than that of the annealed material.

The lattice parameters for the samples annealed at 1800°C for 12 hours plus 10 days at 900°C are shown in Fig. 32. From this figure we can see that a_o decreases with increasing Pt concentration and shows a break in the slope at stoichiometry. This is because the Nb and Pt sites are not crystallographically equivalent, and that the Pt radius (1.37Å) is smaller than that of Nb (1.51Å).

The quenched samples showed a small or zero lattice expansion (Table XIV). The Debye-Scherrer x-ray films of all the as-cast samples did not show the high angle lines (above the (611) line) or else they were considerably broadened; samples with 19 at.%Pt and more than 24 at.%Pt also showed evidence of second phase[69]. After high temperature heat treatment all samples showed very sharp high angle lines (up to 622) with α_1 and α_2

Figure 32

Lattice parameter, a_o, vs. composition for the A-15 phase of Nb-Pt. Open circles are experimentally determined data points for samples annealed at 1800°C for 12 hours plus 900°C for 10 days. Solid curve is least squares fit to modified Geller model.

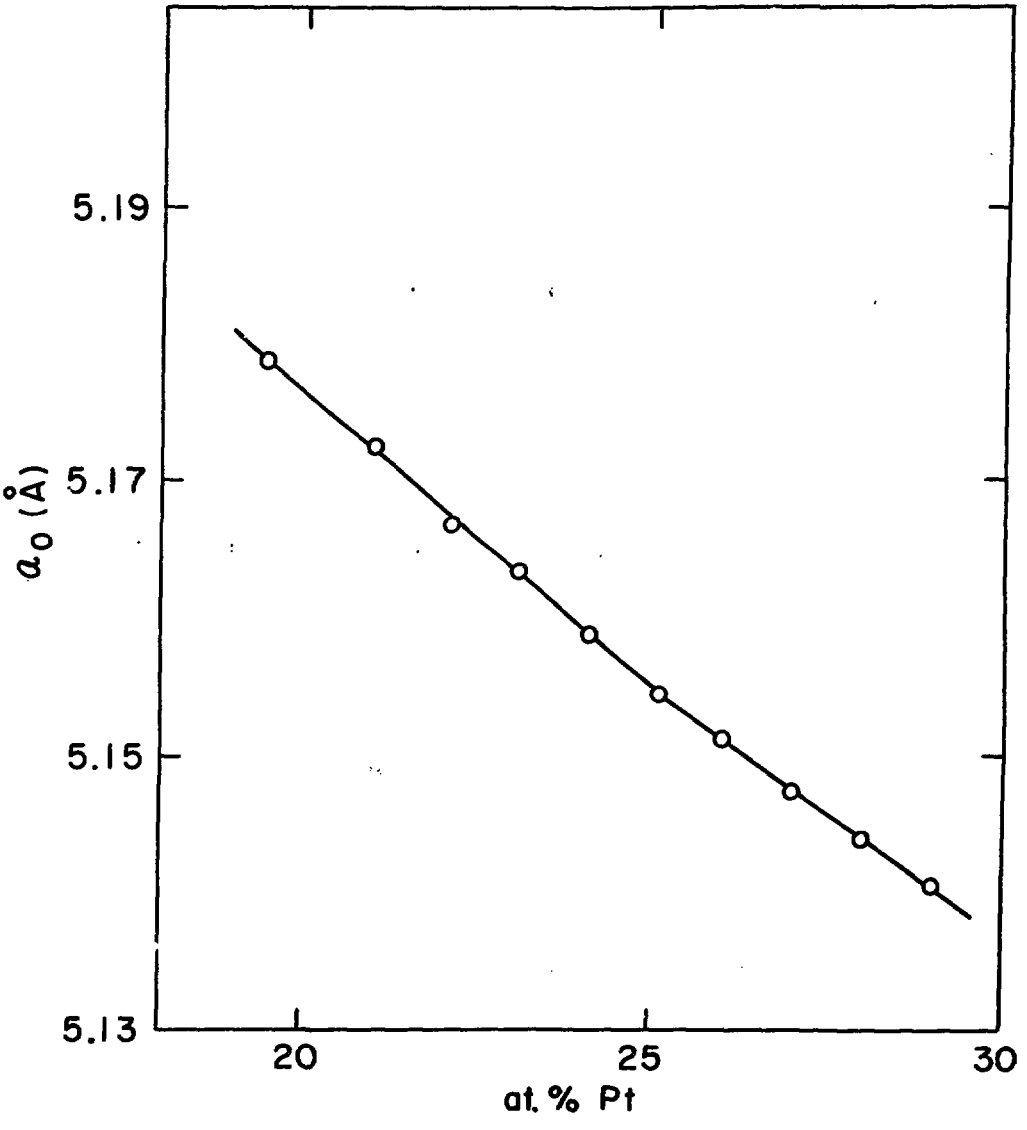

Fig. 32

splitting well resolved and no evidence of second phase except for the sample with 5 wt.% of bcc phase.

The long range order parameter was obtained from the stoichiometric material and two other compositions, 29.1 and 21 at.%Pt, after annealed at 1800°C for 12 hours plus 10 days at 900°C. Data were also collected from a sample with 21 at.%Pt which had been given a long term anneal of 30 days at 900°C following a 12 hour anneal at 1800°C (designated $Nb_{79}Pt_{21}$(II)). Except for 29.1 at.%Pt, the samples were mixed with high purity Si powder. Least square refinement of the integrated intensity data in each case was carried out with three variable parameters for the A-15 phase; an occupation parameter x as defined by the formula $(Nb_{3-x}Pt_x)[Pt_{1-x-y}Nb_{x+y}]$, an overall Debye-Waller factor B, and an instrumental scale factor. Scattering factors for neutral atoms and appropriate dispersion corrections were obtained by interpolation of published values[18] between 0.05Å^{-1} intervals of sin θ/λ. The results of these refinements are listed in Table XV. The accuracy of S determined in this way is about ±0.03.

It is evident that the three materials which had been given the normal annealing treatment, 12 hours at 1800°C plus 10 days at 900°C, are highly ordered, the amount of residual disorder being about 5% if the disorder due to nonstoichiometry is disregarded. The small negative value obtained for x in the sample of $Nb_{79}Pt_{21}$(II) which had been annealed for 30 days at 900°C obviously has no physical meaning and implies that more

TABLE XV

Results of Least-Squares Refinement of X-ray Diffractometer Data for Some A-15 Phases in the Nb-Pt System

	$Nb_{70.9}Pt_{29.1}$	$Nb_{74.9}Pt_{25.1}$	$Nb_{79}Pt_{21}$(I)	$Nb_{79}Pt_{21}$(II)
x	0.185(14)	0.036(9)	0.051(9)	-0.019(9)
B($Å^2$)	0.4(1)	0.3(1)	0.5(1)	0.4(1)
S_A	0.79	0.96	0.92	1.03
S_B	0.96	0.96	0.73	0.77
R	0.052	0.049	0.043	0.051
R_w	0.075	0.056	0.061	0.057
T_c(K)	5.1	10.7	4.8	6.2
a_o(Å)	5.1405	5.1545	5.1725	5.1725

realistic errors in x would be about double the statistical ones. This could easily arise from uncertainties in the scattering factors or an oversimplified model for the Debye-Waller factor. Nevertheless, the relative values of x for the two samples of 21 at.%Pt certainly suggest that the previously noted increase in T_c of about 1.5K following the prolonged anneal results from the elimination of a samll amount of residual disorder.

The effect of high energy (E>1MeV) neutron irradiations on T_c of Nb-Pt for different compositions is shown in Fig. 33 and the data are summarized in Table XVI. These irradiated samples are the same shown in Fig. 31, annealed 12 hours at 1800°C plus 10 days at 900°C. The upper curve of Fig. 33 shows the T_c of the unirradiated samples and the lower the irradiated, in terms of increasing fluence. In each of these curves, all the samples were irradiated at the same time to insure that they received the same neutron dose. A decrease in T_c is observed for all compositions with increasing fluence and also that the depression in T_c is less pronounced as we departure from the stoichiometric composition. At fluences higher than $2.6 \times 10^{19} n/an^2$ all compositions approach the same T_c (~2.4k), as shown by the horizontal line in Fig. 33. Figure 34a and b show the same data as a function of fluence for different compositions; in Fig. 34a we have the Nb-rich side of stoichiometry and in Fig. 34b the Pt-rich side. Here, we see more clearly some of the previous observations (Fig. 33), especially the saturation region above $2.6 \times 10^{14} n/cm^2$, common for all compositions.

Figure 33

Superconducting transition temperature, T_c, vs. composition of Nb-Pt unirradiated and irradiated to different neutron fluences (E > 1 MeV).

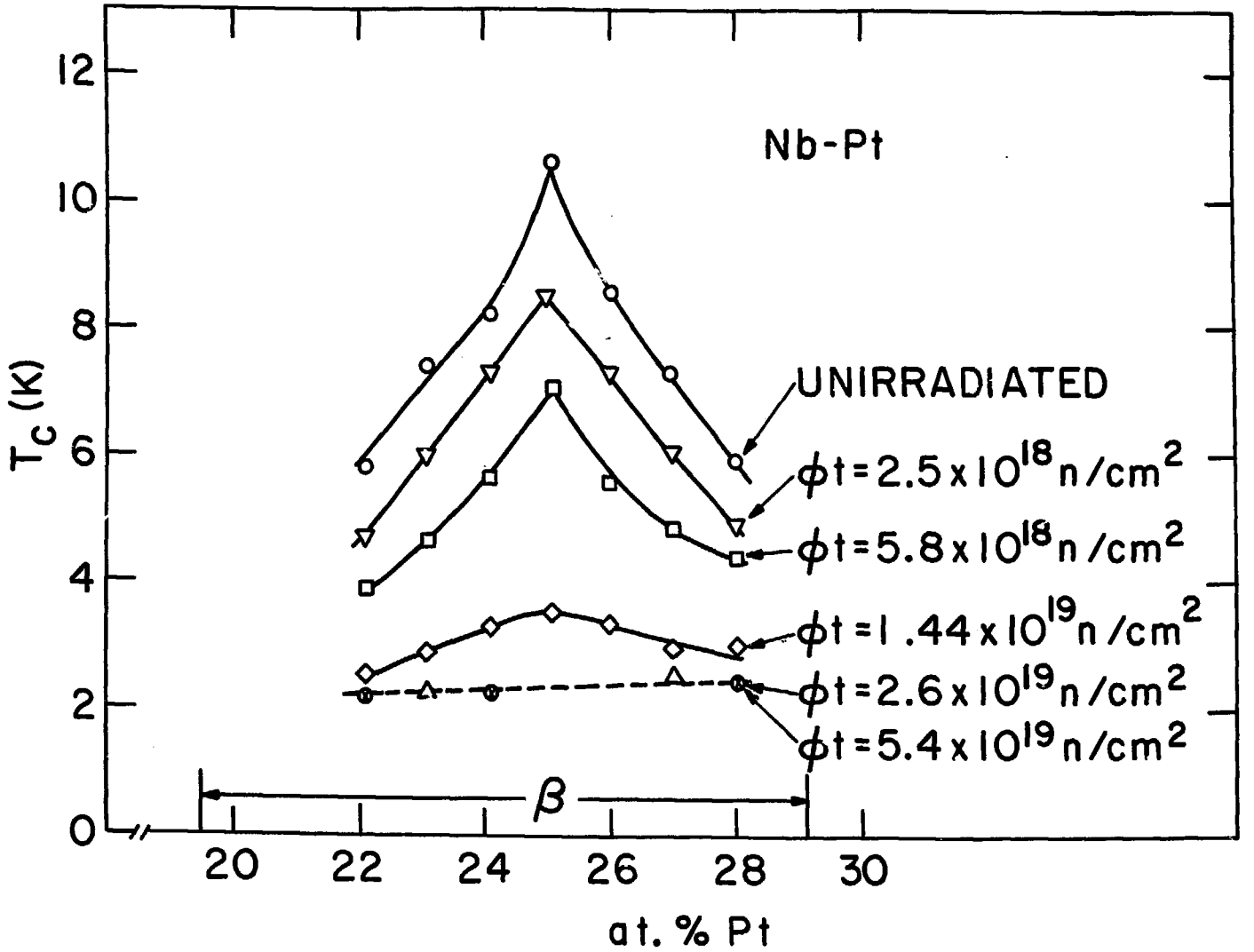
Nb-Pt
UNIRRADIATED
$\phi t = 2.5 \times 10^{18}$ n/cm^2
$\phi t = 5.8 \times 10^{18}$ n/cm^2
$\phi t = 1.44 \times 10^{19}$ n/cm^2
$\phi t = 2.6 \times 10^{19}$ n/cm^2
$\phi t = 5.4 \times 10^{19}$ n/cm^2
β
T_c (K)
at. % Pt
0
2
4
6
8
10
12
20
22
24
26
28
30

Fig. 33

TABLE XVI

Summary Data of Neutron Irradiated Nb-Pt

	$Nb_{77.9}Pt_{22.1}$				$Nb_{76.9}Pt_{23.1}$				$Nb_{75.9}Pt_{24.1}$			
$\phi t (n/cm^2)$	T_{c1}	T_{c3}	ΔT_c	a_o	T_{c1}	T_{c3}	ΔT_c	a_o	T_{c1}	T_{c3}	ΔT_c	a_o
0	7.57	5.81	0.86	5.167±0.001	8.33	7.43	0.27	5.1635±0.0005	8.57	8.23	0.15	5.1590±0.0005
2.5×10^{18}	6.26	4.71	0.41	-	7.09	6.02	0.33	5.1645±0.001	7.61	7.27	0.12	-
5.8×10^{18}	4.50	3.90	0.35	-	5.02	4.64	0.25	5.1665±0.001	6.79	5.63	0.33	-
1.44×10^{19}	2.70	2.54	0.16	-	3.12	2.90	0.21	5.170±0.001	3.38	3.28	0.14	-
2.6×10^{19}	-	-	-	-	2.42	2.27	0.18	5.1715±0.001	-	-	-	-
5.4×10^{19}	2.35	2.23	0.16	-	-	-	-	-	2.34	2.24	0.15	-

	$Nb_{74.9}Pt_{25.1}$				$Nb_{74}Pt_{26}$				$Nb_{73}Pt_{27}$			
$\phi t (n/cm^2)$	T_{c1}	T_{c3}	ΔT_c	a_o	T_{c1}	T_{c3}	ΔT_c	a_o	T_{c1}	T_{c3}	ΔT_c	a_o
0	10.88	10.63	0.34	5.1545±0.0005	10.12	8.55	0.45	5.1515±0.0005	7.78	7.29	0.21	5.1475±0.0005
2.5×10^{18}	8.64	8.49	0.21	5.156±0.001	8.25	7.32	0.23	-	6.79	6.06	0.35	5.149±0.001
5.8×10^{18}	7.12	7.04	0.45	5.1575±0.0005	6.46	5.58	0.25	-	5.32	4.88	0.22	5.152±0.001
1.44×10^{19}	3.69	3.54	0.14	5.1610±0.0005	3.59	3.38	0.14		3.34	2.99	0.40	5.156±0.001
2.6×10^{19}	-	-	-	5.164±0.001	-	-	-	-	2.71	2.53	0.20	5.157±0.001

TABLE XVI(Cont'd)

	$Nb_{72}Pt_{28}$			
$\phi t (n/cm^2)$	T_{c1}	T_{c3}	ΔT_c	a_o
0	6.79	5.91	0.40	5.144±0.001
2.5×10^{18}	5.82	4.91	0.47	-
5.8×10^{18}	4.82	4.42	0.22	-
1.44×10^{19}	3.20	3.01	0.16	5.1515±0.001
2.6×10^{19}	-	-	-	-
5.4×10^{19}	2.58	2.45	0.18	-

Figure 34a.

Superconducting transition temperature, T_c, as a function of neutron fluences (E > 1 MeV), for the Nb-rich side of stoichiometry in the A-15 phase of Nb-Pt.

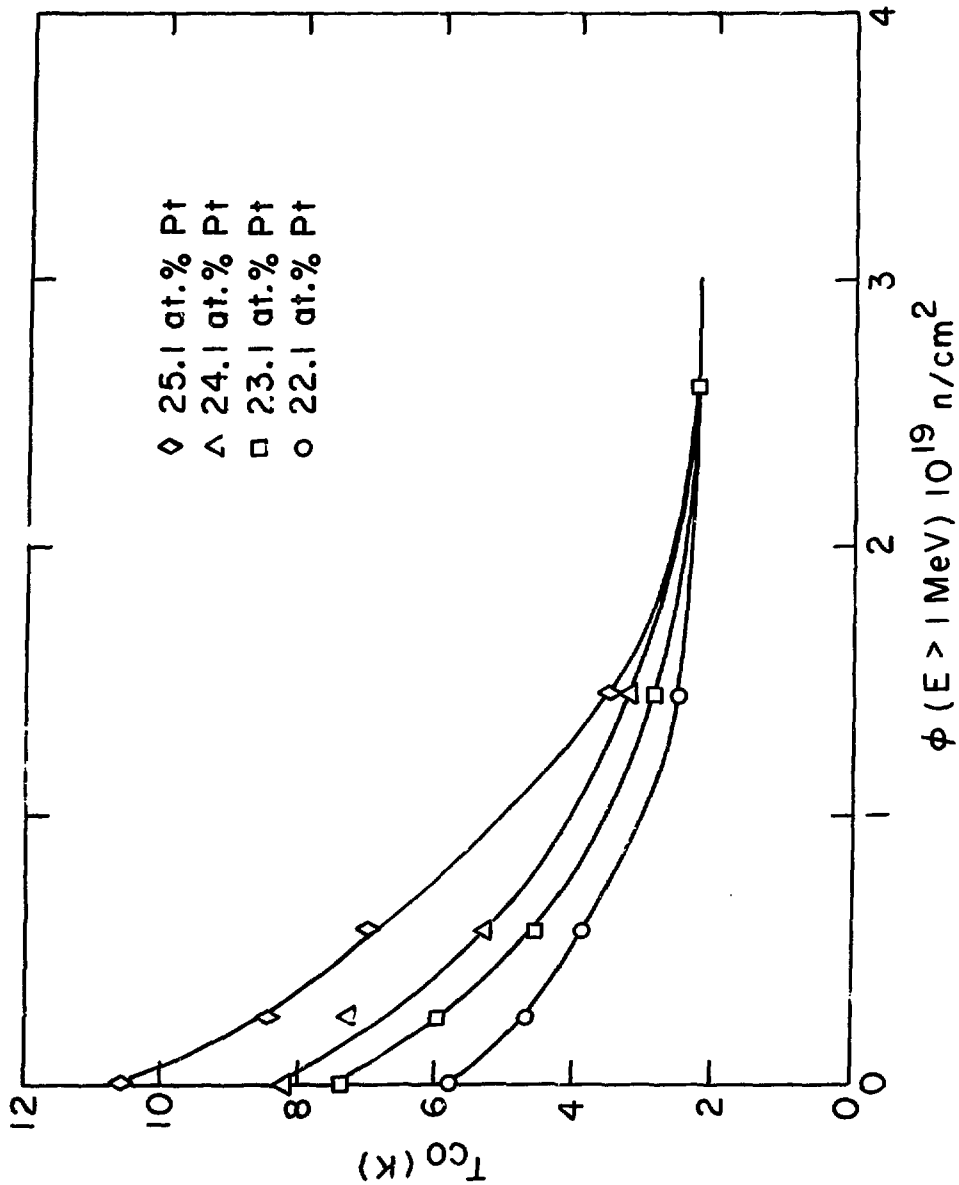
◇ 25.1 at.% Pt
△ 24.1 at.% Pt
□ 23.1 at.% Pt
○ 22.1 at.% Pt
T_{Co} (K)
ϕ (E > 1 MeV) 10^{19} n/cm^2
0
2
4
6
8
10
12
0
1
2
3
4

Fig. 34.a

Figure 34b.

Superconducting transition temperature, T_c, as a function of neutron fluence (E > 1 MeV), for the Pt-rich side of stroichiometry in the A-15 phase of Nb-Pt.

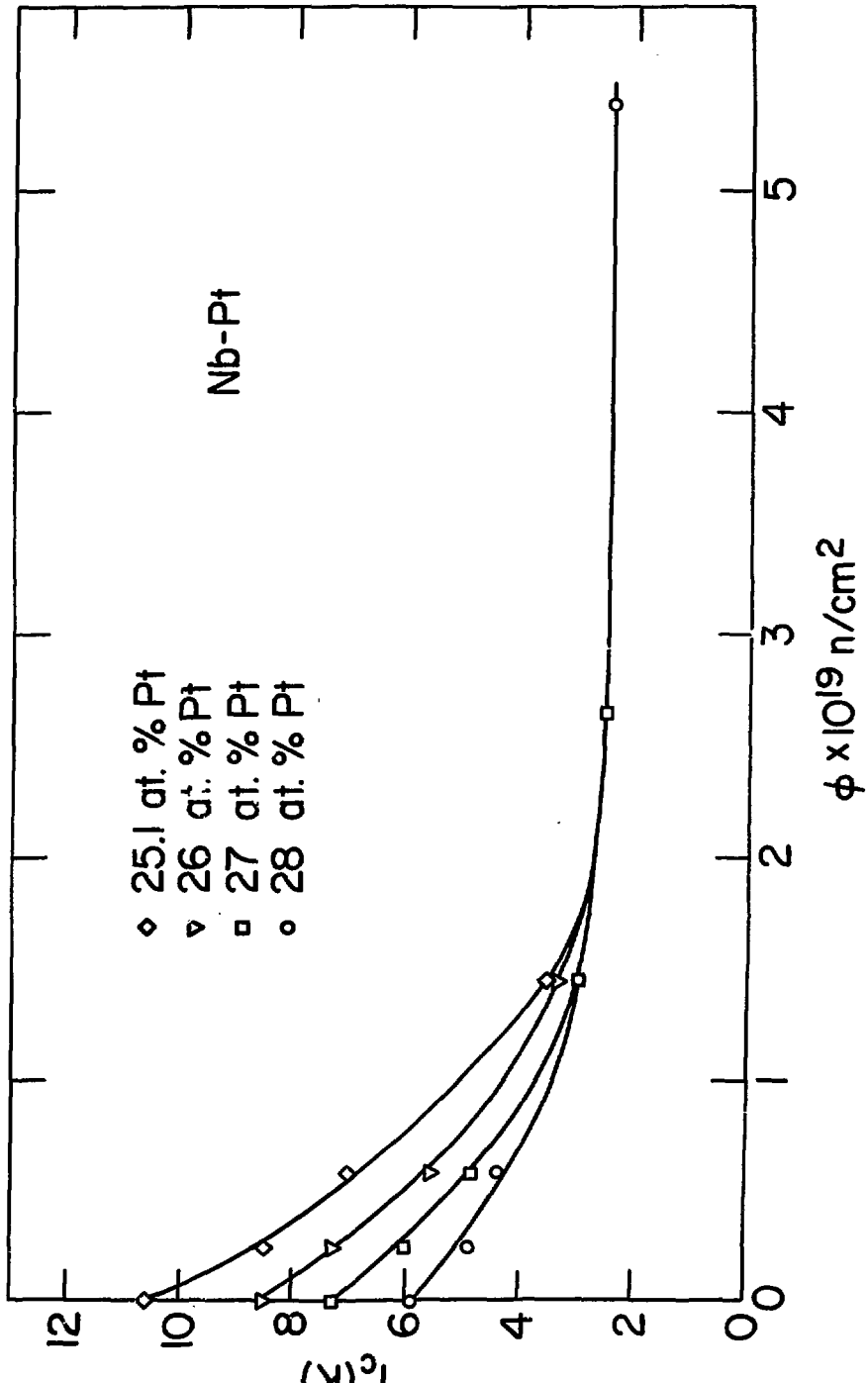
Nb-Pt
◇ 25.1 at. % Pt
▽ 26 at. % Pt
□ 27 at. % Pt
○ 28 at. % Pt
T_c(K)
0
2
4
6
8
10
12
$\phi \times 10^{19}$ n/cm^2
0
1
2
3
4
5

Fig. 3.1.b

These results for single phase samples encompassing both sides of stoichiometry show surprisingly the same general characteristic as previously observed for the Nb-rich side of the Nb-Al system where some second phase was present. Another interesting fact that occurs in the Nb-Pt system is that by changing the composition to 19 at.%Pt (sample with 5% bcc phase and corrected composition: 19.5 at.%Pt) the same T_c for the neutron irradiated sample at the saturation region is obtained. This latter observation is essentially the same noted in the CVD Nb_3Ge(IV) material prepared with an unusually low T_c.

The transition widths, ΔT_c, for Nb-Pt (Table XVI) show, as in Nb-Al, a small or no increase at low fluences and a decrease at high fluences.

The lattice parameter, a_o, of the irradiated samples are shown in Fig. 35a and b. Fig. 35a shows the lattice parameter of the unirradiated and irradiated samples at $1.44 \times 10^{19} n/cm^2$ for different compositions and Fig. 35b shows how a_o expands as a function of fluence for 23.1, 25.1 and 27 at.%Pt. From these two figures we see that for a given fluence the lattice parameter is expanded by a constant factor in all compositions (Fig. 35a) and that the a_o dependence on fluence is the same for different compositions (Fig. 35b). This behavior of a_o for both sides of stoichiometry of Nb-Pt is similar to that observed in the Nb-rich side of Nb-Al.

The lattice parameter of the sample with 25.1 at.%Pt after being irradiated to a fluence of $5.8 \times 10^{18} n/cm^2$ shows an

Figure 35a.

Lattice parameter, a_o, as a function of composition, for Nb-Pt unirradiated and irradiated to 1.44×10^{19} n/cm^2.

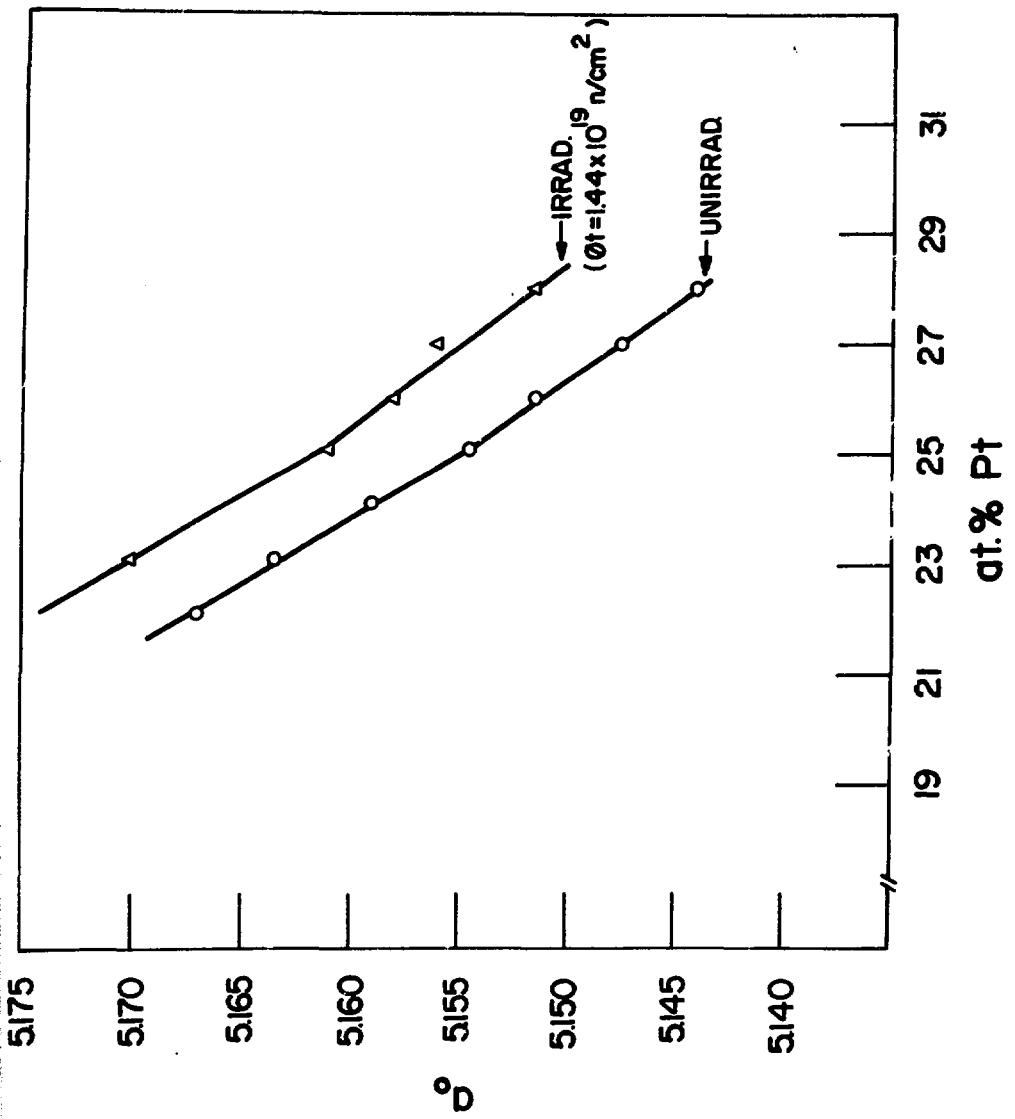
IRRAD.
(Øt=1.44x10^19 n/cm^2)
UNIRRAD
at.% Pt
19
21
23
25
27
29
31
°D
5.175
5.170
5.165
5.160
5.155
5.150
5.145
5.140

Fig. 35.a

Figure 35b.

Lattice parameter, a_o, as a function of neutron fluence, for Nb-Pt alloys in the A-15 phase field.

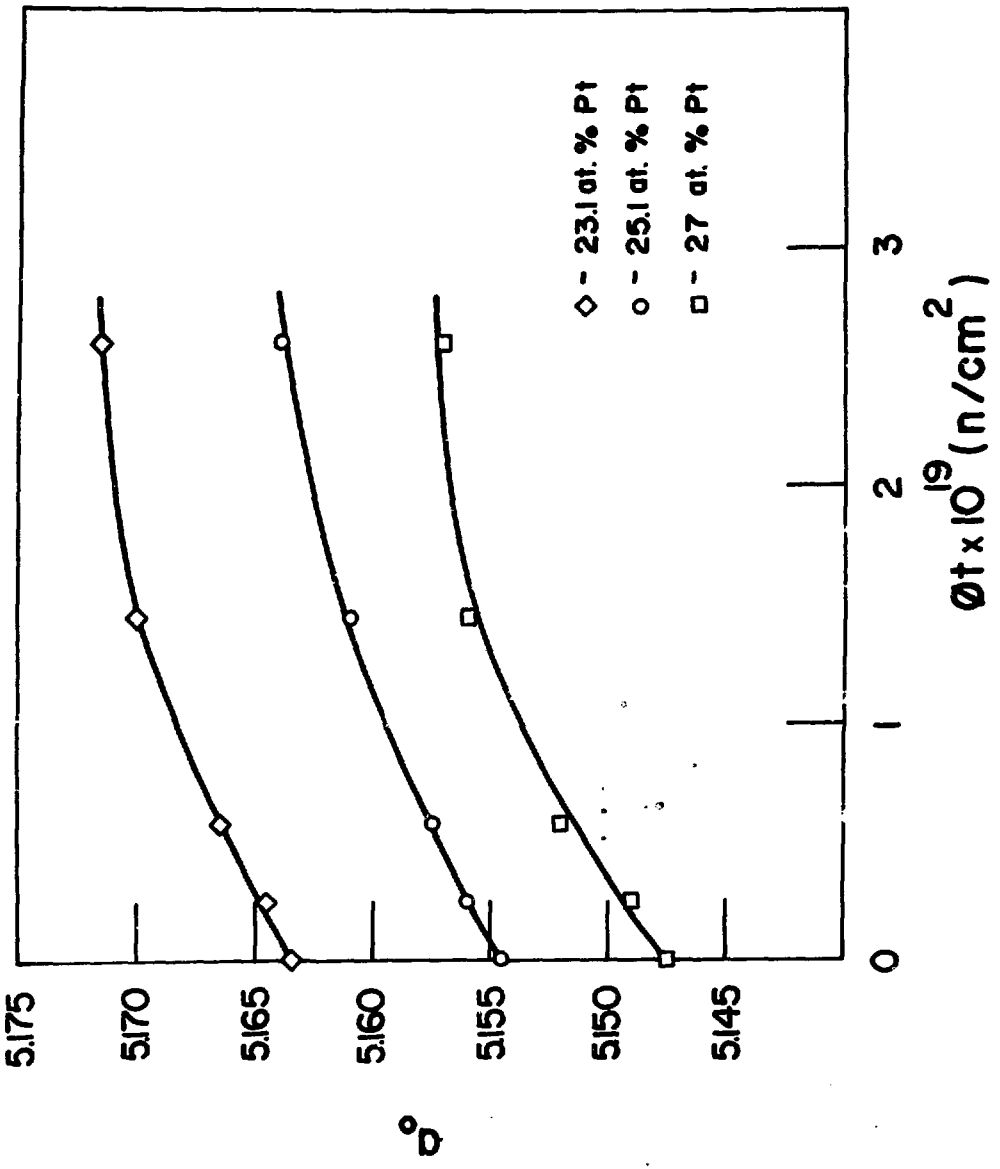
◇ - 23.1 at. % Pt
○ - 25.1 at. % Pt
□ - 27 at. % Pt
5.175
5.170
5.165
5.160
5.155
5.150
5.145
°D
0
1
2
3
Øt x 10^19 (n/cm^2)

Fig. 35.b

increase of 0.06%. The T_c of this irradiated sample (7.04K) is the same as that observed in this same sample after being rapidly quenched from high temperatures (7.13K) where an expansion in a_o of only 0.02% was measured which again suggests the lack of correlation of a_o with T_c.

From the Debye-Scherrer x-ray patterns we observe that the intensities of all the difference lines decrease with increasing fluence and after a fluence of $2.6 \times 10^{19} n/cm^2$ all the difference lines could no longer be observed in the x-ray films. This could not be attributed to the increase of the γ-radiation background as other structure lines with intensities equivalent or smaller than the difference lines, like the (222) line, were clearly visible even at high fluences where the difference lines could not be observed. This decrease in intensity of the difference lines with fluence imply a decrease in the long range order parameter which was confirmed by the LRO measurements in some of the irradiated samples. These observations proved to be a useful tool for a quick qualitative observation of the decrease in the LRO. Here, as in the Nb-Al system, no line broadening was noted even in the most heavily irradiated samples. Also, no large lattice expansions were observed at high fluences (Fig. 35 b).

The long range order parameter of the irradiated stoichiometric sample was measured at fluences of $5.8 \times 10^{18} n/cm^2$ and $1.44 \times 10^{19} n/cm^2$ with T_c of 7.04K and 3.54K and a_o of 5.1575Å and 5.1610Å, respectively, were obtained. The data collection and the refinement procedures were the same as described

previously. The final parameters are summarized in Table XVII, and Fig. 36 shows how T_c varies with the percentage of Nb sites occupied by Pt atoms. Fig. 36 also includes the LRO measurements of Flukiger[11] in a samples with composition close to stoichiometry quenched from different temperatures with different cooling rates. From this figure we can see that the T_c depression with increasing disorder for these two processes (irradiation and quenching) are quite similar, even though no low T_c data exists for the quenched samples due to the limits of this technique.

Figures 37 and 38 show how T_c recovers with the isochronal anneal for three samples with compositions 23.1, 25.1 and 27 at.%Pt irradiated to a fluence of $1.44 \times 10^{19} n/cm^2$ and also the sample with 27 at.%Pt irradiated to $2.6 \times 10^{19} n/cm^2$. From these figures we can see that T_c begins to show recovery only above 400^oC independent of composition or fluence, as observed previously in the Nb-Ge and Nb-Al samples. However, here the rate of recovery is less pronounced as in the Nb-Ge and Nb-Al.

V-Ga: For the V-base A-15 compounds V-Ga has the largest range of homogeneity and one of the highest critical temperatures (~15.5K). The phase diagram of this system is well known principally by the work of van Vucht et. al.[70] and with the A-15 phase studies in more details by Das et al.[43] and Flukiger et al.[71]. The superconducting properties of the A-15 phase of this system have been the subject of several investigations[42-44,70-74] and the purpose of this study was to study the A-15 phase of V-Ga in a similar manner to the Nb-Al system as described previously.

TABLE XVII

SUMMARY DATA OF LRO MEASUREMENTS ON $Nb_{74.9}$ $Pt_{25.1}$ NEUTRON IRRADIATED

	UNIRRAD.	5.8×10^{18} n/cm^2	1.44×10^{19} n/cm^2
X	0.036(9)	0.094(14)	0.311(13)
B(Å^2)	0.3(1)	0.34(1)	0.59(15)
S_A	0.96	0.87	0.58
S_B	0.96	0.88	0.59
R	0.049	0.080	0.145
R_W	0.056	0.071	0.114
T_c(K)	10.63	7.04	3.54
a_o(Å)	5.1545	5.1575	5.1610

Figure 36

Superconducting transition temperature, T_c, as a function of the percentage of Nb sites occupied by Pt atoms. Circles and squares represent respectively, radiation-induced and thermally-induced disorder[11].

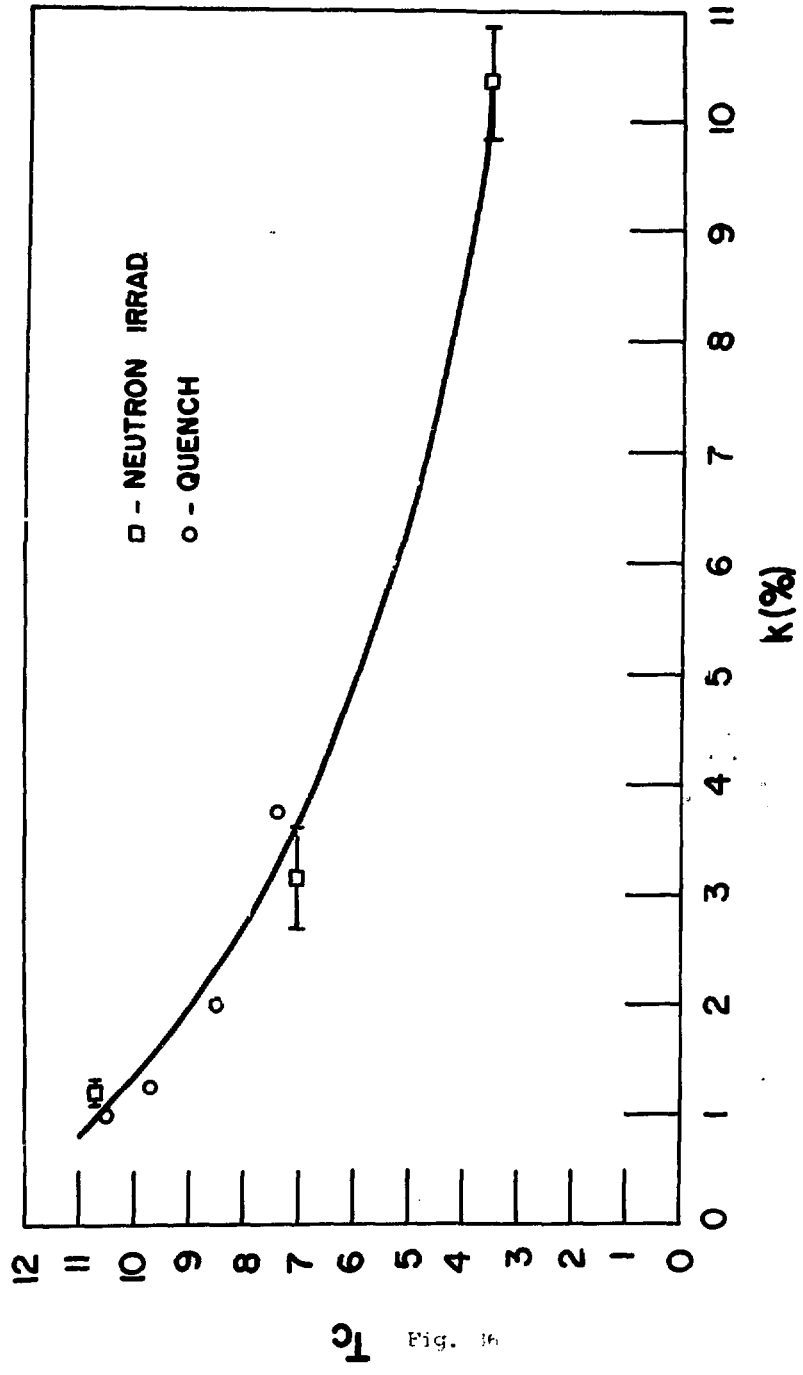

Fig. 16

Figure 37

Isochronal annealing curve showing the recovery of T_c for two Nb-Pt alloys irradiated to a fluence of $1.44 \times 10^{19} n/cm^2$. Lattice parameters are also given. Upper circles represent T_c onsets, and vertical bars indicate transition widths (10-90%).

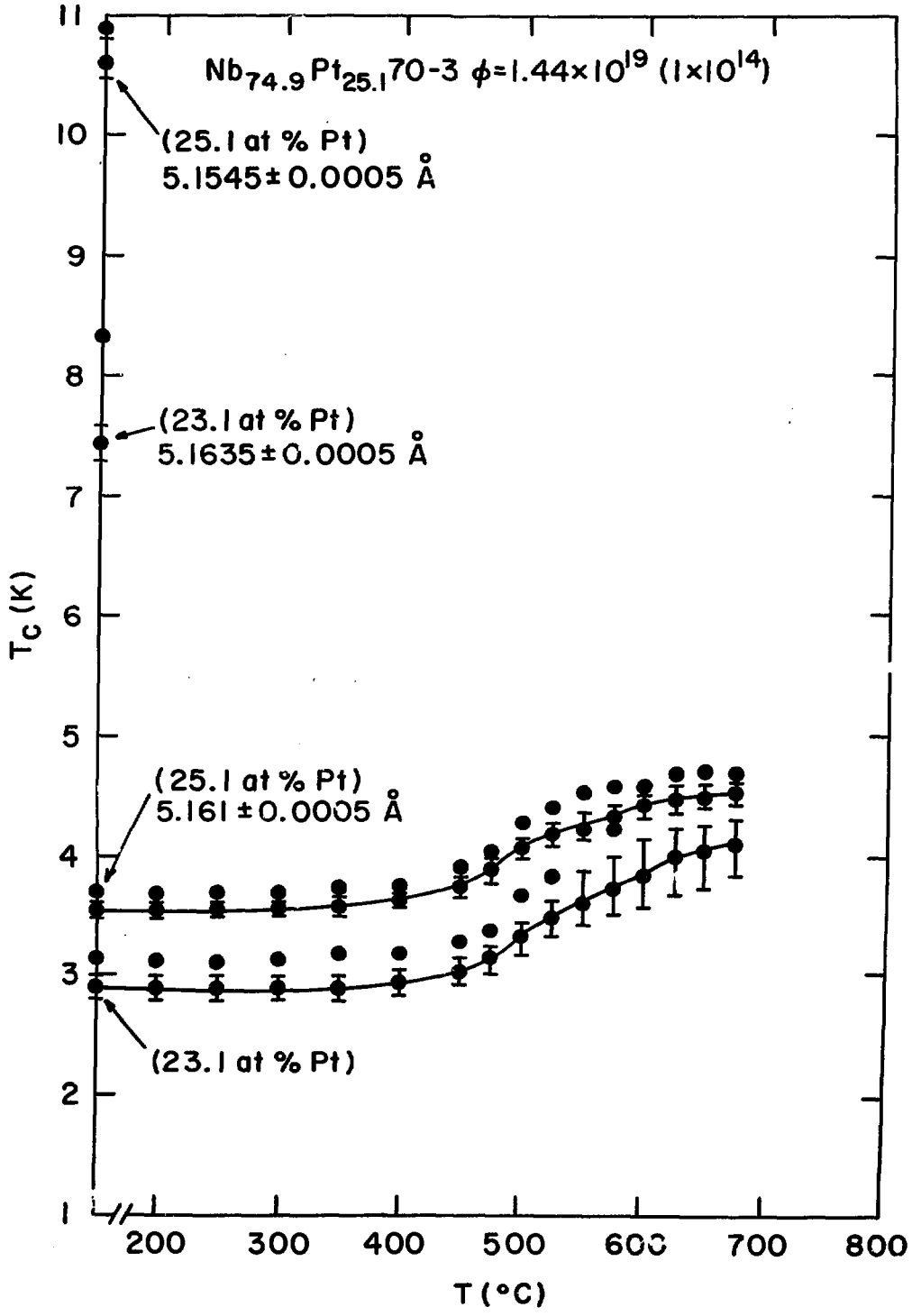
$Nb_{74.9}Pt_{25.1}$70-3 ϕ=1.44×10^{19} (1×10^{14})
(25.1 at % Pt)
5.1545±0.0005 Å
(23.1 at % Pt)
5.1635±0.0005 Å
(25.1 at % Pt)
5.161±0.0005 Å
(23.1 at % Pt)
T_c (K)
T (°C)
1
2
3
4
5
6
7
8
9
10
11
200
300
400
500
600
700
800

Fig. 37

Figure 38

Isochronal annealing of T_c for $Nb_{73}Pt_{27}$ neutron irradiated to two different fluences. Upper circles represent T_c onsets, and vertical bars indicate transition widths (10-90%).

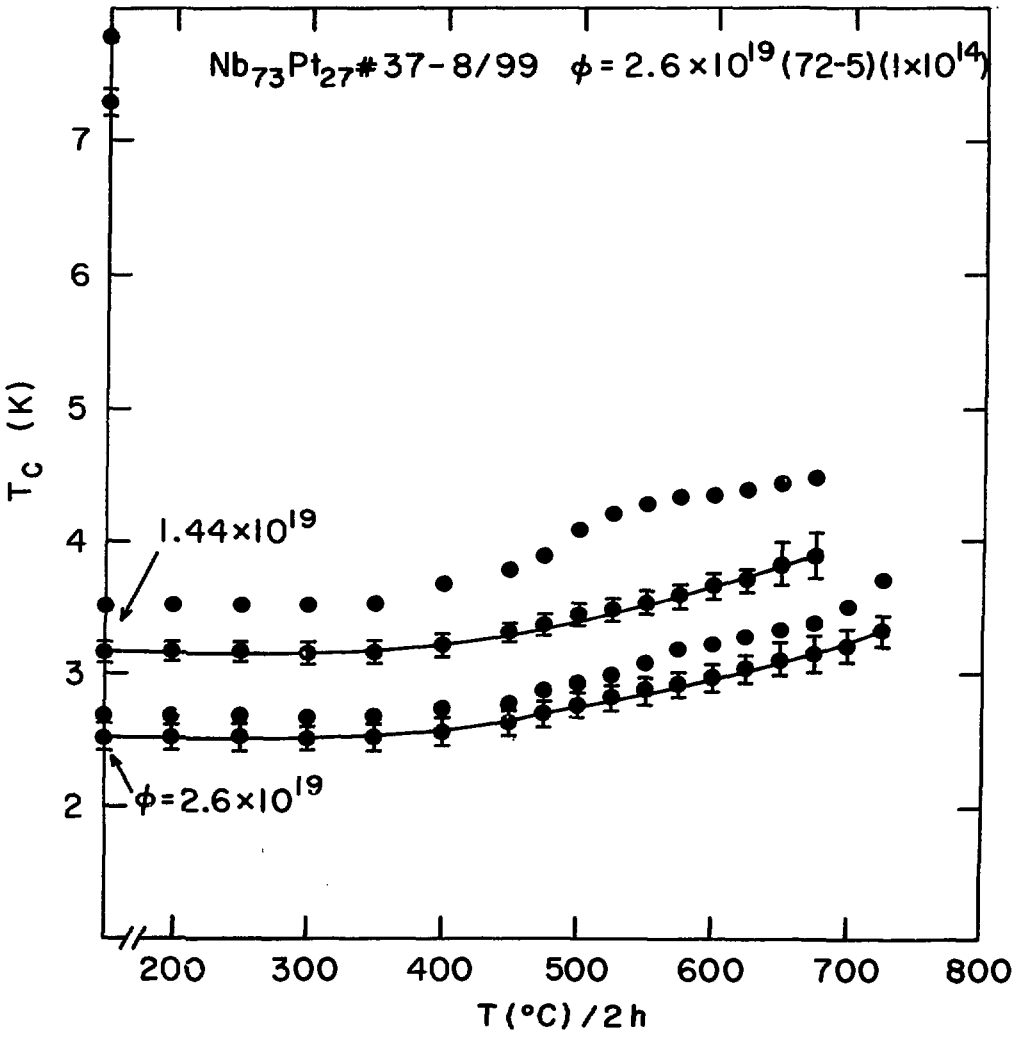
Nb73Pt27#37-8/99 φ = 2.6×10^19 (72-5)(1×10^14)
Tc (K)
7
6
5
4
3
2
1.44×10^19
φ=2.6×10^19
200
300
400
500
600
700
800
T(°C)/2h

Fig. 38

In the homogeneity range of the A-15 phase (21-31.5 at.% Ga[43]) several samples with different compositions were prepared. After casting, these samples were heat treated for 6 hours in the V-rich solid solution field, at 1400°C, to homogenize the alloys. The samples were then retransformed to the A-15 structure by annealing for 24 hours in the A-15 field (1100°C-1200°C), and finally annealed at low temperatures (650°C) for one week, with these treatments homogeneous single phase (>95%) A-15 samples were obtained. The complete heat treatment for each composition is summarized in Table XVIII together with their T_{c1}, T_{c3}, ΔT_c and a_o. The superconducting transition temperature, T_{c3}, and the lattice parameter, a_o, for the annealed samples are shown in Fig. 39, as a function of at.%Ga. From this figure we can see that T_c is a maximum at the stoichiometric composition and decreases on both sides of stoichiometry with an average slope of ~1.5K/at.%Ga. It is interesting to note that the same slope was also found in the Nb-Pt system, however, the sharp peak in T_c at stoichiometry observed in the Nb-Pt does not occur in V-Ga.

From the lattice parameters of these annealed samples, shown in Fig. 39 we can see that a_o increases with increasing Ga concentration, where in Nb-Pt a decrease was observed. This is because the Ga radius (1.38Å) is larger than the V(1.31Å). A break in the slope at stoichiometry was also observed, as in Nb-Pt, and previously noted in this system[42,43]. The T_c and a_o dependence with composition are in good agreement with previous

TABLE XVIII

Summary of Data for A-15 Phase of V-Ga

COMPOSITION	HEAT TREATMENT	T_{c1}	T_{c3}	ΔT_c	a_o	REMARKS
$V_{79.5}Ga_{20.5}$	As Cast	14.16	11.05	3.69	N.M.	A-15+Nb_{SS}
$V_{79.5}Ga_{20.5}$	2 hrs 1400°C+48 hrs 1150°C+ + 1 week 650°C	9.92	9.74	0.22	4.814 ±0.001	A-15+Nb_{SS}
$V_{77.8}Ga_{22.2}$	As Cast	14.30	12.19	3.49	N.M.	A-15
$V_{77.8}Ga_{22.2}$	6 hrs 1400°C+24 hrs 1200°C+ +1 week 650°C	12.85	12.41	0.45	4.815 ±0.001	A-15
$V_{76.4}Ga_{23.6}$	As Cast	14.21	14.15	0.08	N.M.	A-15
$V_{76.4}Ga_{23.6}$	6 hrs 1400°C+24 hrs 1200°C+ +1 week 650°C	15.42	14.80	0.48	4.816 ±0.001	A-15
$V_{75.2}Ga_{24.8}$	As Cast	-	-	-	N.M.	A-15
$V_{75.2}Ga_{24.8}$	6 hrs 1400°C+48 hrs 1170°C+ +1 week 650°C	15.46	15.31	0.23	-	A-15
$V_{74.7}Ga_{25.3}$	As Cast	14.31	14.16	0.27	N.M.	A-15
$V_{74.7}Ga_{25.3}$	6 hrs 1400°C+24 hrs 1200°C +1 week 650°C	15.53	14.28	1.30	4.8185 ±0.001	A-15
$V_{73.5}Ga_{26.5}$	As Cast	14.22	14.06	0.27	N.M.	A-15
$V_{73.5}Ga_{26.5}$	6 hrs 1400°C+24 hrs 1150°C+ +1 week 650°C	15.32	12.98	0.90	4.8195 ±0.001	A-15
$V_{71.9}Ga_{28.1}$	As Cast	14.36	9.84	3.24	N.M.	A-15
$V_{71.9}Ga_{28.1}$	6 hrs 1400°C+24 hrs 1150°C+ +1 week 650°C	13.18	10.20	2.46	4.8225 ±0.001	A-15
$V_{70.4}Ga_{29.6}$	As Cast	14.33	8.28	5.58	N.M.	A-15
$V_{70.4}Ga_{29.6}$	6 hrs 1350°C+24 hrs 1100°C+ +1 week 650°C	10.28	7.98	1.55	4.825 ±0.001	A-15

N.M. - Not Measured

Figure 39

Superconducting transition temperature, T_c, (midpoints) and lattice parameter, a_o, vs. composition for the V-Ga system.

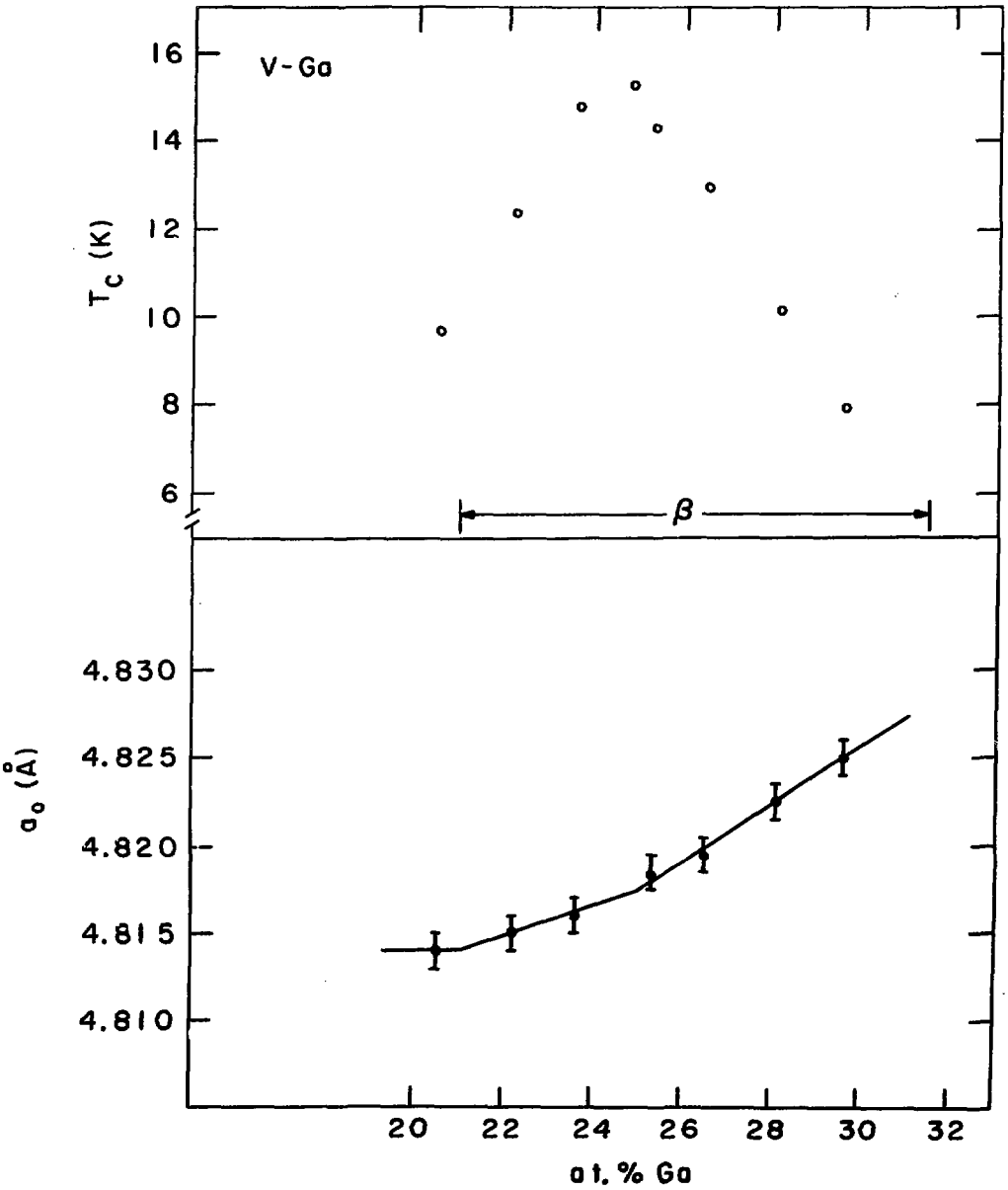
V-Ga
16
14
12
10
8
6
T_c (K)
β
4.830
4.825
4.820
4.815
4.810
a_o (Å)
20
22
24
26
28
30
32
at. % Ga

Fig. 39

work[43,71,73] where the long range order parameter was also measured which indicated that the annealed samples are nearly fully ordered.

The samples with different compositions were irradiated with high energy neutrons in the same manner as the previous Nb-base A-15 compounds. However, only a slight T_c depression (≲3K) was observed even at high fluences (2.6 x 10^{19}n/cm^2) and a rather random T_c distribution with fluence for the different composition was observed. The reasons for this are not clear at the present time, as other irradiated V-base A-15 compounds, such as α irradiated V_3Si and V_3Ge[75], and neutron irradiated V_3Si[76] and V_3Ga[77] do behave as would be expected.

A V_3Si sample[76] neutron irradiated to a fluence of 2.6 x 10^{19}n/cm^2 had its T_c (16.7K) depressed to 2.6K and after 2 years at room temperature a T_c increase of 0.8K was observed. This sample was isochronally annealed for 2 hours at each temperature, and the results are shown in Fig. 40. From this figure we can see that T_c starts to show recovery at temperatures lower than the Nb-base compounds (~400°C) and even at 250°C some recovery is observed. This result, together with the fact that the thermal neutron absorption cross section[78] of V is more than 4 times greater than that of Nb and the thermal conductivity[78] of V is only half that of Nb, may indicate that the V-Ga samples were overheated during radiation and some of the damage annealed out. Different geometries of the Al capsule and packing of the samples with Al powder to improve the

Figure 40

Isochronal annealing curve for neutron irradiated V_3Si. Upper circles represent onset temperatures, while error bars represent transition widths (10-90%).

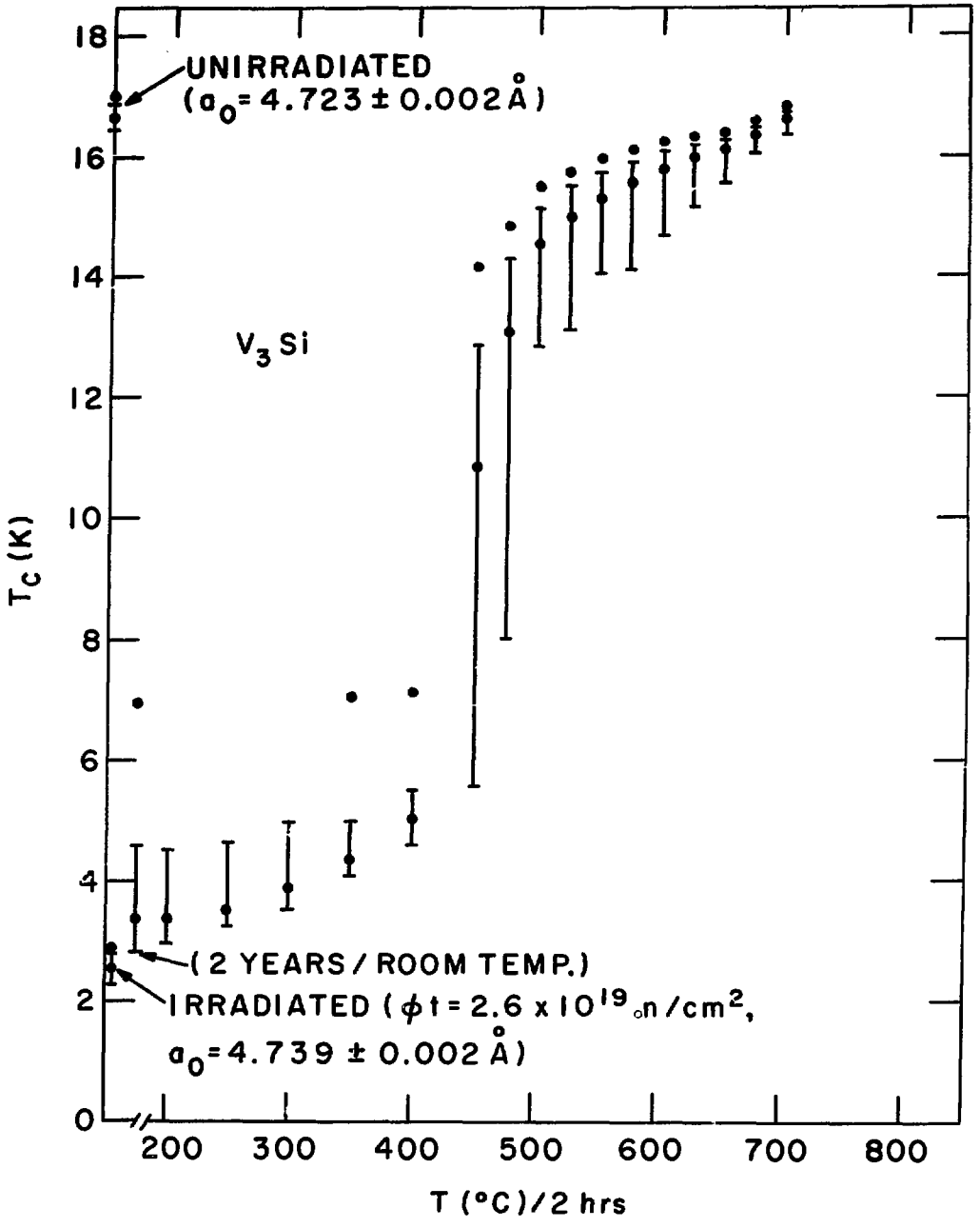
UNIRRADIATED
(a_0 = 4.723 ± 0.002 Å)
V_3Si
(2 YEARS / ROOM TEMP.)
IRRADIATED ($\phi t = 2.6 \times 10^{19}$ n/cm^2,
a_0 = 4.739 ± 0.002 Å)
T_c (K)
T (°C)/2 hrs
0
2
4
6
8
10
12
14
16
18
200
300
400
500
600
700
800

Fig. 40

thermal conductivity were used, but no significant change was obtained.

$\underline{Mo_3Os}$: The interest in studying this system lies in the fact that both elements are transition metals while in the previous systems studied the B elements (Ge, Al and Ga) were non-transition metals or have the f-band nearly full, like Pt. Besides, this system has the highest T_c (12-13K)[11,12,79,80] of these sd-sd type bonding A-15 compounds.

Here we studies the effect of neutron induced disorder on T_c and a_o, coupled with isochronal anneals.

The phase diagram of Mo-Os was investigated by Taylor et al.[81], where the A-15 phase of Mo_3Os forms at 2210°C via a peritectoid reaction with a homogeneity range very narrow, ranging from about 24.0 to 25.5 at.%Os at 1000°C. Due to this narrow range of the A-15 phase no composition studies were possible. A stoichiometric sample was arc-cast and subjected to the following heat treatment: 15 hours/1850°C + 25 hours/1450°C + 10 days/1000°C + 9 days/950°C + 20 days/800°C. After these heat treatments, x-ray diffraction analyses indicated the sample to be single phase and of the A-15 structure type with lattice parameter a_o = 4.968±0.001Å, and a transition temperature, T_{c3}, of 12.62K, is good agreement with previously reported value[11,12,19,79,80]. This sample was neutron irradiated to fluences of 1 x 10^{20} n/cm^2 and the results are summarized in Table XIX. Fig. 41 shows the T_c dependence on fluence together with the results of a neutron irradiated Nb_3Al sample[64], an A-15 compound with sd-sp type

TABLE XIX

Summary of Data for Mo_3Os Neutron Irradiated

FLUENCES	T_{c1}	T_{c3}	ΔT_c	a_o	S_A
0	12.77	12.64	0.21	4.968±0.001	0.89
2.5×10^{18} n/cm^2	12.37	12.26	0.21	4.970±0.001	0.86
5.8×10^{18} n/cm^2	12.36	11.99	0.21	4.971±0.001	0.82
1.7×10^{19} n/cm^2	11.17	11.06	0.15	-	0.69
4.9×10^{19} n/cm^2	10.47	10.31	0.19	4.976±0.001	0.44
1.03×10^{20} n/cm^2	10.29	10.09	0.28	4.9785±0.001	0.20

Figure 41

Superconducting transition temperature, T_c, against neutron fluence (E > 1 MeV) for Mo_3Os. Neutron irradiated Nb_3Al is shown for comparison.

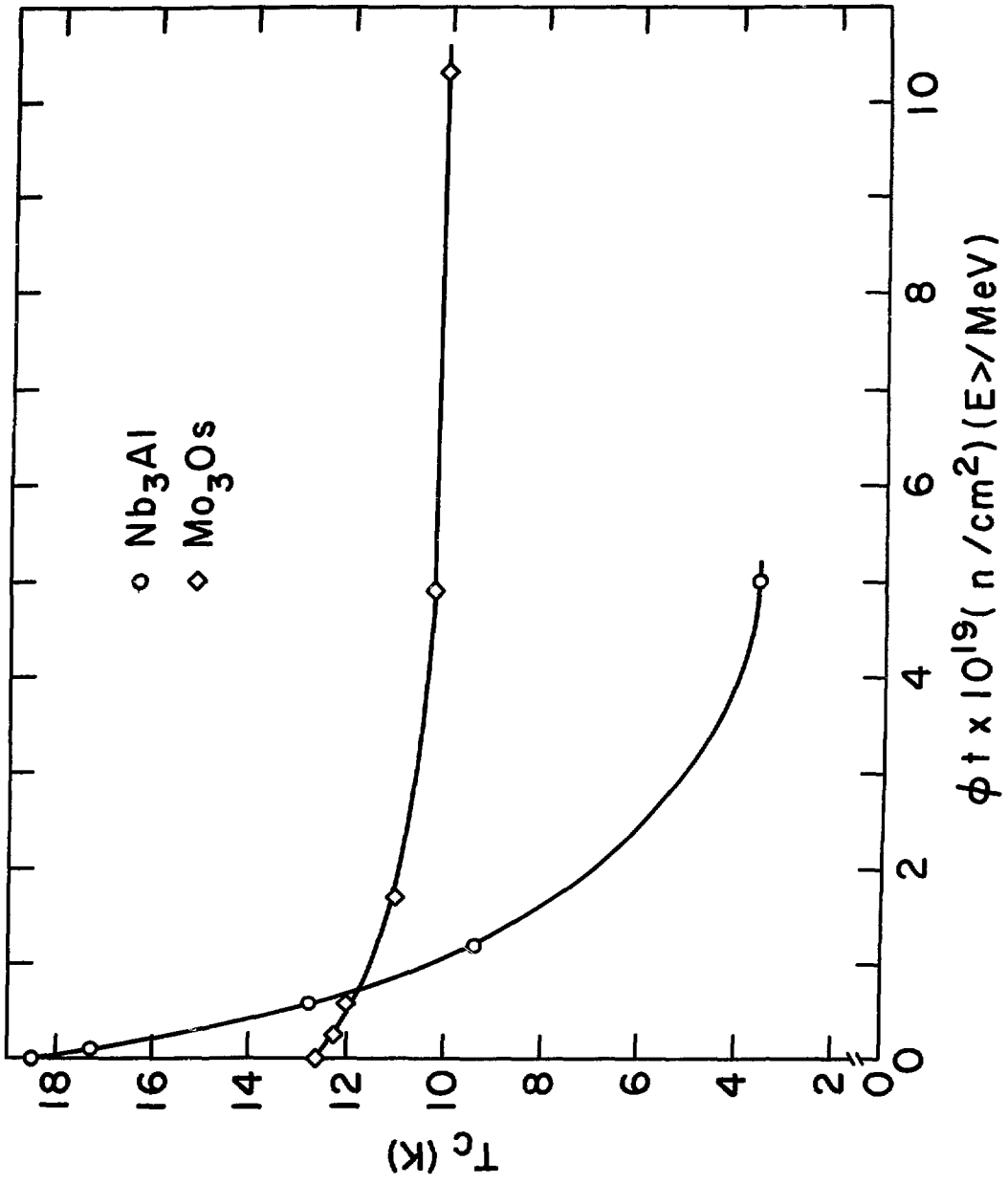
T_c (K)
18
16
14
12
10
8
6
4
2
0
0
2
4
6
8
10
$\phi t \times 10^{19}$(n /cm^2) (E>/ MeV)
o Nb_3Al
◇ Mo_3Os

Fig. 41

bonding. It is clearly seen from this figure that the depression of T_c, for a given neutron fluence, for Mo_3Os is considerably less than for Nb_3Al. Where the depression of T_c for Nb_3Al was about 3.1K, 5.7K and 14.9K, the corresponding values for Mo_3Os were 0.4K, 0.6K and 2.3K respectively. At high fluences ($>5 \times 10^{19} n/cm^2$) the transition temperature of Mo_3Os approached a saturation of about 10K.

Fig. 42 shows how the lattice parameter of the same sample of Fig. 41 depends on fluence together with the a_o's of irradiated Nb_3Al[64]. From this figure we can see that the lattice parameter of Mo_3Os expands with increasing fluence ($\frac{\Delta a_o}{a_o} = 0.16$ %, at $4.9 \times 10^{19} n/cm^2$) but this expansion is less pronounced than for Nb_3Al ($\frac{\Delta a_o}{a_o} = 0.33$ at $5 \times 10^{19} n/cm^2$). At high fluences no large lattice expansion was observed as in Nb_3Ge.

From the Debye-Scherrer x-ray films of these samples we could clearly observe the decrease in intensity of the difference lines with increasing fluence. After a fluence of $4.9 \times 10^{19} n/cm^2$ no difference line could be observed in the x-ray films. This behavior, as observed previously in other systems studied, indicates a decrease in the degree of order.

Flukiger[11] and Flukiger et al.[80] have determined the long range order parameter, S_A, as a function of T_c for Mo_3Os over the range $0.79 \leq S_A \leq 0.87$ and $11.75 \leq T_c \leq 12.45$ by annealing techniques. We previously observed, in the Nb-Pt system (Fig.36), that the T_c dependence on the order parameter is the same for neutron irradiated samples and for those samples subjected to different

Figure 42

Lattice parameter, a_o, against neutron fluence (E > 1 MeV). Nb_3Al is shown for comparison.

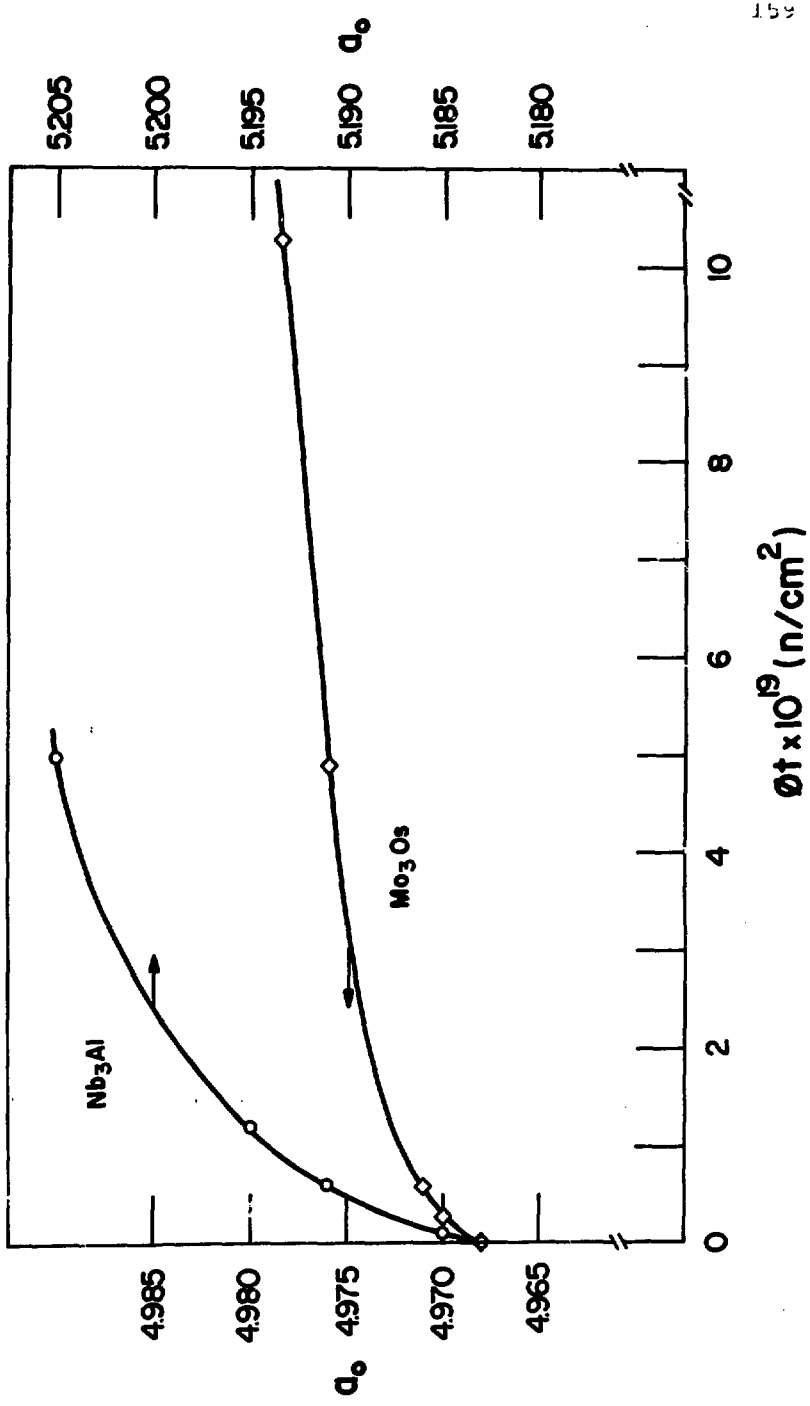
5.205
5.200
5.195
5.190
5.185
5.180
a_o
Nb_3Al
Mo_3Os
4.985
4.980
4.975
4.970
4.965
a_o
0
2
4
6
8
10
$\phi t \times 10^{19} (n/cm^2)$

Fig. 42

heat treatments. Applying this to Mo_3Os and using Flukinger's data, the T_c dependence on S_A for the irradiated Mo_3Os can be obtained using the Aronin expression[82]. Aronin has pointed out that the long range order parameter can be related to the neutron fluence by a relation of the type $S = Soe^{-k\phi t}$, where So is the value of S before irradiation, ϕt the neutron fluence and k is a proportionality constant independent of fluence. In systems where S has been measured as a function of neutron fluence, such as Cu_3Au[82], Ni_3Mn[82] and Nb_3Al[64], the above relationship agrees well with observation. For our neutron irradiated Mo_3Os samples having T_{c3} values of 12.26K, 11.99K and 11.06K, corresponding to fluences of 2.5×10^{18}, 5.8×10^{18} and $1.7 \times 10^{19} n/cm^2$ respectively, order parameters of 0.86, 0.82 and 0.69 were obtained from Flukiger's data. With these order parameters it was possible to calculate a value of k, enabling us to extend the range of S_A from 0.79-0.87 to 0.20-0.89, as seen in Fig. 43. The value of k was $1.4 \times 10^{-20} cm^2/n$ with an estimated uncertainty of ±0.4, and So = 0.89. As a function of S_A also shown in Fig. 43 is the T_c of neutron irradiated Nb_3Al[64]. We see that the depression of T_c for a given change in S_A is considerably greater for Nb_3Al, a sd-sp type A-15 compound, than for the Mo_3Os, a sd-sd type. Which may indicate that the type of bonding is responsible for the different behavior of these two types of A-15 compounds with respect to the effect of ordering on T_c.

A pure Mo(T_c = 0.9K) was irradiated to a fluence of $1.5 \times 10^{20} n/cm^2$ and no superconducting transition was found to the lower limit of our T_c apparatus (~1.3K).

Figure 43

Superconducting transition temperature, T_c, as a function of the Bragg-Williams long range order parameter for neutron irradiated and quenched Mo_3Os (see text). Neutron irradiated Nb_3Al is shown for comparison.

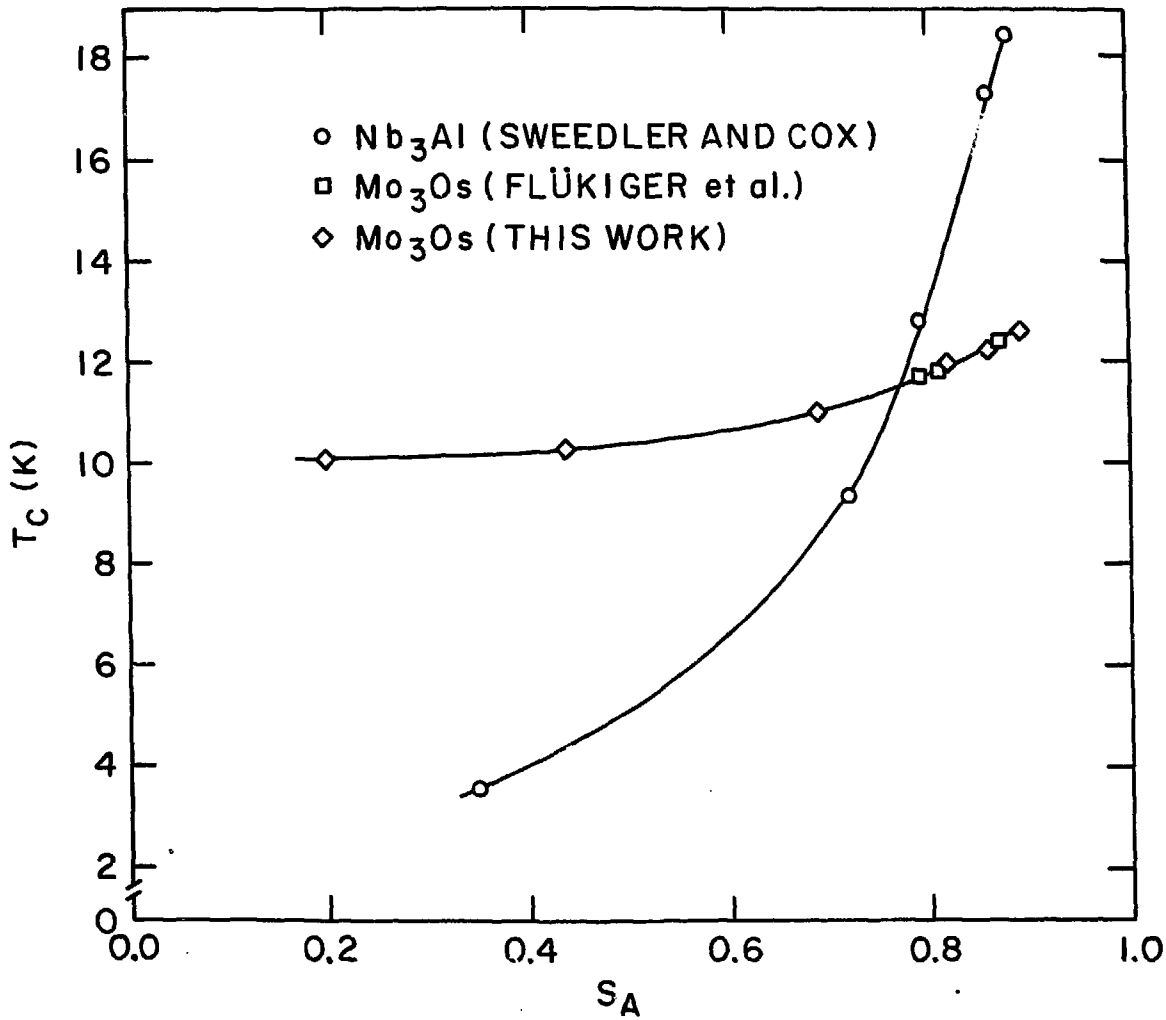
18
16
14
12
10
8
6
4
2
0
0.0
0.2
0.4
0.6
0.8
1.0
T_C (K)
S_A
o Nb_3Al (SWEEDLER AND COX)
□ Mo_3Os (FLÜKIGER et al.)
◇ Mo_3Os (THIS WORK)

Fig. 43

An isochronal anneal (2 hours at each temperature) was made in the most heavily irradiated Mo_3Os ($1.03 \times 10^{20} n/cm^2$) and the results are shown in Fig. 44. From this figure we can see that there is no recovery of T_c until 700°C.

Figure 44

Isochronal annealing curve of T_c for Mo_3Os irradiated to a fluence of $1.03 \times 10^{20} n/cm^2$. Upper circles represent T_c onsets, and vertical bars indicate transition widths (10-90%).

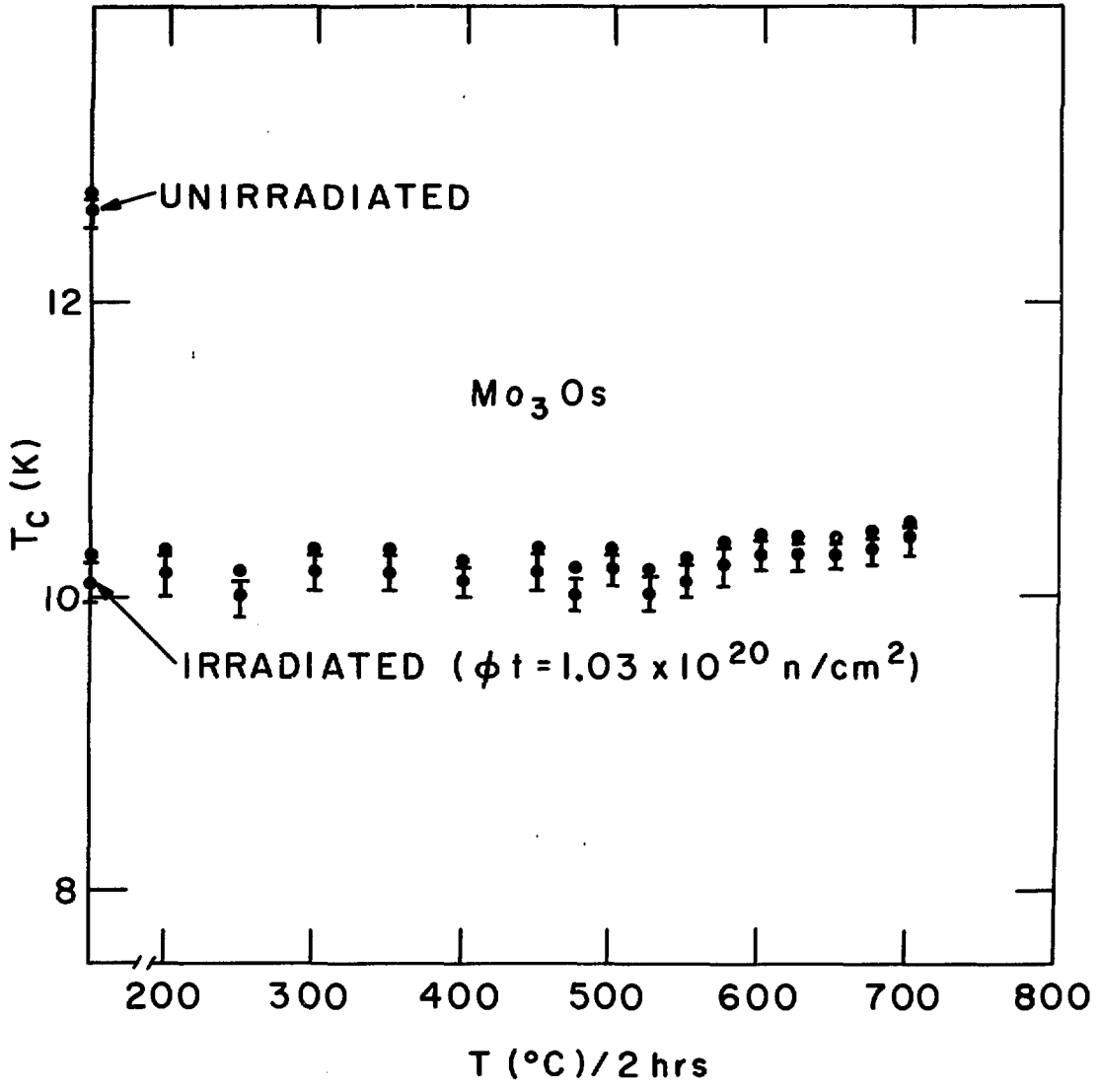
UNIRRADIATED
12
Mo_3Os
T_c (K)
10
IRRADIATED ($\phi t = 1.03 \times 10^{20}$ n/cm^2)
8
200
300
400
500
600
700
800
T (°C)/2 hrs

Fig. 44

IV. DISCUSSION

The effects of neutron irradiation, annealing, and compositional changes on T_c, a_o, and the degree of order for the A-15 materials will now be discussed.

Before proceeding, we want to summarize here the following general observations, made from this investigation:

a) The superconducting transition temperature, T_c, of the A-15 compounds studied is greatly depressed when exposed to high energy neutron irradiation at 140°C, amounting to more than 80% of the unirradiated values except for Mo_3Os where the highest depression observed was only 20%. T_c is also depressed in nonstoichiometric alloys but the rate of depression is less pronounced as we deviate to either side of stoichiometry. At high fluences T_c approaches a saturation value and the same final T_c value is reached by the different compositions of a given A-15 compound.

The transition temperature of the irradiated material is recovered with isochronal and isothermal anneals. In the isochronal anneals all the Nb-base compounds, independent of composition or fluence, start to show recovery of T_c between 400-500°C. The V_3Si shows some recovery at 250°C while Mo_3Os shows no recovery until 700°C.

T_c also decreases with rapid quenching from high temperatures, amounting to more than 40% of the original annealed value, the decrease being more pronounced at stoichiometry.

The superconducting transition temperature is a maximum at the stoichiometric composition when this composition exists in

thermodynamic equilibrium in the homogeneity range of the A-15 phase (Nb-Pt and V-Ga). When this latter does not occur, the maximum T_c is observed at the nearest point to stoichiometry (Nb-Al). In the Nb-Ge system the high T_c obtained by non-equilibrium techniques is due to the formation of a metastable stoichiometric Nb_3Ge. The transition temperature also decreases as we depart to either side of stoichiometry, with a slope ranging from 2.6K/at.% in Nb-Al to 1.5K/at.% in Nb-Pt and V-Ga. Long term low temperature anneals normally increase T_c.

b) As a general trend, the transition width, ΔT_c, shows a small or zero increase at low fluences but a significant decrease is observed at high doses. In the isochronal and isothermal recovery anneals ΔT_c increases as T_c starts to recover reaching a maximum when T_c recovers about 50% of the unirradiated value and decreases again as T_c begins to approach its final value.

There is a large increase in the transition width after the rapid quench, in some cases, to more than 4 times the width of the original annealed sample. No systematic variation in ΔT_c was observed with the change in composition.

c) The lattice parameter, a_o, expands with neutron irradiation for all the A-15 compounds studies here. The rate of lattice expansion is high at low fluences ($<1 \times 10^{19} n/cm^2$) and decreases at high doses where T_c approaches saturation. A lower a_o expansion (~50%) was observed in the Nb-Pt and Mo_3Os systems when compared to Nb_3Ge and Nb-Al. Independent of composition, the same a_o expansion with fluence is observed for a given A-15

compound. The lattice parameter can also be completely recovered with isochronal anneals (Nb_3Ge and Nb-Al) but the a_o recovery does not seem to correlate with the recovery of T_c (Nb-Al).

With the rapid quench from high temperatures, the Nb-Pt system shows a small or zero lattice expansion which is at least 3 times smaller than that observed with neutron irradiation for the same T_c's. However, in the Nb-Al system a more similar expansion is observed between the two processes (quench and irradiation).

The lattice parameter variation with composition depends on the system investigated, an a_o increase (decrease) occurs with the increase of B concentration when the atomic radius of the A atom is smaller (larger) than that of the B atom. A difference in slopes, Δa_o/at. %, occurs at stoichiometry as we go from one side of stoichiometry to the other. The lattice parameter remains unchanged (Nb-Pt) or a small contraction was noted (Nb-Al) with the long term low temperature anneals.

d) The Debye-Scherrer x-ray films show a decrease in the intensities of the difference lines with increasing fluence and these lines are no longer visible or very weak at high fluence. No line broadening was observed even in the saturation region of T_c, except for Nb_3Ge samples irradiated to 2.6×10^{19} and 5×10^{19} n/cm^2. All the difference lines reappear with the isochronal anneals. With rapid quenching some line broadening could be observed in the high angle region, while no line broadening was observed by changing composition.

e) The long range order parameter, S, decreased with increasing fluence and T_c approached a saturation faster than S approaches zero. The LRO parameter also recovers with the isochronal anneal (Nb-Ge). The disorder introduced by the rapid quench from high temperatures correlates with T_c in the same manner as that created by neutron irradiation (Nb-Pt). The higher order parameter occurs at the stoichiometric composition and a change in this composition to either side of stoichiometry is coupled with a decrease in the LRO parameter. The long term low temperature anneal increased the LRO parameter.

From these observations we note that the superconducting transition temperature can be depressed (>40%) by changing composition, rapid quenching from high temperatures and neutron irradiation, and also in these two latter cases T_c can be recovered by annealing. For the changes in T_c a similar change was always observed in the long range order parameter, which suggests a correlation between these two parameters.

Labbé and Friedel[83] proposed a model for the A-15 compounds, where the high T_c's in this structure result from a very high density of states at the Fermi level, N(0). This peak in the density of states arises from the A-atom chains and any interruption in their continuity will affect the peak and cause a decrease in T_c. The observed crystallographic disorder will certainly affect the integrity of the chains and change T_c. However, it should be pointed out here that the sharp peak at the Fermi level of the A-15 compounds can also be affected, as T_c is, by other

effects, such as addition of gases[84,85], magnetic impurities[86,87] or stress[88], where the crystallographic disorder is probably not the principal cause of the changes in T_c as are here with irradiation, rapid quencing, annealing and composition.

The first experimental evidence of this correlation was obtained by Sweedler and Cox[64] in neutron irradiated Nb_3Al. They observed an initial depression rate[89] of 2.2 ± 0.2K per % of Nb sites occupied by Al atoms. Here for neutron irradiated Nb_3Ge, Nb_3Pt and Mo_3Os we obtain 3.3 ± 0.2, 1.4 ± 0.2 and 0.4 ± 0.2K per % of A sites occupied by B atoms, respectively. Similar values for Nb_3Pt and Mo_3Os are observed with the rapid quench. It is interesting to note that the sensitivity of T_c on the order parameter depends on the A-15 system. This sensitivity to disorder may be attributed to the directionality[90] of the bonding between the atoms in the A-15 structure and, as the Mo_3Os results suggest, the depression of T_c also depends on the nature of the B atom, if it is a transition or a non-transition element. Recently, Staudenman et al.[91] demonstrated in a precise x-ray study of the valence electron density distribution in the superconducting A-15 compound V_3Si that the bonding along the V-chains are of the covalent type. If this type of bonding is also true for the other A-15 compounds the integrity of the linear chains formed only by transition metals will be very sensitive to the nature of the B atom when it interupts a chain.

The T_c depression with irradiation has been observed to fall in a similar manner for most of the A-15 compounds[10], and a

universality in the defect that causes the T_c depression has been suggested[92]. Soll et al.[93] also showed that the T_c depression of Nb_3Sn for various types of irradiations (neutrons, oxygen ions and deuterons) are equivalent, when normalized to the energy transferred to each lattice atom. From our neutron irradiation results of samples with different compositions some interesting observations on this subject arises. Fig. 45 a shows the irradiation results in the Nb-rich side of the Nb-Pt system where, as previously mentioned, the rate of depression of T_c decreases as we go off-stoichiometry. Comparing the slopes, $\Delta T_c/\Delta\phi t$, of these curves we note that they all have the same slope for a given T_c. In other words, the irradiation effect on T_c of an off-stoichiometry sample, for example point C in Fig. 45 a that follows the path CD, is equivalent to a stoichiometric sample already irradiated until point B that follows the path BD. These two curves (CD and BD) are only separated by a constant factor. From this figure we can also observe that going from point A to B by neutron irradiating a stoichiometric sample to a fluence of $3.2 \times 10^{18} n/cm^2$ (point B in Fig. 45 a) is equivalent to going from point A to C by changing the composition of the stoichiometric sample to 24.1 at.% Pt (point C), as far as T_c is concerned. These same observations were also found for the Pt-rich side of stoichiometry and all the off-stoichiometric curves shifted to the right by a constant factor, ϕt equivalent, until they match the stoichiometric curve as shown in Fig. 45 b. This curve, that gives the dependence of T_c with fluence for the stoichiometric Nb_3Pt, also includes the dependence of all the off-

Figure 45a

Superconducting transition temperature, T_c, for neutron irradiated Nb-Pt alloys illustrating procedure for obtaining master curve as discussed in details in text.

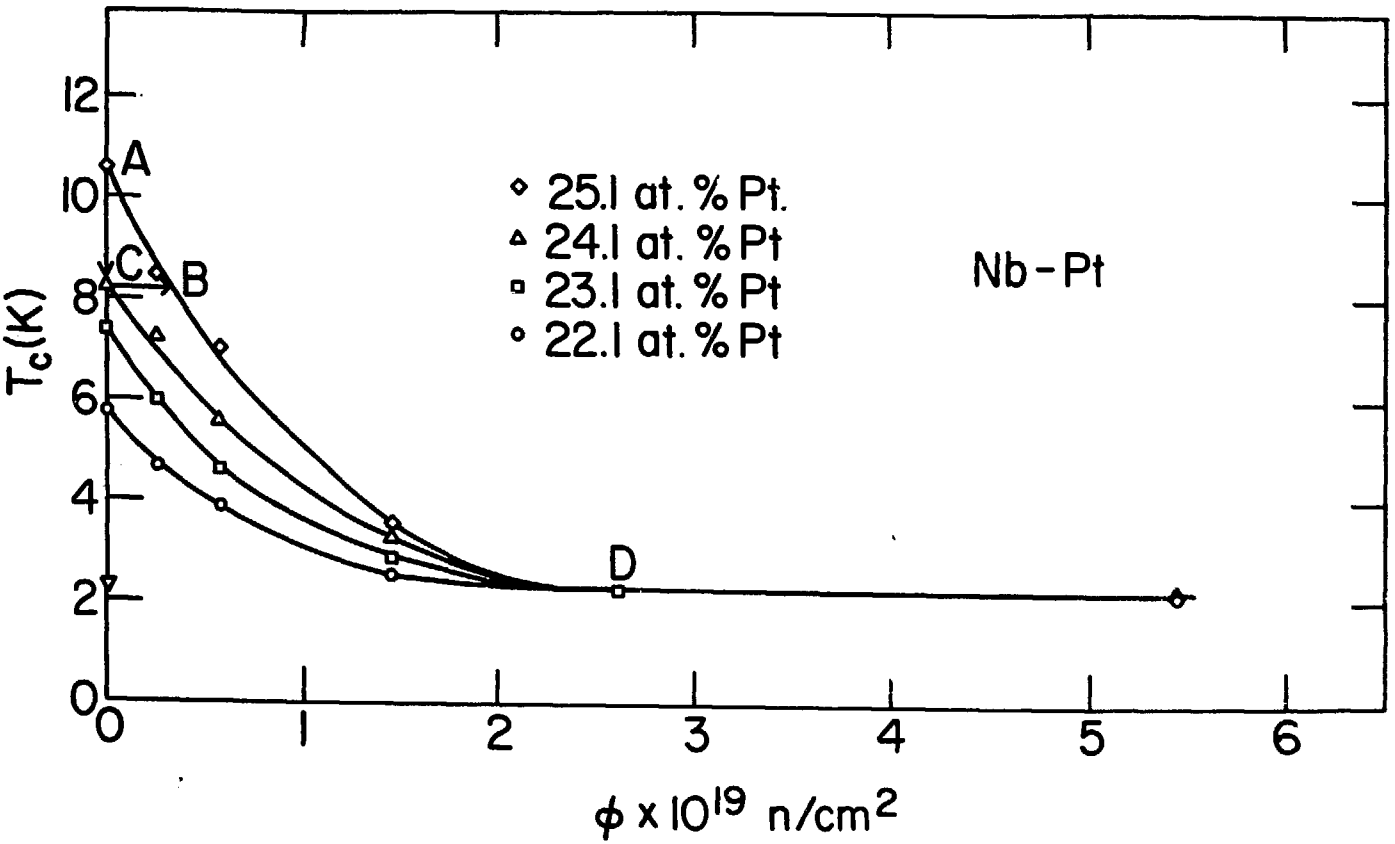
12
10
8
6
4
2
0
T_c(K)
A
B
C
D
◇ 25.1 at. % Pt.
△ 24.1 at. % Pt
▫ 23.1 at. % Pt
○ 22.1 at. % Pt
Nb-Pt
0
1
2
3
4
5
6
$\phi \times 10^{19}$ n/cm^2

Fig. 45.a

Figure 45b.

Master curve for the superconducting transition temperature T_c of neutron irradiated and compositionally variant samples in the Nb-Pt system. For detailed explanation see text.

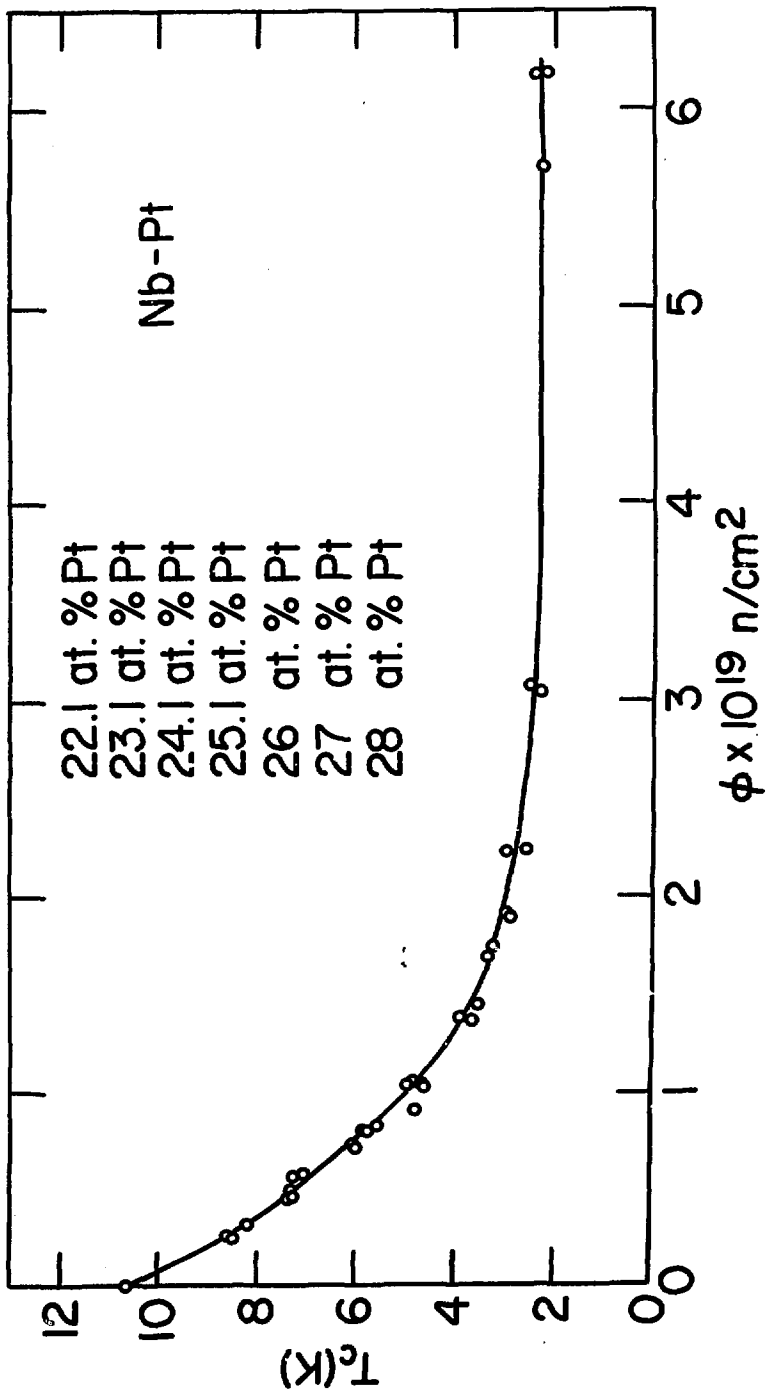
Nb-Pt
22.1 at. % Pt
23.1 at. % Pt
24.1 at. % Pt
25.1 at. % Pt
26 at. % Pt
27 at. % Pt
28 at. % Pt
T_c(K)
$\phi \times 10^{19}$ n/cm^2
0
2
4
6
8
10
12
0
1
2
3
4
5
6

Fig. 45.b

stoichiometric samples and have implicitly the T_c variation with composition. In this sense we can say that this curve suggests a universal correlation between T_c and the defect that cause its depression in the Nb-Pt system. This same analysis can also be made for the neutron irradiated Nb-Al samples with different compositions, and the master curve for this system with the off-stoichiometric curves shifted to the right by the equivalent fluences is shown in Fig. 46.

Observing the initial slopes in the depression of Tc with fluence, $\Delta T_c/\Delta\phi t/_{\phi t = 0}$, not only for different compositions of a given system but also between different Nb-base compounds we note that they all scale with T_c (Fig. 47). The higher the T_c, the greater the initial slope which probably is also a reflection of the structural stability of these A-15 compounds. This observation led us to extend the idea of equivalent fluences to different compounds. As the higher T_c and slope belong to the Nb_3Ge system we assume this as the master curve for all the other Nb-base A-15 compounds. The results are shown in Fig. 48 with the equivalent fluence for the systems Nb-Pt (Fig. 45 b), Nb-Al (Fig. 46), and Nb_3Sn and Nb_3Ga from Ref. 77. A plot of $(T_c-T_c^{sat})$ vs. ϕt was used due to the different T_c's in the saturation region for different systems. A striking overlap of all these curves can be observed from this figure which indicate, now in a more generalized form, the universality of the T_c dependence on the defect that causes its depression. As mentioned earlier, the cause of the depression of T_c with irradiation, quenching, annealing and

Figure 46

Master curve for the superconducting transition temperature T_c of neutron irradiated and compositionally variant samples in the Nb-Al system. For detailed explanation see text.

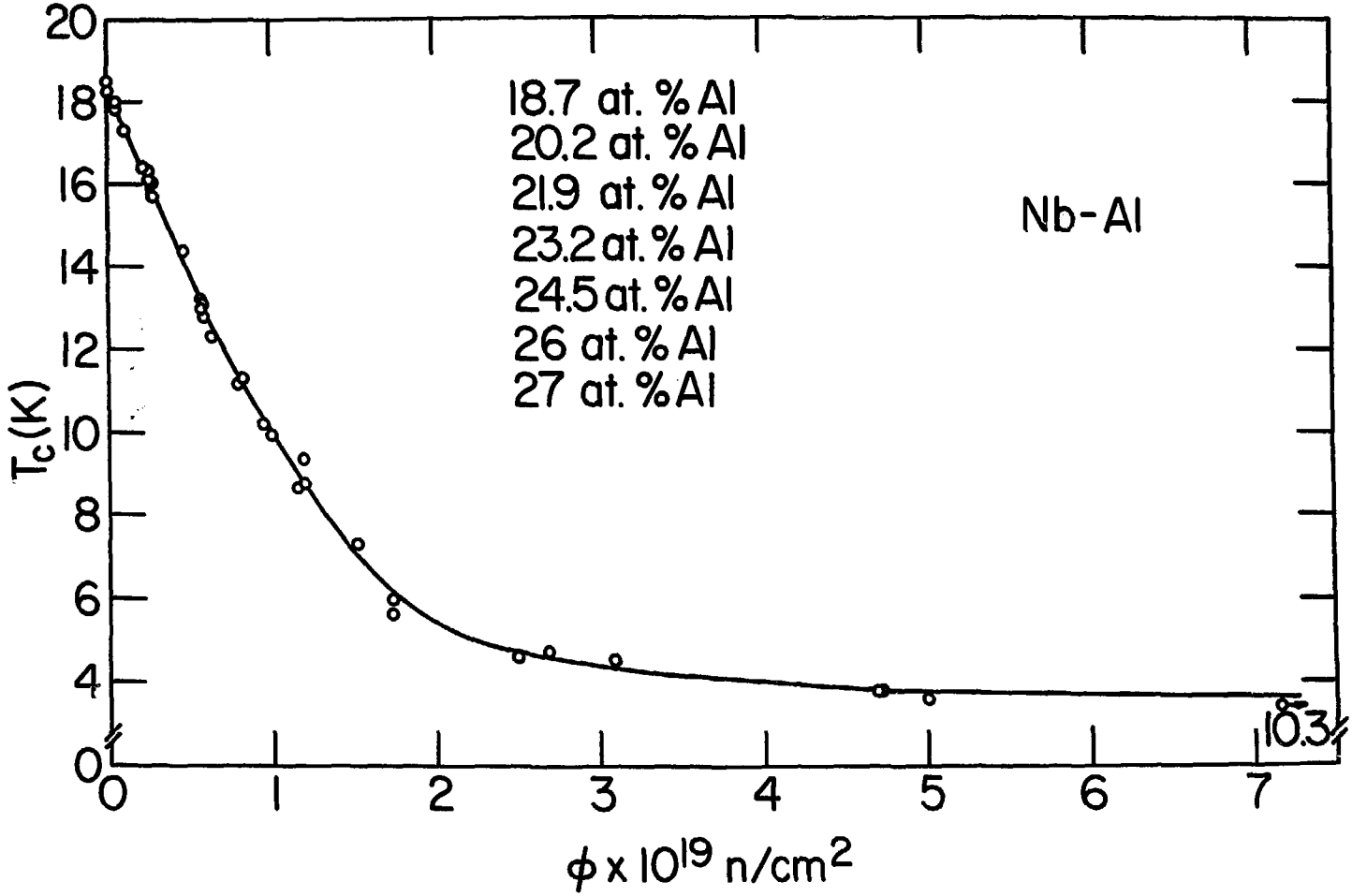
18.7 at. % Al
20.2 at. % Al
21.9 at. % Al
23.2 at. % Al
24.5 at. % Al
26 at. % Al
27 at. % Al
Nb-Al
T_c(K)
$\phi \times 10^{19}$ n/cm^2
10.3

Fig. 46

Figure 47

Initial depression rate of the superconducting transition temperature, $\Delta T_c/\Delta\Phi|_{\Phi=0}$, against T_c for neutron irradiated Nb-base A-15 compounds and α-particle irradiated V-base A-15 compounds.

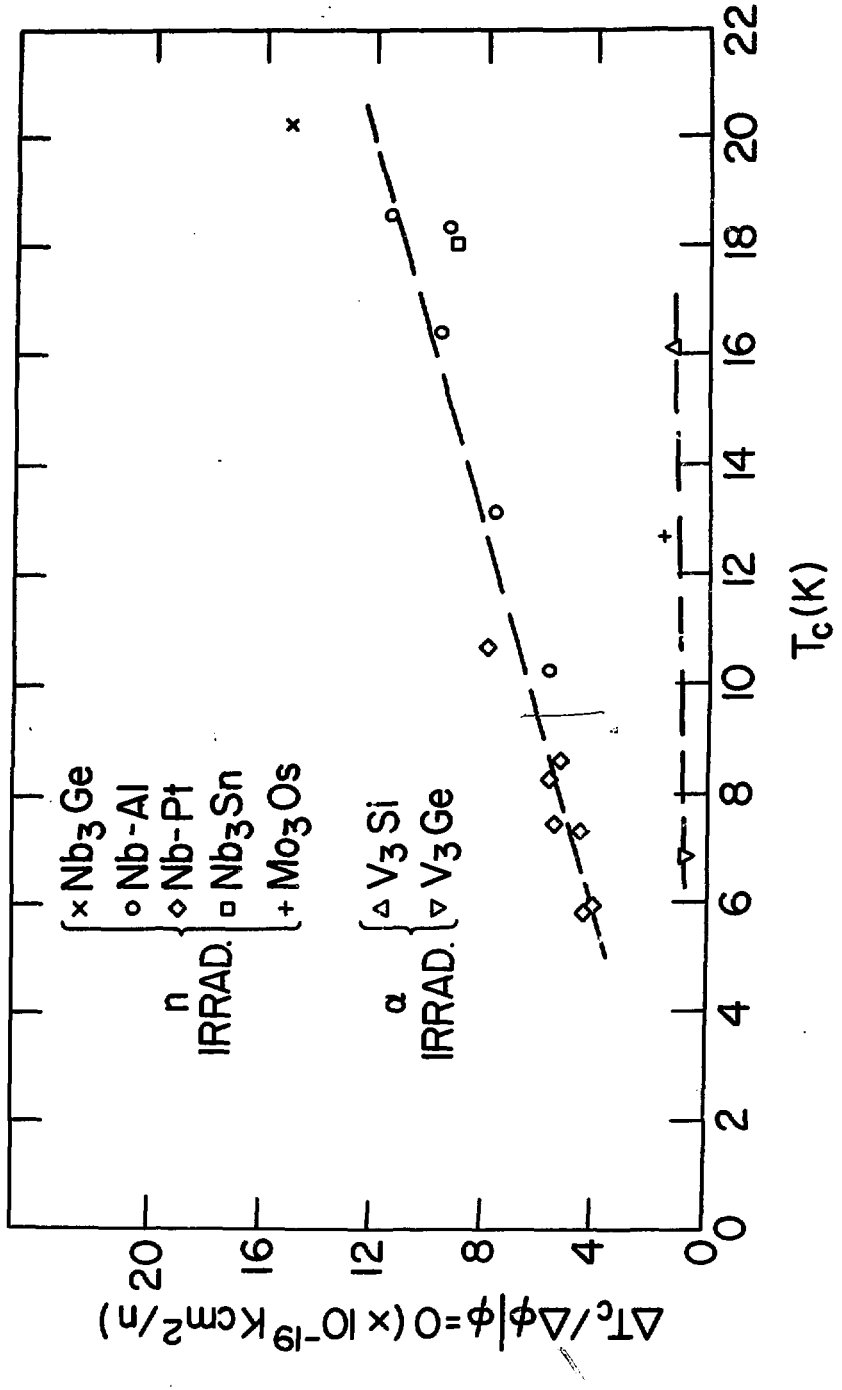
$\Delta T_c/\Delta\phi|_{\phi=0}$ ($\times 10^{-19}$ K cm^2/n)
T_c(K)
n IRRAD.
× Nb_3Ge
○ Nb-Al
◇ Nb-Pt
□ Nb_3Sn
+ Mo_3Os
α IRRAD.
△ V_3Si
▽ V_3Ge

Fig. 47

Figure 48

Master curve for the superconducting transition temperature of neutron irradiated and compositionally variant Nb-base A-15 compounds. $T_{c\ sat}$ is the saturation value of T_c for each system. For complete description see text.

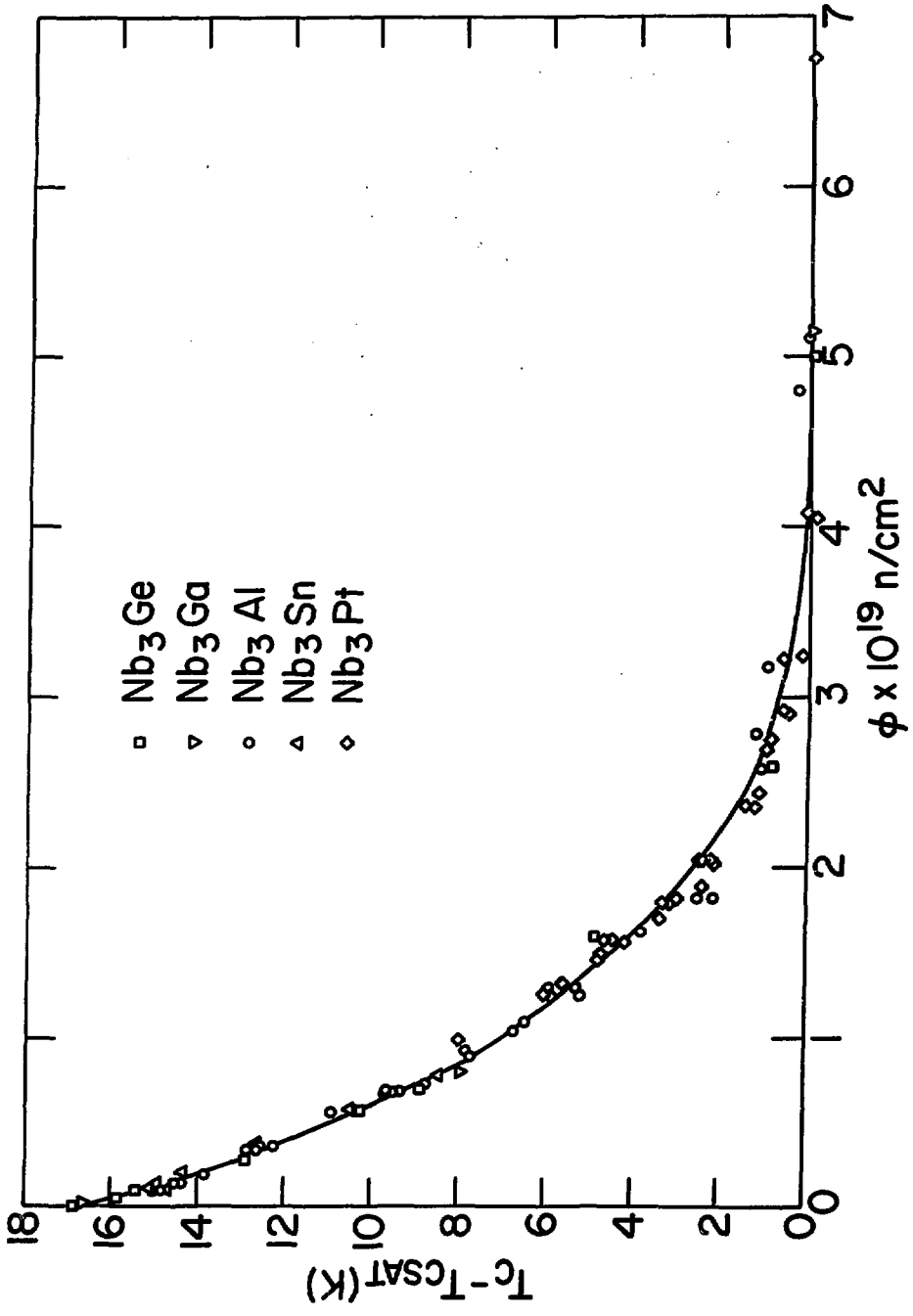
Nb3Ge
Nb3Ga
Nb3 Al
Nb3Sn
Nb3Pt
Tc-TcSAT(K)
φ x 10^19 n/cm^2
0
2
4
6
8
10
12
14
16
18
1
3
5
7

Fig. 48

composition for a given system is the crystallographic disorder. To understand the overlap of the curves for different systems in terms of crystallographic disorder is not so obvious as all these compounds are nearly fully ordered. However, the scaling of T_c with the different Nb-base A-15 compounds can be related through the sensitivity of T_c with atomic disorder. This is because the initial rate of depression of T_c with disorder depends on the system (Nb_3Ge = 3.3; Nb_3Al = 2.2; Nb_3Pt = 1.4K per % of Nb sites occupied by B atoms) and this also scales with T_c (Nb_3Ge, T_c = 20.2K; Nb_3Al, T_c = 18.6K and Nb_3Pt, T_c = 10.6K). It should be emphasized here that the choice of Nb_3Ge as the master curve for the Nb-base compounds is because this is the highest T_c available but if another Nb-base A-15 compound with a higher T_c could be synthesized, like Nb_3Si, this would be the master curve for all the others, including Nb_3Ge.

A comparison between this curve for Nb-base A-15 compounds with other systems like V_3Si and Mo_3Os neutron-irradiated (see Fig. 47) shows that they have different slopes and it's possible that each one, V-base or Mo-base A-15 compounds, have their own master curve. From the results of Poate et al.[75] where V_3Si and V_3Ge have been irradiated with α-particles (Fig. 47) we note that this is true for these two V-base systems (V_3Si, $T_c$sat = 2.4K, ϕt equiv. = 0 and V_3Ge, $T_c$sat = 1.0K, ϕt equiv. = 1.05 x $10^{17}\alpha/cm^2$) but are very different when compared to Nb_3Ge and Nb_3Sn also α-irradiated, which seem to support the suggestion of different T_c dependences for each system.

We have shown that T_c correlates with the crystallographic disorder whether the samples of a given system were neutron irradiated or rapidly quenched. It will be of great interest to know if this is also true for other processes that change T_c where a change in the order parameter also occur like annealing and composition, as a unique relation should exist between T_c and the crystallographic disorder for a given system. From the annealing studies made here no systematic measurements of the order parameter were done that permit this kind of analysis, however, this parameter was measured as a function of composition in the Nb-Pt system where also the correlation of T_c with disorder for irradiated and quenched samples were observed. A difficulty arises with the interpretation of the dependence of the LRO parameter with composition because by definition there are two order parameters, S_A and S_B, one for each side of stoichiometry. However, this problem can be avoided if we consider the disorder in terms of the percentage of sites occupied. As follows from the A_3B stoichiometry, with the same degree of deviation from stoichiometry, the number of wrongly occupied sites is three times greater in the A-rich side (B site disorder) than in the B-rich side (A site disorder). So, in a plot of T_c against percent of Nb sites wrongly occupied, the wrongly occupied site occupation number of a sample in the Nb-rich side must be divided by three to be equivalent to a sample in the Pt-rich side with the same degree of deviation from stoichiometry.

With this procedure, the results of T_c and

the order parameter measurements for different compositions is shown in Fig.49, together with the previous irradiated and quenched results and the sample with 21 at.% Pt that received a long term-low temperature anneal. Samples with intermediate compositions had their LRO parameters obtained by interpolating the experimental data. From Fig.49 we can see that there is a good correlation of T_c with the percentage of wrongly occupied sites for all of these processes. This result is not so surprising if we recall that in the universality of the defect with irradiation shown previously, the master curve also included the T_c dependence with composition. This universality in the defect involving different systems of a certain kind, strongly suggest that this correlation of T_c and disorder observed in the Nb-Pt system will also occur in other A-15 compounds. It should be noted however that a correlation with resistance ratio, $\rho(300\ K)/\rho(25\ K)$, has also been observed in Nb_3Ge[94] and Nb_3Sn[95] films for different growing conditions and α-particle irradiations. This condition may indeed reflect the disorder discussed here.

We observed from this investigation that a maximum in T_c occurs exactly at the stoichiometric composition when the homogeneity range of the A-15 phase includes this composition, as in Nb-Pt and V-Ga. This has also been observed in other systems, as V-Pt[11] and V-Si[44] that have a broad homogeneity range.

Figure 49

Superconducting transition temperature, T_c, as a function of the percentage of wrongly occupied sites for irradiated, quenched, composition, and annealed Nb-Pt samples.

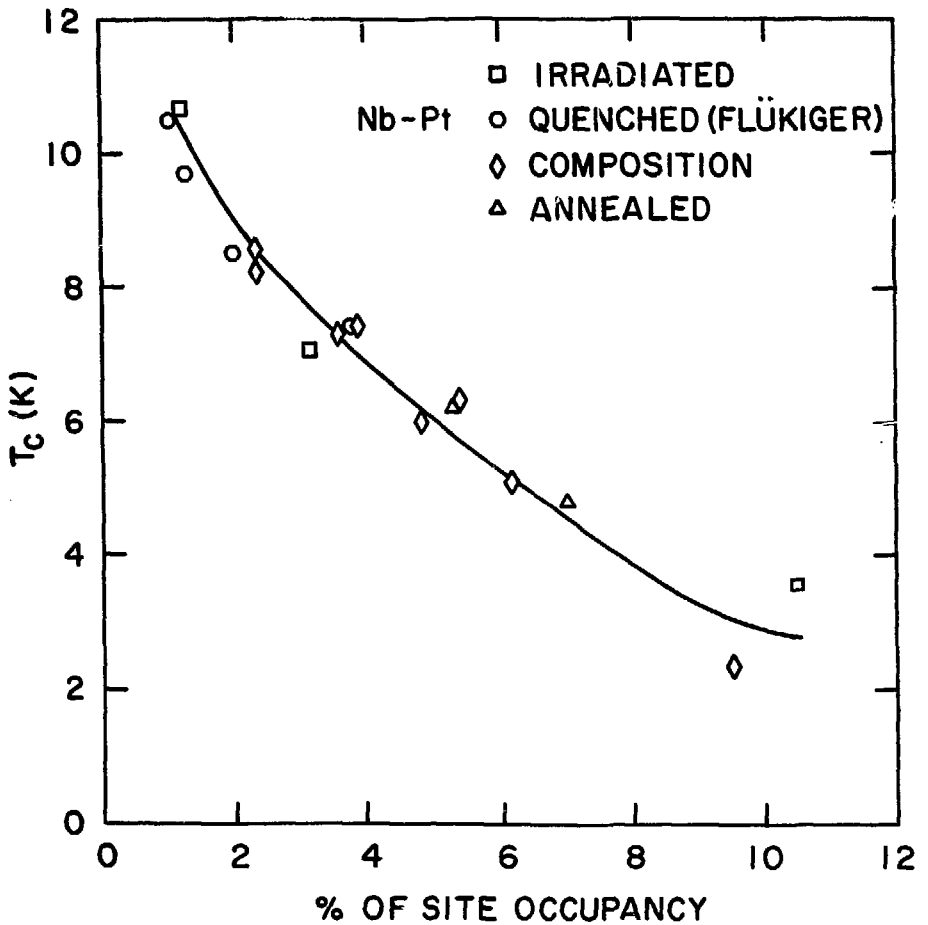
Nb-Pt
IRRADIATED
QUENCHED (FLÜKIGER)
COMPOSITION
ANNEALED
T_c (K)
% OF SITE OCCUPANCY
0
2
4
6
8
10
12

Fig. 49

These results are consistent with the correlation mentioned above since the LRO parameter is also a maximum at the stoichiometric composition. However, in a few other A-15 compounds[11,80,96] the maximum T_c does not occur at the stoichiometric composition. T_c increases or decreases with the composition, having its maximum at one of the A-15 phase boundaries. These compounds usually have a low transition temperature ($\lesssim$5 K) and are composed of two transition metals. The most striking example of these compounds is Nb-Ir. Within the homogeneity range of the A-15 phase[97] (21.5 to 28.5 at.% In) the superconducting transition temperature rises linearly from <0.1 K at 22 at.% Ir to the maximum value of 3.3 K beyond the stoichiometric composition at 28 at.% Ir according to Flukiger[11] who investigated this system. In three arc melted samples (22.5, 25 and 27.2 at.% Ir) similar behavior in T_c was observed. After a high temperature heat treatment (10 hrs/ 1800°C) followed by a long term-low temperature anneal (70 days/ 900°C) no significant change would be observed in T_c, beside a small increase at stoichiometry (1.31 K-1.52 K). Debye-Scherrer x-ray films and diffractometer scans show in all these samples two unidentified extra peaks (d=1.054Å and d=0.921Å). A similar result was also found in the V-Ir system,[96] where a second phase was observed in all samples except at stoichiometry. Interesting results were obtained by Koch and Scarbrough[98] on the effect of

interstitial impurities on T_c of the σ phase of Nb-Ir. After annealing single-phase samples in a partial pressure of air T_c, previously a sharp transition at 2.2 K, rises to 3.7-4.1 K. Whether the measured T_c is from the A-15 phase or from a second phase or impurity is not known, but a more detailed analysis of these compounds would be necessary to determine if they are really an exception to the maximum in T_c at stoichiometry.

A correlation between T_c and the lattice parameter expansion have also been proposed[92] but from our results such correlation could not be found. In Fig. 50 we show T_c/T_{co} (T_{co} is the unirradiated T_c) vs $\Delta a_o/a_o$ for the neutron-irradiated A-15 compounds and Nb_3Sn and V_3Si from Ref. 77. We see the different lattice expansions of Mo_3Os and Nb-Pt as compared to the other A-15 compounds. From the irradiation results of samples with different compositions we also observe that T_c does not correlate with a_o as the expansions of the latter with fluence is constant for the different compositions while the T_c depression is not. This lack of correlation is also observed in the T_c dependence of a_o for Nb-Al (26 at.% Al) irradiated to 5×10^{19} n/cm^2 and the recovery anneal curve shown in Fig. 51, where two different paths can be observed with irradiation and annealing. Similar observations occur in quenched and irradiated Nb_3Pt where the two T_c's are equal but a lattice expansion three times larger occur with irradiation than from quenching.

Figure 50

Reduced transition temperature, T_c/T_{co}, against lattice expansion, $\Delta a_o/a_o$, for neutron irradiated A-15 compounds.

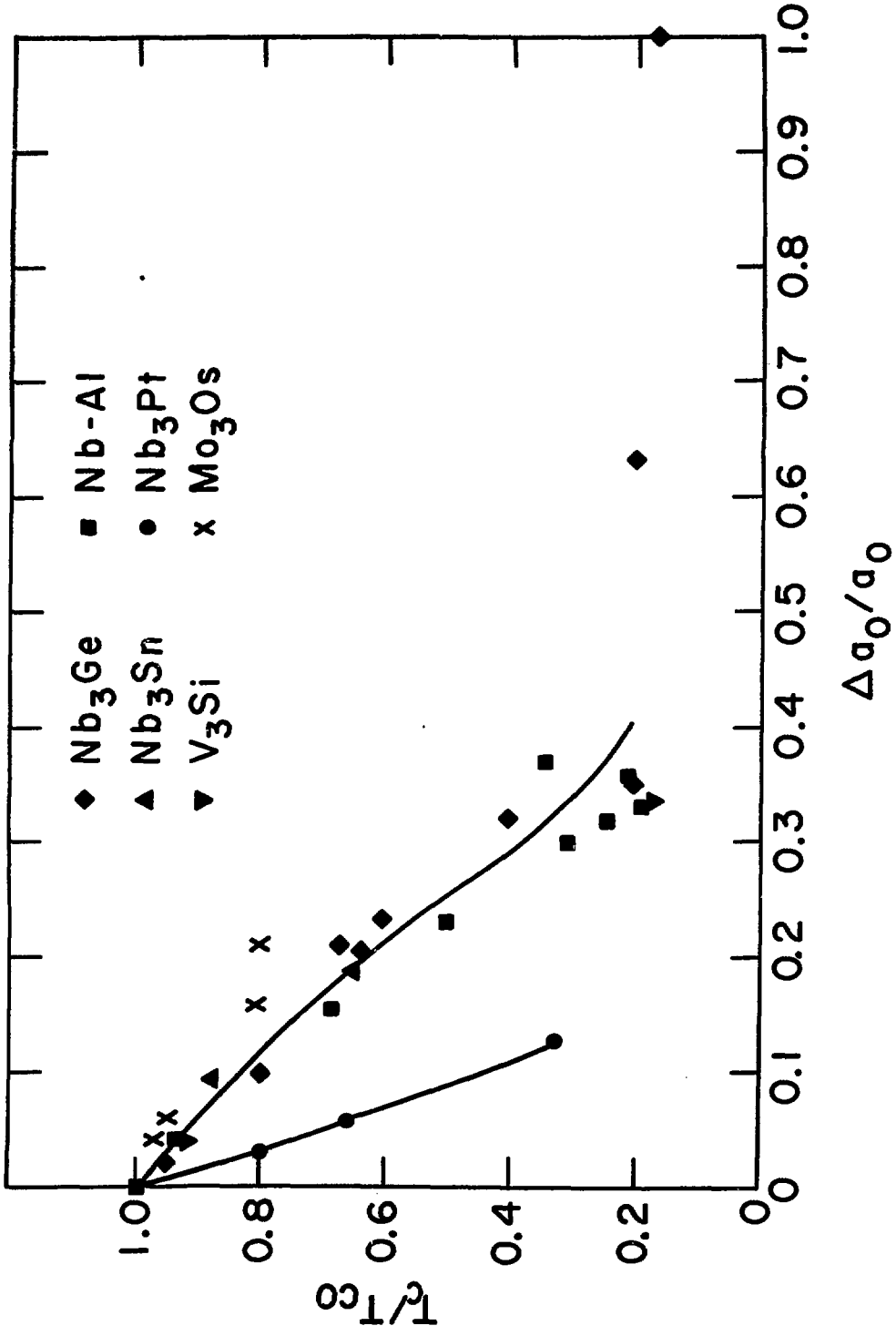
Nb-Al
Nb_3Pt
Mo_3Os
Nb_3Ge
Nb_3Sn
V_3Si
T_c/T_{co}
$\Delta a_o/a_o$
1.0
0.8
0.6
0.4
0.2
0
0.1
0.2
0.3
0.4
0.5
0.6
0.7
0.8
0.9
1.0

Fig. 50

Figure 51

Superconducting transition temperature, T_c, as a function of lattice parameter, a_o, for Nb_3Al neutron irradiated (circles) and annealed (squares).

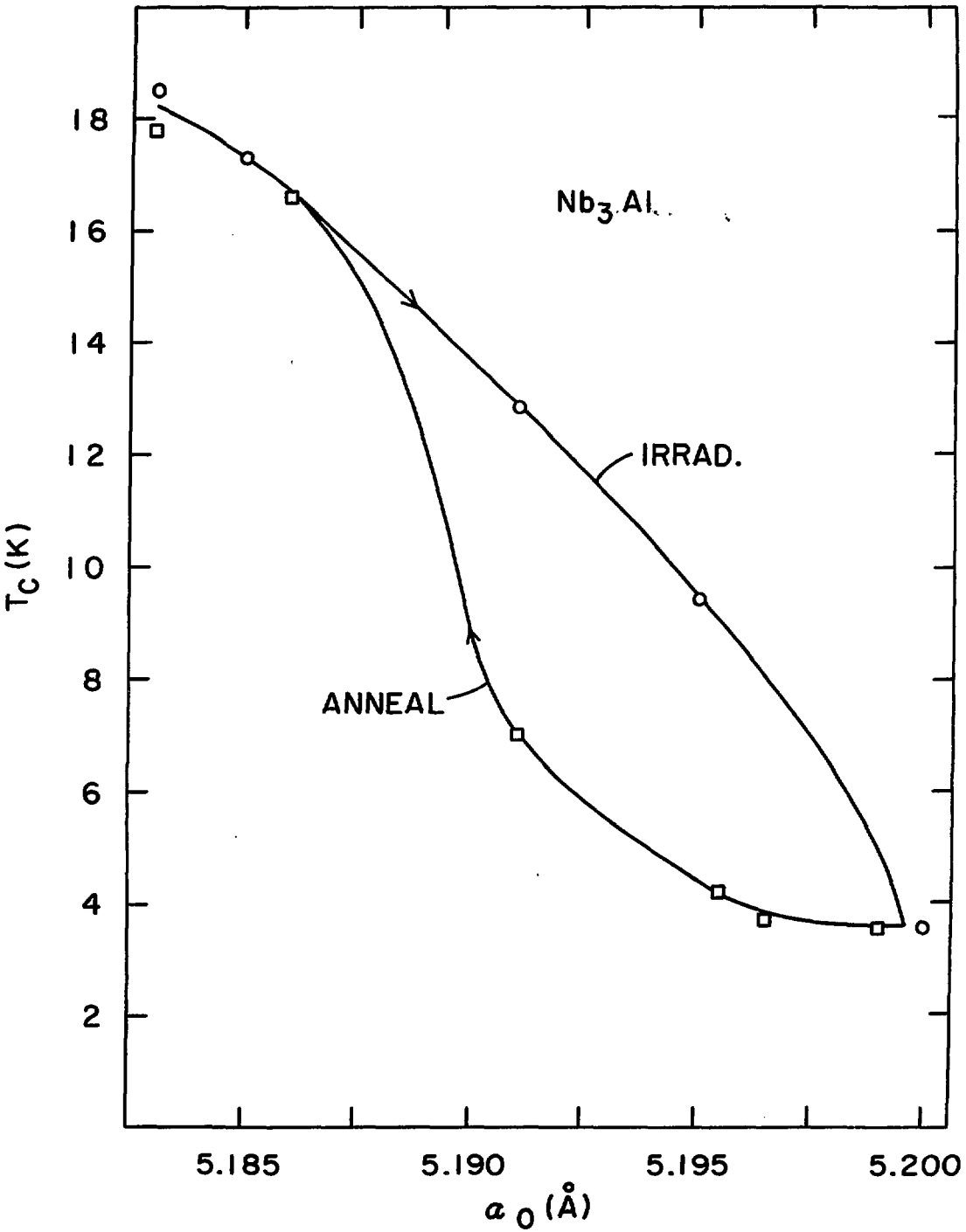
Nb3Al
IRRAD.
ANNEAL
Tc (K)
18
16
14
12
10
8
6
4
2
5.185
5.190
5.195
5.200
a0 (Å)

Fig. 51

The observed large lattice expansion in the irradiated samples may not be due only to the crystallographic disorder, since it is known[99] that during neutron irradiation other defects are also created that may account for this expansion. From these results we note that the a_o expansion is smaller for A-15 compounds involving only transition metals than when a non-transition element is present. This variation in the lattice expansion with the nature of the B element may be related with the type of bonding between the atoms in the A-15 structure and the change in atomic size when the atoms occupy different sites.

The variation of the lattice parameter for the different A-15 compounds can be satisfactorily accounted for by a simple model first proposed by Geller.[100] This relates a_o to the effective radii of nearest neighbor A and B atoms as follows:

$$a_o = \frac{4}{\sqrt{5}} (r_A + r_B)$$

and implies that the principal geometrical feature of the structure is contact between these atoms. The original values tabulated by Geller have recently been revised and updated by Johnson and Douglass,[35] and the overall agreement for more than 60 compounds is quite striking.

For off-stoichiometric materials, a simple extension of this model is to assume that the effective radii in the A and B sites are just an average of the Geller radii i.e.

$$\bar{r}_A = N_A^A r_A + N_B^A r_B$$

where N_A^A and N_B^A are respectively the fractions of A and B atoms on A sites. An analogous expression holds for the B sites.

Applying these expressions to a system like Nb-Pt where the homogeneity range encompasses both sides of stoichiometry and comparing them with the measured values of a_o yield a discrepancy, as illustrated in Fig.52, in which the broken line corresponds to the calculated values of the lattice parameter based upon Geller radii for Nb and Pt of 1.51Å and 1.37Å respectively,[35] and the order parameters listed in Table XV. It is seen that on the Pt-rich side the model gives a very good fit to the slope of the data points. A decrease of about 0.05% in r_{Nb} and r_{Pt} would make the fit almost exact. However, on the Nb-rich side, the model is clearly inadequate, with the implication that the B-site radius of Nb is significantly smaller than 1.51Å and must be considered as an additional variable i.e.

$$\bar{r}_A = N_A^A r_A^A + N_B^A r_B$$

$$\bar{r}_B = N_A^B r_A^B + N_B^B r_B \ .$$

A least-squares fit to the data in Fig.52 with r_{Nb}^A, r_{Nb}^B and r_{Pt} as variable parameters yielded the respective values 1.516Å, 1.425Å and 1.365Å, with standard errors of about 0.002Å. It is to be noted that the values of the Geller radii r_{Nb}^A and r_{Pt} are

Figure 52

Lattice parameter, a_o, vs. composition for the A-15 phase of Nb-Pt. Open circles are experimentally determined data points for samples annealed at 1800°C for 12 hours plus 900°C for 10 days. Dashed curve is calculated from Geller radii r_{Nb}=1.51Å and r_{Pt}=1.37Å. Solid curve is least squares fit to modified Geller model as described in text.

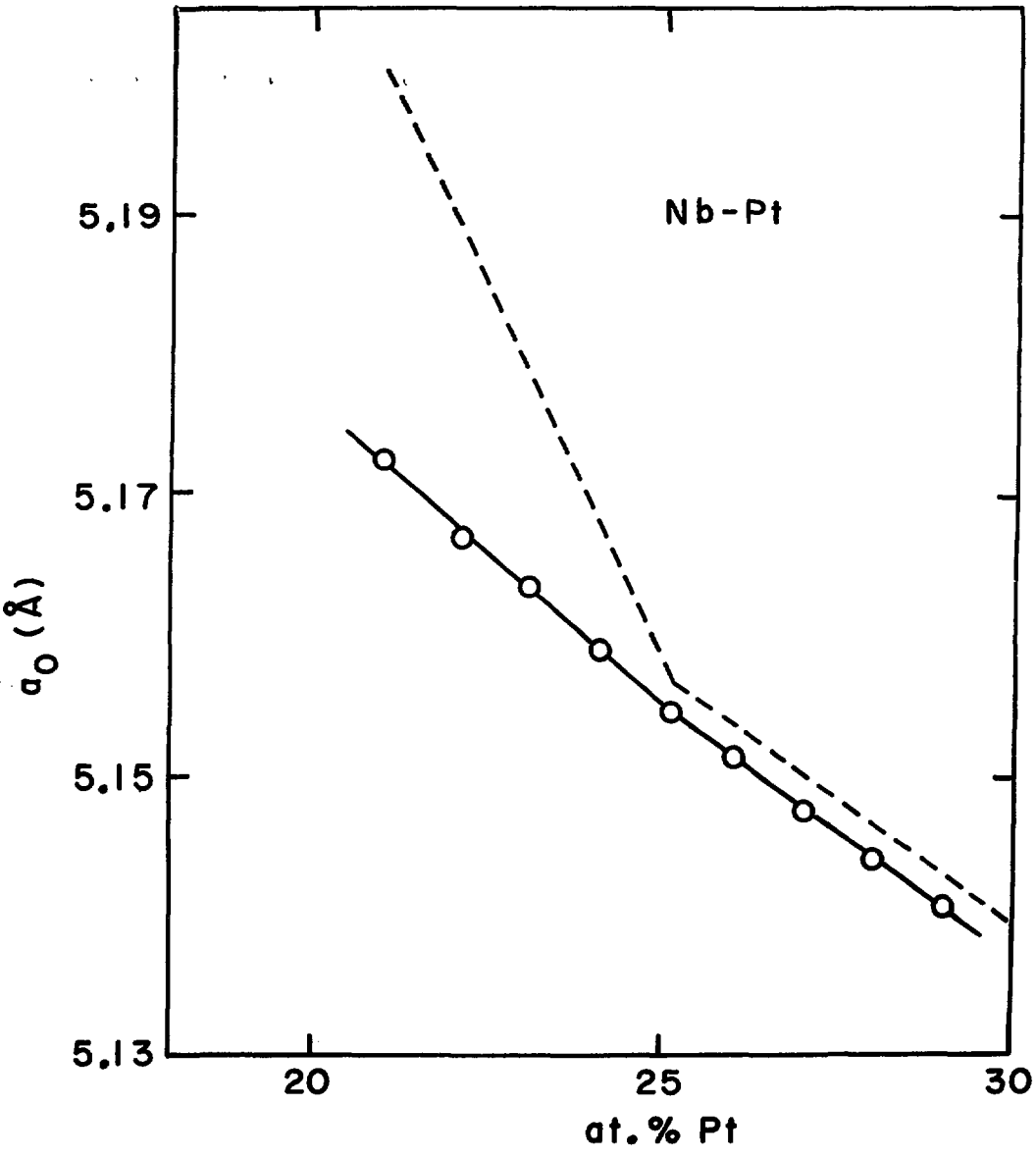

Fig. 52

uniquely determined in this analysis, whereas previous compilations are relative to some arbitrary fixed value, as first pointed out by Nevitt.[101] The present analysis therefore indicates that whereas Pt has essentially the same effective Geller radius on either site, Nb has a significantly smaller B site radius of 1.43Å, the same as in the metal. Furthermore, the calculated value of a_o for the hypothetical compound "Nb_3Nb" would be 5.26Å, a fact first noted by Vieland and Wicklund[102] from extrapolation of data in the Nb-Ga and Nb-Ge systems. They also pointed out the similarity between the atomic volume of Nb in "Nb_3Nb" (18.2Å^3) and in the metal (18.0Å^3). A similar analysis of lattice parameter data for the A-15 region of the V-Ga system shows an opposite trend, namely a B site radius for V of 1.37Å, which is larger than the Geller radius of 1.31Å and the same as in the metal. The calculated value of a_o for the hypothetical compound "V_3V" would be 4.794Å. Doing the same extrapolation for the V-base A-15 compounds from the data available in the literature[11,44,103], as shown schematically in Fig. 53, an a_o of 4.796±0.01Å was obtained which gives an atomic volume for V in "V_3V" of 13.79±0.1Å^3 similar to the metal (14.0Å^3). From Fig. 53 we also observe that the lattice parameter increase or decrease with composition for the different Nb or V-base A-15 compounds depends on how the size of the B atom compares with that of the A atom in the B site.

Figure 53

Schematic lattice parameter, a_o, dependence on composition for several Nb-and V-base A-15 compounds, and the extrapolated a_o for the hypothetical compound "Nb_3Nb" and "V_3V" (see text).

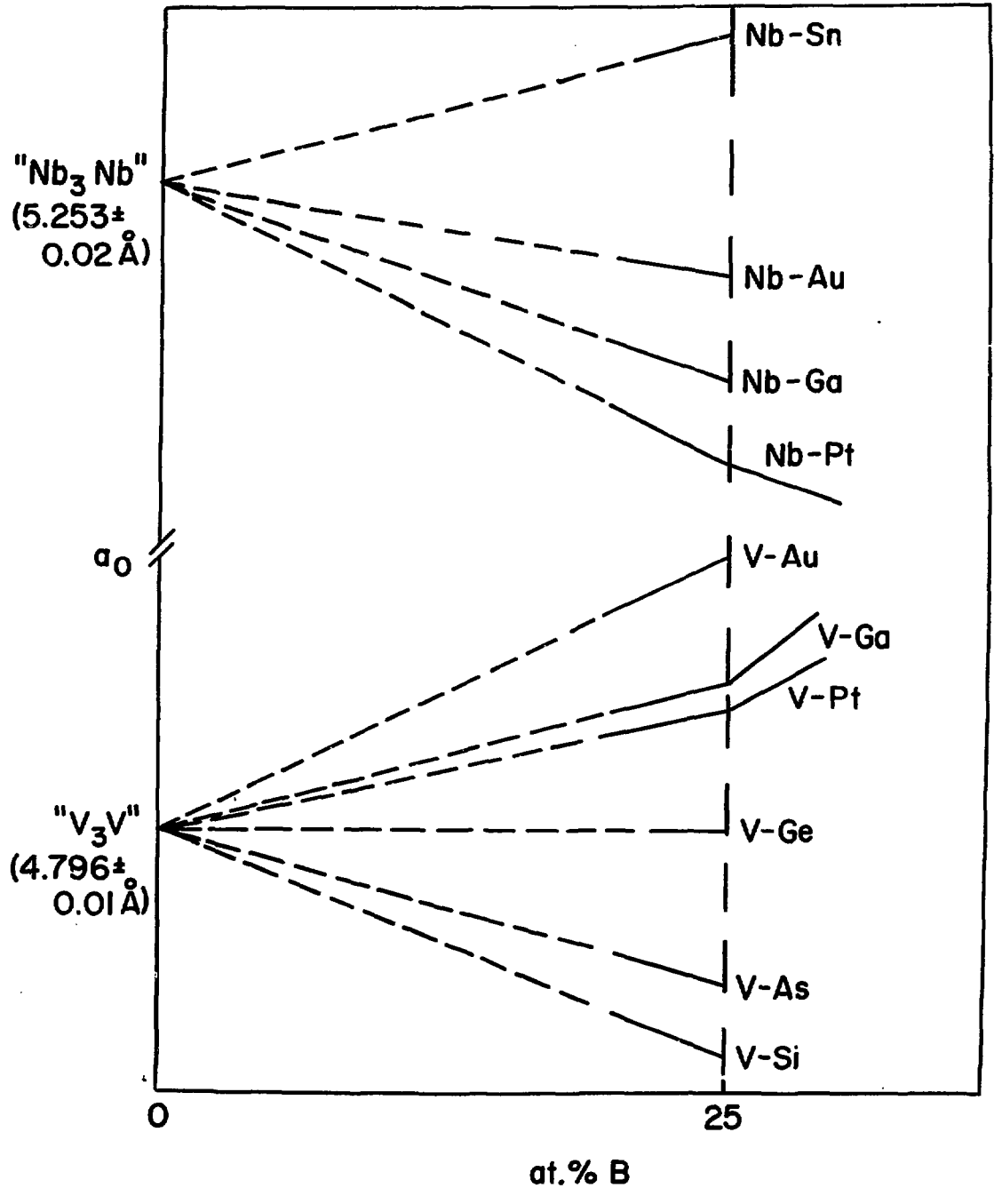
Nb-Sn
"Nb3 Nb"
(5.253±
0.02 Å)
Nb-Au
Nb-Ga
Nb-Pt
a0
V-Au
V-Ga
V-Pt
"V3V"
(4.796±
0.01 Å)
V-Ge
V-As
V-Si
0
25
at.% B

Fig. 53

For example in V-Si system, Si has an atomic radius (1.33Å), smaller than V at the B site (1.37Å) so an a_o decrease occurs with increasing Si concentration, while in the V-Au system an a_o increase is observed because the atomic radius of Au (1.41Å) is larger than the V at the B site, and in the V-Ge system a very small change in a_o with composition is observed because the Ge radius (1.36Å) is similar to the V at the B site. Analogous interpretation is valid for the Nb-base A-15 compounds.

Figure 54 shows the slopes of the lattice parameters with composition, $\Delta a_o/\Delta$at.%, against the atomic radius of the B atoms for several Nb and V-base A-15 compounds. From this figure we see that within experimental errors there is a good correlation between these two parameters for Nb and V-base A-15 compounds and that the slope is zero when the radius of the B element is equal to the radius of the A atom in the B site, as predicted. The extrapolated straight lines for Nb and V-base A-15 compounds shown in Fig. 53 are given by

$$a_o = \left(\frac{\Delta a_o}{\Delta \text{at.\%}}\right) \text{at.\%} + \begin{matrix} 4.796 \text{ (V-base)} \\ 5.253 \text{ (Nb-base)} \end{matrix}$$

where the a_o dependence on composition (A-rich side) can be obtained for all Nb and V-base A-15 compounds. Using this relation for Nb_3Si and V_3Al (see Fig. 54) we obtain an a_o value of 5.05Å and 4.84Å, respectively, which are in good agreement with the values

Figure 54

Slopes of the lattice parameters with composition, $\Delta a_o/\Delta$at.%, against the atomic radius of the B atoms for several Nb-and V-base A-15 compounds (see text).

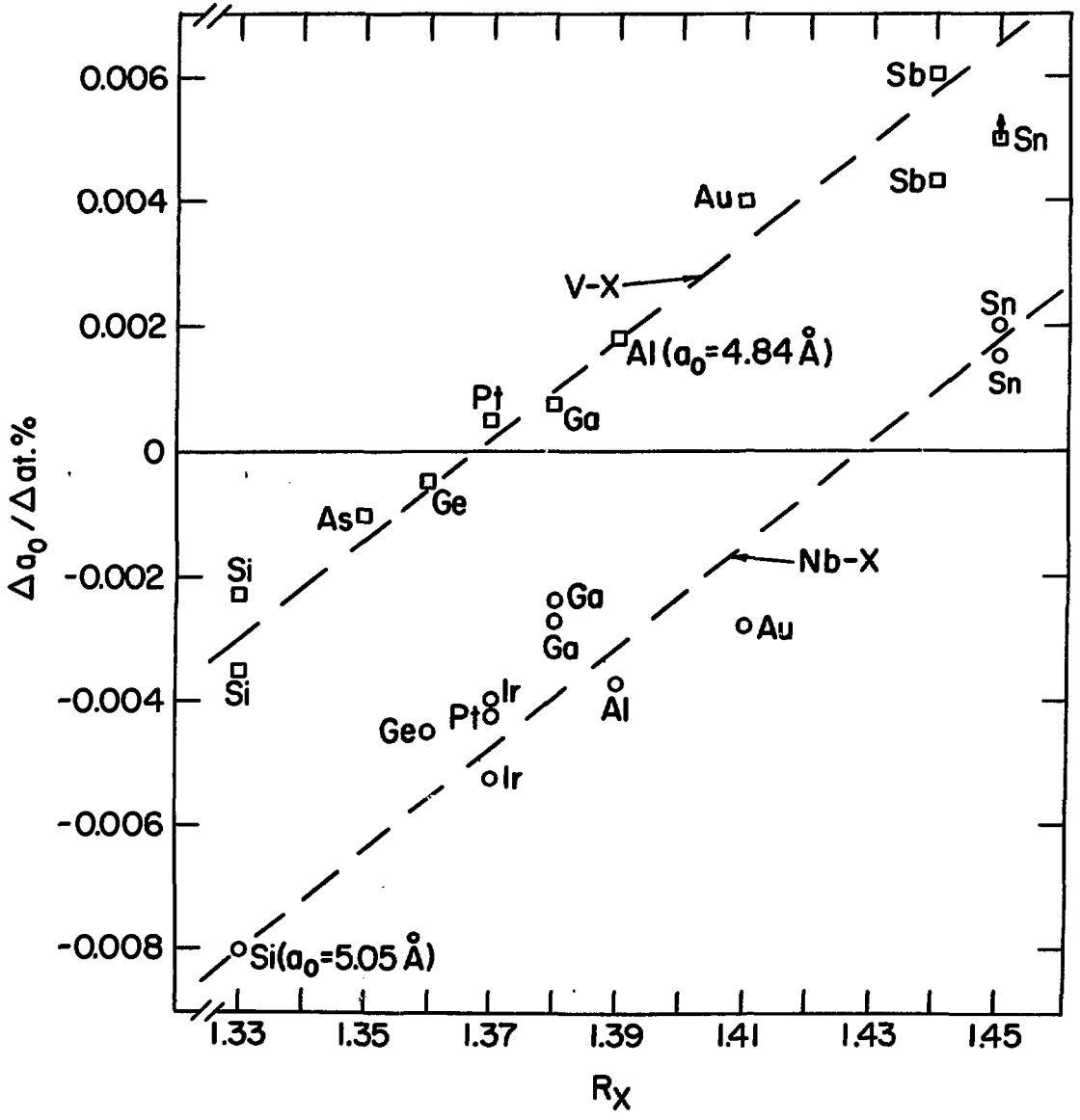
0.006
0.004
0.002
0
-0.002
-0.004
-0.006
-0.008
Δa0 / Δat.%
1.33
1.35
1.37
1.39
1.41
1.43
1.45
RX
Sb
Sn
Sb
Au
V-X
Sn
Al (a0=4.84 Å)
Sn
Pt
Ga
As
Ge
Si
Nb-X
Ga
Ga
Au
Si
Ir
Al
Geo
Pt
Ir
Si(a0=5.05 Å)

Fig. 54

predicted by Geller and entrapolated from pseudo-binary compounds.[104]

The concept of two different radii for atoms with coordination number greater than twelve in intermetallic compounds has previously been advanced by Shoemaker and Shoemaker.[105] The origin of the deformation undoubtedly lies in the pronounced covalent character of the bonding along the chains, and strong covalent bonding of this type has recently been demonstrated.[91]

Therefore, the lattice parameter changes with composition can be accounted by the different sizes and positions of the atoms in the A-15 structure and no obvious correlation exists with the superconducting transition temperature.

REFERENCES

1. G. F. Hardy and J. K. Hulm, Phys. Rev. 93, 1004 (1954).
2. B. T. Matthias, T. H. Geballe, S. Geller and E. Corenzwit, Phys. Rev. 95,, 1435 (1954).
3. J. R. Gavaler, Appl. Phys. Lett. 23, 480 (1973); L. Testardi, J. H. Wernick and W. A. Roger, Solid State Commun. 15, 1 (1974).
4. R. A. Hein, in Science and Technology of Superconductivity, Gregory et al. (Eds.), Plenum, New York (1973) p. 333.
5. M. Weger and B. Goldberg, Solid State Phys. 28, 1 (1973).
6. L. R. Tesstardi, in Physical Acoustics, Principles and Methods, Vol. 10, W. P. Mason and R. N. Thurston (Eds.), Academic Press, New York (1973) p. 194.
7. L. D. Hartsough, J. Phys. Chem. Solids 35, 1691 (1974).
8. Yu. A. Izyumov and Z. Z. Kurmaev, Sov. Phys.-Usp. 17, 356 (1974).
9. D. Dew-Hughes, Cryogenics 15, 435 (1975).
10. A. R. Sweedler, D. G. Schweitzer and G. W. Webb, Phys. Rev. Lett. 33, 168 (1974).
11. R. Flukiger, Thesis, University of Geneva (1972).
12. R. D. Blaugher, R. A. Hein, J. E. Cox and R. M. Waterstrat, J. Low Temp. Phys. 1, 531 (1969).
13. D. Dew-Hughes and V. G. Rivlin, Nature 250, 723 (1974).
14. L. R. Newkirk, F. A. Valencia, A. L. Giorgi, E. G. Sklarz and T. C. Wallace, IEEE Trans. on Mag. MAG 11-2, 221 (1975);

L. R. Newkirk, F. A. Valencia and T. C. Wallace, Proc. of Fifth International Conf. on CVD, London, England, Sept. 1975.

15. C. S. Pande, R. Caton and S. Moehlecke, J. Mater. Sci. 11, 2338 (1976).

16. G. W. Webb, RCA Laboratories, Interim Report, April 1973.

17. A. Müller, Z. Naturforsch. 25A, 1659 (1970).

18. International Tables for X-Ray Crystallography, Vol. 4, The Kynsch Press, Birmingham (1974).

19. See for example: E. C. Van Reuth and R. M. Waterstrat, Acta Cryst. B24, 186 (1968).

20. H. P. Klug and L. E. Alexander, X-Ray Diffraction Procedures, New York, John Wiley & Sons, 1954.

21. The neutron irradiation effects on quartz have been the subject of several studies (see Ref. 22 and other thereafter) and as a general conclusion the action of neutrons on the structure of quartz resembles the action of heat; the lattice expands. For example, after a fluence (E>10 keV) of $1x10^{20}$ n/cm^2 a decrease of 15% in the density of quartz was observed. The observed loss of He exchange gas at high fluence can be understood with these large lattice expansions of the quartz ampoles where the small He atoms can begin to diffuse out, after a certain dose.

22. G. K. Krivokonevr, L. S. Solntseva, B. K. Pergamenshchik and V. V. Korenevskii, Izvestiya Akademii Nauk SSSR, Neorganicheskie Materialy, Vol. 10, 1988 (1974).

23. J. R. Gavaler, M. A. Janocko and C. K. Jones, J. of Appl. Phys. 45, 3009 (1974).

24. L. R. Testardi, R. L. Meek, J. M. Poate, W. A. Royer, A. R. Storm and J. H. Wernick, Phys. Rev. 11, 4304 (1975).

25. Y. Tarutani, M. Kudo and S. Taguchi, Proc. of ICEC 5477, IPC Science and Technology Press (1974).

26. H. Lutz, H. Wiesmann, Y. A. Bashkirov, O. F. Kammerer, M. Strongin, G. Warren, J. Roche and D. H. Douglass, Proc. of the International Conf. on Low Lying Lattice Vibrational Modes and their Relationship to Superconductivity and Ferroelectricity, San Juan, Puerto Rico, Dec. 1975.

27. G. W. Roland and A. I. Braginski, ICMC-CEC, Kingston, Ontario, Canada, July 1975.

28. B. T. Matthias, T. H. Geballe, R. H. Willens, E. Corenzwit and G. W. Hull, Jr., Phys. Rev. 139, A1501 (1965).

29. J. H. Carpenter, J. Phys. Chem. 67, 2141 (1963).

30. T. B. Reed, H. C. Gatos, W. J. La Fleur and J. T. Rody, Metallurgy of Advanced Electronic Materials, G. E. Brock (Ed.), Interscience (1963), p. 71.

31. This is also deduced both from the observed lattice parameter a_o of the A-15 phase, which is about 5.14Å, close to the

predicted value of 5.13±0.01Å based on a hard-sphere model for stoichiometric completely ordered Nb_3Ge, and also from analyses when these have been made.[25]

32. J. R. Gavaler, J. W. Miller and B. R. Appleton, Appl. Phys. Lett. 28, 237 (1976).

33. A. B. Hallak, R. H. Hammond and T. H. Geballe, Appl. Phys. Lett. (to be published).

34. P. H. Schmidt, E. G. Spencer, D. C. Joy and J. M. Rowell, Superconductivity in d- and f-Band Metals, D. H. Doublass (Ed.), Plenum Press (1976), p. 431.

35. G. R. Johnson and D. H. Douglass, J. of Low Temp. Phys. 14, 575 (1974).

36. The only difference line visible in the x-ray film of the as-deposited material was the (110), which is the first and most intense of the difference lines. This line was not visible in the annealed material. Comparing the film of the annealed material with that of the off-stoichiometric (Nb-rich) arc-melted material the same feature is observed. This decrease in intensity reflects an increase of disorder. However, we want to emphasize here that even if the (110) line was not visible in the x-ray film it could be clearly observed in the diffractometer scans (see Fig. 4 and Table III).

37. A. L. Bowman, T. C. Wallace, J. L. Yarnell and R. G. Wenzel, Acta Cryst. 21, 843 (1966).

38. S. Jagner and S. E. Rasmussen, Acta Cryst. B31, 2881 (1975).

39. R. Pynn, J. D. Axe and R. Thomas, Phys. Rev. B13, 2965 (1976).

40. C. E. Lundin and A. S. Yamamoto, Trans. AIME 236, 864 (1966).

41. R. M. Waterstrat and E. C. Van Reuth, Ordered Alloys-Structural Application and Physical Metallurgy, Proc. of the 3rd Bolton Landing Conference (1969).

42. S. M. Kuznetsova and G. S. Zhdanov, Sov. Phys. Crystallogr. 16, 1077 (1972).

43. B. N. Das, J. E. Cox, R. W. Huber and R. A. Meussner, Metal. Trans. 8A, 541 (1977).

44. A. Junod, J. L. Staudenmann, J. Muller and P. Spitzli, J. Low Temp. Phys. 5, 25 (1971).

45. In this as-deposited sample, Nb_3Ge(I), no difference line could be visible in the x-ray film.

46. The diffractometer scan of Nb_3Ge(I) irradiated to $5x10^{19}$ n/cm^2 (Fig. 10) show two Al peaks from the sample holder (bottom and top) which could not be avoided due to the small amount of material.

47. N. Norman, J. Less Common Metals 4, 52 (1962); G. Brauer, H. Mueller and G. Kuhner, ibid. 533.

48. Some irradiated samples of the Nb_3Ge(I) material were also submitted to a long term low-temperature anneal (31 days at 650°C) and T_c shows a full recover. The samples irradiated to $7x10^{18}$ and $2.6x10^{19}$ n/cm^2 after this anneal has a T_{c1} of

20.61 K and 19.44 K, respectively, while the unirradiated value was of 20.82 K. The same irradiated sample ($7x10^{18}$ n/cm^2) used in the isochronal anneal (until 725°C, T_{c1}=20.67 K) after 31 days at 650°C has a T_{c1} of 21.07 K while the unirradiated Nb_3Ge(I) with the same heat treatment shows no change in T_c. In all, a sharp transition was observed.

49. E. A. Wood, V. B. Compton, B. T. Matthias and E. Corenzwit, Acta Cryst. 11, 604 (1958).

50. E. Corenzwit, J. Phys. Chem. Solids 9, 93 (1959).

51. K. Raetz and E. Saur, Z. Physik 169, 315 (1962).

52. P. R. Sahm and T. V. Pruss, Phys. Lett. 28A, 707 (1969).

53. R. H. Willens, T. H. Geballe, A. C. Gossard, J. P. Maita, A. Menth, G. W. Hull, Jr. and R. R. Soden, Solid State Commun. 7, 837 (1969).

54. V. M. Pan, V. I. Latysheva and A. I. Sudovtsov, Fiz. Metal. Metalloved. 31, 504 (1971).

55. J. G. Kohr, T. W. Eagar and R. M. Rose, Metal. Trans. 3, 1177 (1972).

56. L. Kammerdiner and H. L. Luo, J. Appl. Phys. 43, 4728 (1972).

57. I. Ya. Dekhtyar, V. I. Latysheva, V. S. Mikhalenkov, V. M. Pan, S. G. Sakharova and A. I. Sudovtsov, Fiz. Metal. Metalloved. 33, 656 (1972).

58. P. J. Martin, A. M. Campbell and J. E. Evetts, J. Mater. Sci. 10, 498 (1975).

59. L. Kokot, R. Horyn and N. Iliew, J. Less Common Metals 44, 215 (1976).

60. R. E. Siemens and D. J. Griffiths, Solid State Commun. 18, 1097 (1976).

61. V. V. Baron and E. M. Savitskii, Zh. Neorgan. Khim. 6, 182 (1961).

62. N. A. Nedumov and V. I. Rabezova, Izv. Akad. Nauk SSSR, Otd. Tekhn. Nauk, Met. i Toplivo 4, 68 (1961).

63. V. N. Sveshnikov, V. M. Pan and V. I. Latysheva, Sb. Metallofizika. Fazovye prevrashcheniya (Phase transformations) 22, Kiev. Izd. Nauschnaya mysl', 54 (1968).

64. A. R. Sweedler and D. E. Cox, Phys. Rev. 12B, 147 (1975).

65. N. Q. Lam and S. J. Rothman, Radiation Damage in Metals, N. L. Peterson and S. D. Harkness (Eds.), ASM, Chapter V (1975).

66. R. M. Waterstrat and R. C. Manuszewski, Noble Metal Constitution Diagrams, Part II, No. 5, Report NBSIR 73-415 (1975).

67. J. M. Muller, R. Flukiger, A. Junod, F. Heiniger and C. Susz, Low Temperature Physics LT-13, K. D. Timmerhaus, W. J. O'Sullivan and E. F. Hammel (Eds.), Plenum Press (1974), p. 446.

68. S. T. Zegler, Phys. Rev. 137A, 1438 (1965).

69. The T_c of these samples is nearly independent of composition after 25 at.% Pt (~8 K), very similar behavior was reported previously.[11,67]

70. J. H. N. van Vucht, H. A. C. M. Bruning, H. C. Donkersloot and A. H. Gomes de Mesquita, Philips Res. Reports 19, 407 (1964).

71. R. Flukiger, J. L. Staudenmann and P. Fischer, J. Less Common Metals 50, 253 (1976).

72. C. C. Koch, J. Phys. Chem. Sol. 34, 1445 (1973).

73. R. Flukiger, J. L. Staudenmann, A. Treyvaud and P. Fischer, Low Temp. Phys. LT 14, M. Krusius and M. Vuorio (Eds.), Vol. 2 North-Holland/American Elsevier, New York (1975), p. 1.

74. A. Junod, R. Flukiger, A. Treyvaco and J. Muller, Solid State Commun. 19, 265 (1976).

75. J. M. Poate, R. C. Dynes, L. R. Testardi and R. H. Hammond, Superconductivity in d- and f-Band Metals, D. H. Douglass (Ed.), Plenum Press (1976), p. 489.

76. A. R. Sweedler, D. E. Cox and L. Newkirk, J. of Electronics Materials 4, 883 (1975).

77. A. R. Sweedler, D. E. Cox, D. G. Schweitzer and G. W. Webb, IEEE Trans. on Magnetics, Mag 11, 163 (1975); V_3Ga multifilament wires were also irradiated with deuterons at low temperatures by E. Seibt, IEEE Trans. on Magnetics, Mag 11, 174 (1975).

78. Metals Handbook-AMS, T. Lyman (Ed.), Vol. 1 (1961).

79. D. C. Johnston, Solid State Commun. 11, 1751 (1972).

80. R. Flukiger, A. Paoli and J. Muller, Solid State Commun. 14, 443 (1974).

81. A. Taylor, N. J. Doyle and B. J. Kagle, J. Less Common Metals 4, 436 (1962).

82. L. R. Aronin, J. of Appl. Phys. 25, 344 (1954).

83. J. Labbé and J. Friedel, Journale de Physique 27, 153, 303, 708 (1966).

84. L. J. Vieland and R. W. Cohen, RCA Report (1970).

85. E. M. Savitskii, V. V. Baron, Yu. V. Efimov, M. I. Bychkova and L. F. Myzenkova, Superconducting Materials, K. D. Timmerhaus (Ed. Trans.), Plenum Press (1973).

86. G. H. Bongi, R. Flukiger, A. Treyvaud and P. Fischer, J. Low Phys. 23, 543 (1976).

87. N. E. Alekseevskii, C. Bazan, A. B. Mitin, T. Mydlarz, E. P. Krasnoperov and B. Raczka, Phys. Stat. Sol. 77B, 451 (1976).

88. E. M. Savitskii, V. V. Baron, A. A. Korostelin, A. R. Kadyrbaev, V. N. Sumarokov and V. R. Gusev, Sov. Phys. Dokl. 21, 211 (1976).

89. The T_c dependence on the order parameter is linear for low fluences, where the slopes ($\Delta T_c/\Delta S$) were taken.

90. P. B. Allen and R. C. Dynes, Phys. Rev. B12, 905 (1975).

91. J. L. Staudenmann, S. P. Cooper and J. M. Muller, Solid State Commun. 19, 29 (1976).

92. L. R. Testardi, Cryogenics, Feb. 67 (1977).

93. M. Söll, K. Böning and H. Bauer, J. Low Temp. Phys. 24, 631 (1976).

94. J. M. Poate, L. R. Testardi, A. R. Storm and W. M. Augustyniak, Phys. Rev. Lett. 35, 1290 (1975).

95. J. M. Poate, R. C. Dynes, L. R. Testardi and R. H. Hammond (to be published).

96. J. E. Cox, J. Bostock and R. M. Waterstrat, Proc. LT 13, 480 (1972).

97. B. C. Giessen, R. Koch and N. J. Grant, Trans. AIME 230, 1268 (1964).

98. C. C. Koch and J. O. Scarbrough, Phys. Rev. B3, 742 (1971).

99. G. J. Dienes and G. H. Vineyard, Radiation Effects in Solids, Interscience (1957).

100. S. Geller, Acta Cryst. 9, 885 (1956); 10, 380 (1957).

101. M. V. Nevitt, Trans. AIME 212, 350 (1958).

102. L. J. Vieland and A. W. Wicklund, Phys. Lett. 49A, 407 (1974).

103. A. Muller, Z. Naturforsch. 24a, 1134 (1969).

104. L. A. Pendrys and D. H. Douglass, J. Low Temp. Phys. 23, 367 (1976).

105. C. B. Shoemaker and D. B. Shoemaker, Trans. AIME 230, 486 (1964).